Electropolishing Effects on Surface Roughness of Additively Manufactured Aluminum

Nadia Eslami

A Thesis

in The Department of

Chemical and Materials Engineering (CME)

Presented in Partial Fulfillment of the Requirements

for the Degree

of Master of Applied Science (Chemical Engineering) at

Concordia University

Montreal, Quebec, Canada

August 2025

CONCORDIA UNIVERSITY
School of Graduate Studies

This is to certify that the thesis prepared

By: Nadia Eslami

Entitled: Electropolishing Effects on Surface Roughness of Additively Manufactured Aluminum

and submitted in partial fulfillment of the requirements for the degree of

Master's Degree in Chemical Engineering

complies with the regulations of the University and meets the accepted standards with respect to originality and quality.

Signed by the final examining committee:

Dr.Pantcho Stoyanov Chair

Dr. Pantcho Stoyanov Examiner

Examiner

Dr.Rolf wuthrich Thesis Supervisor(s)

Thesis Supervisor(s)

Approved by

Dr.Sana Jahanshahi-Anbuhi Chair of Department or Graduate Program Director

Dr.Mourad Debbabi Dean of Faculty

Abstract for Masters

Investigating how electropolishing influences the surface roughness of aluminum parts fabricated through additive manufacturing (3D printing), with a focus on optimizing process parameters and comparing electrolyte systems.

Nadia Eslami, Masters

Concordia University,2025

Producing complex metal components, particularly with aluminum-based alloys, has been significantly advanced by the growing adoption of 3D printing technologies. However, the surface finish of 3D-printed parts remains a key challenge, often requiring post-processing to meet the quality standards for functional applications. Electropolishing is a promising surface finishing technique that can enhance the smoothness and uniformity of metal parts by selectively dissolving microscopic surface asperities.

The present research investigates the effect of electropolishing on the surface roughness of 3D-printed aluminum-based alloys, specifically AlSi10Mg and a custom alloy referred to as CP1. The study focuses on evaluating and optimizing key process parameters—including electrolyte composition, applied voltage, polishing duration, and bath temperature—to determine their influence on surface quality. Two electrolytic systems are explored: a conventional acidic mixture (phosphoric and sulfuric acid) and a neutral organic system (ethylene glycol with sodium chloride).

Surface roughness changes are quantified using both portable contact profilometry and confocal laser scanning microscopy, enabling detailed analysis of topographical improvements. Comparative assessments between the two alloys and electrolyte systems offer insights into the electropolishing behavior of different microstructures and alloy chemistries.

The findings contribute to a deeper understanding of electropolishing as a viable finishing method for improving the surface condition of additively manufactured aluminum components and guiding process selection for industrial applications requiring high surface quality.

Acknowledgements

I am truly grateful for all of those who have supported me throughout this journey from the bottom of my heart.

Above all, I would like to share my sincere appreciation to Dr. Rolf Wuthrich, my supervisor, for his amazing advice, knowledge, and guidance during this process.

Furthermore, I would like to express my gratitude to the following members of my thesis defense committee: Professor Christian Moreau, Professor Ivan Kantor, professor Pantcho P. Stoyanov Their thoughtful suggestions and insightful criticism contributed to improving this work.

I would also like to thank Dr. Zahra Chaghazardi for her significant participation on this project. Her constant support and technical expertise helped me get through this work.

My dear Vi, your presence has helped me on this road, raising my mood and making me feel alive again. I am deeply grateful.

My colleagues in the lab have been a wonderful source of cooperation, support, and knowledge. Thank you for your contributions and for making this experience an enriching one.

Woman-Life-Freedom

Table of Contents

List of Figures

List of Tables

Nomenclature

Symbol	Definition
Ra	Arithmetic average roughness
Rq	Root mean square roughness
Rz	Average maximum height of profile
V	Applied voltage during electropolishing
t	Polishing time
T	Bath temperature
WL	Weight loss rate ($mg/cm^2/min$)

Nomenclature

Term	Definition
Electropolishing (EP)	Electrochemical process that removes asperities to smooth a metal surface
Additive Manufacturing (AM)	Layer-by-layer 3D printing of metal or polymer components
Powder Bed Fusion (PBF)	AM technique using laser or electron beam to melt powder selectively
Profilometry	Surface roughness measurement method using stylus or optical techniques
CLSM	Confocal Laser Scanning Microscopy

Acronyms

Acronym	Full form
AM	Additive Manufacturing
PBF	Powder Bed Fusion
HIP	Hot Isostatic Pressing
CLSM	Confocal Laser Scanning Microscopy
EP	Electropolishing

1. Introduction

1.1Background on 3D Printing Technology

Additive Manufacturing (AM), commonly known as 3D printing, has evolved from a rapid prototyping technique into an advanced manufacturing process capable of producing fully dense, high-strength metal components across various industries [1-3]. Metal additive manufacturing (AM) technology allows to produce highly intricate and customized components. It offers significant cost reductions by enabling a rapid transition from design to final part production, minimizing manufacturing steps by eliminating assembly processes, and reducing both material and energy waste [4-6].

Metal additive manufacturing (AM) has become a game-changer across multiple industries due to its versatility. One of the first sectors to adopt this technology was aerospace, where it is used to create lightweight and complex parts like turbine blades and fuel nozzles, helping improve efficiency and reduce material waste [3], [7]. In the medical field, AM enables the production of patient-specific implants, leading to more precise surgeries and better patient outcomes. For example, laser-based AM can manufacture implants tailored to an individual's anatomy [8]. Both the biomedical and aerospace industries have been using additive manufacturing since 2011 [9].

Other industries, such as automotive and energy, benefit from AM's ability to consolidate multiple components into single structures, eliminating the need for fasteners and welding while improving structural integrity and reducing production costs [10].

1.2 Powder Bed Fusion (PBF) for Aluminum Components

Aluminum alloys play a crucial role in additive manufacturing (AM) due to their exceptional strength-to-weight ratio, making them highly desirable for aerospace, automotive, and RF applications where both weight efficiency and mechanical performance are critical [11].

Among the various AM techniques, Powder Bed Fusion (PBF) is one of the most widely used processes for fabricating aluminum parts. This method utilizes a high-energy laser or electron beam to selectively melt fine metal powders, building components layer by layer based on a Computer-Aided Design (CAD) model. PBF enables the production of complex geometries with high precision and minimal material waste [12]. A defining characteristic of PBF is its extremely

high cooling rates, typically ranging from 10^3 to 10^8 K/s, depending on the process parameters and material properties. These rapid solidification conditions significantly affect the microstructure, mechanical properties, and residual stresses of the printed material, influencing its overall performance [10-11].

Common Aluminum Alloys in PBF

Two aluminum alloys, AlSi10Mg and CP1 (Al-Fe-Zr), have gained significant attention in PBF due to their unique properties and suitability for high-performance applications.

AlSi10Mg: One of the most extensively studied aluminum alloys in AM, AlSi10Mg is valued for its excellent castability, low thermal expansion, and high strength-to-weight ratio. The microstructure of AlSi10Mg consists of a fine cellular-dendritic network, with ultrafine silicon particles dispersed along grain boundaries. This refined microstructure enhances tensile strength, ductility, and thermal stability, making it a preferred material for lightweight structural components in the aerospace and automotive industries [13-16].

CP1 (Al-Fe-Zr): Recently, CP1 alloys have gained increasing interest due to their exceptional thermal stability and refined grain structures. The addition of Zirconium (Zr) promotes the formation of Al_3Zr particles, which encourage equiaxed grain formation during solidification. This grain refinement enhances tensile strength while reducing susceptibility to hot cracking, making CP1 alloys particularly well-suited for high-temperature aerospace structural applications [17-18].

Both AlSi10Mg and CP1 offer unique advantages in PBF-based manufacturing, allowing for the development of lightweight, high-performance aluminum components tailored for demanding industrial applications.

1.3 Challenges of Surface Roughness in 3D-Printed parts

While metal additive manufacturing (AM) offers significant mechanical advantages, its widespread application requires high surface quality and durability under cyclic loading conditions [19-21]. One of the key challenges of AM parts is their layer-by-layer fabrication process, which inherently leads to high surface roughness [22]. This roughness impacts aesthetics, dimensional accuracy, corrosion resistance, and mechanical performance. One prominent contributor to this issue is the “stair-stepping effect,” which arises when inclined or curved surfaces are built from stacked horizontal layers. Because these layers cannot fully conform to sloped geometries, small

step-like discontinuities form along the surface. The severity of this effect depends on factors such as layer thickness, build orientation, and printer resolution. Shallower build angles and thicker layers typically exacerbate the issue, increasing surface roughness and decreasing dimensional fidelity. The stair-stepping effect not only affects appearance but can also reduce fatigue life, disrupt fluid flow, and complicate post-processing. While techniques like electropolishing or machining can alleviate it, stair-stepping remains an inherent limitation of layer-based AM technologies [22-23].

Beyond geometric limitations, surface roughness is also significantly affected by loosely bound or partially fused powder particles that adhere to the surface during fabrication [22]. These particles often persist even in regions where the stair-step effect should be minimal, introducing additional texture and irregularities. For instance, Strano et al. reported that even near-vertical surfaces (80°–90°), which theoretically should exhibit low roughness due to reduced layering effects, still showed average roughness values around 14 µm—only slightly better than the 16 µm observed on shallow angles (5°–45°) [22]. This suggests that residual powder plays a key role in surface texture formation. Furthermore, horizontal surfaces generally appear smoother compared to vertical faces, which tend to accumulate more surface defects due to their orientation during powder deposition and melting [24]. To mitigate both stair-stepping and particle-related roughness, strategies like using smaller powder particles and reducing layer thickness are often employed. However, these adjustments come at a cost: fine powders are more expensive due to lower manufacturing yields, and thinner layers increase production time [25-26].

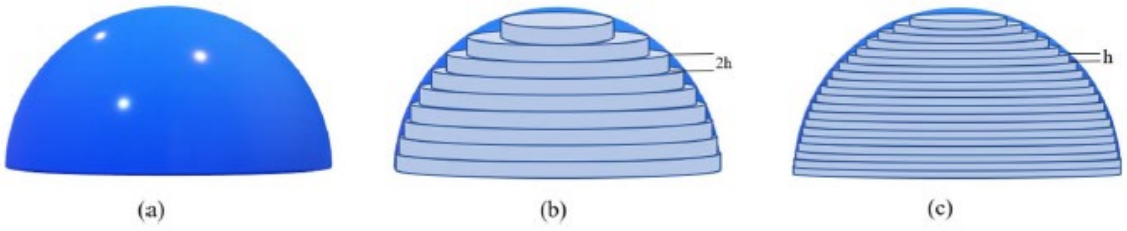

Figure 1.1 The stair-step effect in additive manufacturing parts: (a) 3D design, (b) AM part with a layer thickness 2 h, and (c) AM part with a layer thickness h The stair-step effect is reduced compared to situation (b) at the cost of build time [27].

In biomedical applications, surface smoothness is especially important to prevent bacterial growth and minimize tissue damage, making as-built AM parts unsuitable for direct use without further processing [27]. Despite their mechanical benefits, powder bed fusion (PBF) components typically

exhibit an arithmetic average roughness (Ra) between 5 and 15 µm, which is significantly rougher than conventionally manufactured parts. This high surface roughness can negatively affect fatigue resistance, corrosion behavior, and functional performance, particularly in applications demanding precise dimensions and smooth finishes [11-14].

The layered deposition process of AM contributes to these surface irregularities, which are further aggravated by partially sintered powder particles and process-induced defects. Such surface irregularities pose serious concerns in demanding applications, where they may compromise fatigue resistance, promote corrosion [2],[30], and in the case of aerodynamic components, contribute to higher drag and increased energy usage [31].

Defects and Remedies in PBF of Aluminum Alloys:

- Porosity: Metallurgical Porosity caused by gas entrapment or oxide inclusions. Also Keyhole Porosity which results from excessive energy input leading to unstable melt pools [28]**.**
- Cracking**:** Hot Cracking observed in high-strength alloys due to rapid cooling rate [29].
- Oxidation**:** The formation of oxide films on the surface of a molten or partially solidified layer can hinder proper fusion with the subsequent deposited layer, leading to poor interlayer bonding and reduced mechanical integrity [30]

1.4 Microstructural and Mechanical Characteristics of PBF-Processed Aluminum

The unique solidification conditions in Powder Bed Fusion (PBF) significantly influence the microstructure and mechanical properties of aluminum alloys. The combination of rapid cooling rates, steep thermal gradients, and restricted elemental diffusion results in refined grain structures, residual stress accumulation, and the formation of metastable phases, all of which impact the final performance of the material [10], [30].

The rapid solidification inherent in PBF promotes grain refinement, leading to the formation of ultrafine cellular or dendritic structures. The morphology of these microstructures depends on the alloy composition and processing parameters, such as laser power, scanning speed, and hatch spacing. This refined grain structure enhances key mechanical properties, particularly by

increasing strength and hardness, making PBF-processed aluminum alloys well-suited for high-performance applications [11-12].

However, the high cooling rates in PBF introduce steep thermal gradients, which generate significant internal residual stresses within the material. These stresses can compromise part integrity, leading to distortion or microcracking, particularly in complex geometries. To mitigate these effects, post-processing treatments, such as stress-relief annealing, hot isostatic pressing (HIP), or shot peening, are often necessary to minimize mechanical weaknesses and enhance dimensional stability [31].

Additionally, the limited time for elemental diffusion during the rapid solidification process prevents the formation of stable equilibrium phases. Instead, PBF-processed aluminum alloys frequently develop supersaturated solid solutions and refined secondary phases, leading to the presence of metastable phases. These metastable structures can significantly impact hardness, ductility, and thermal stability, necessitating further heat treatments, such as aging or solution treatment, to achieve a more stable microstructure and optimize mechanical properties [13], [32].

Overall, the microstructural and mechanical characteristics of PBF-processed aluminum alloys emphasize the importance of careful process optimization and post-processing strategies to ensure enhanced performance for demanding industrial applications.

1.5 Electropolishing and Alternative Post-Processing

Due to the limited effectiveness of corrective measures during fabrication, post-processing is often necessary to achieve the desired surface finish and mechanical performance in AM parts. Various post-processing techniques are used to enhance the surface quality of aluminum AM components. The table below provides a comparison of these methods, highlighting their advantages and limitations.

Table 1.1 omparison of Surface Roughness Measurement Methods: Advantages and Limitations (continued on next page)

Post-Processing Method	Description	Advantages	Limitations
Mechanical-Based Processes			
Mechanical Surface Finishing (Mass Finishing)[33],	Uses abrasive media to polish surfaces, rely on direct tool-part	Adaptable to various materials, effective for	Limited effectiveness for complex geometries,

[34], [35], [36], [37]	contact to improve surface quality. mainly suitable for simpler geometries.	batch processing, cost-efficient.	can introduce residual stress and surface deformation, may contaminate the oxide layer, and requires direct contact, making uniform polishing difficult
Ultrasonique Nano Crystal Surface Modification (UNSM)[38], [39]	Uses ultrasonic vibrations to plastically deform surfaces, enhancing fatigue and corrosion resistance.	Improves fatigue life and corrosion resistance, suitable for high-stress applications.	Requires specialized equipment and frequent tool replacement, increasing cost and complexity.
Thermal-Based Treatments			
Heat Treatment[40], [41]	Thermal processes applied after metal additive manufacturing to enhance mechanical properties. Techniques include peak hardening and annealing.	Improves microstructure, enhances fatigue resistance, relieves residual stress, increases yield and ultimate tensile strength	Can reduce hardness, may require controlled environments (e.g., vacuum annealing), and can be time-consuming.
Hot Isostatic Pressing (HIP)[42], [43], [44]	A heat treatment process that applies high temperature and pressure to densify metal	Improves fatigue resistance, reduces residual stress, refines	Requires specialized equipment, can be costly, and may alter material

	AM parts, reducing porosity and enhancing mechanical properties	microstructure, and enhances ductility.	properties depending on treatment conditions.
Chemical & Electrochemical Methods			
Chemical Surface Finishing[45], [46], [47]	A surface treatment method where a corrosive solution forms a viscous oxide film on the part, leading to selective dissolution of protruding areas and surface smoothening.	Cost-effective for batch processing, ensures consistency over large areas. does not cause surface tension due to the absence of physical contact.	Slow polishing rate, requires handling hazardous chemicals like hydrofluoric acid, necessitating special equipment and training
Electropolishing (EP)[2], [48]	Electrochemical removal of asperities, resulting in a smooth, mirror-like finish.	Achieves low roughness, preserves geometry, and allows batch processing, making it efficient for large-scale applications.	Limited to conductive materials, generates chemical waste.
Laser-Based Method			
Laser Surface Modification[49], [50]	Employs focused lasers to treat surfaces, reducing porosity and improving density.	Provides high precision and control, ideal for targeted treatments.	Requires high energy, risk of warping if not controlled properly.

Among the various post-processing methods reviewed, electropolishing has proven to be highly effective for improving the surface quality of 3D-printed AlSi10Mg components. In a study by Yu et al. [51], the surface roughness (Sa) of AlSi10Mg produced by laser powder bed fusion was

reduced by 68% through electropolishing. In addition, electropolishing is well-suited for complex geometries, as it avoids direct tool contact and can access recessed or internal surfaces, making it a highly efficient, geometry-preserving, and scalable option for batch processing of delicate or intricate additive manufactured components [52]. While other methods, such as mechanical finishing and chemical treatments, provide alternative solutions, they often come with limitations such as surface deformation, excessive costs, or slow processing rates. Given its superior balance of effectiveness and scalability, electropolishing stands out as the optimal technique for enhancing surface quality in aluminum alloys. The next chapter will delve deeper into the experimental methodology used to optimize electropolishing parameters for AlSi10Mg and CP1.

1.6 Objectives of the Study

This study investigates the effect of electropolishing on the surface roughness and morphology of 3D-printed aluminum components, with a specific focus on:

- Optimizing electropolishing parameters for AlSi10Mg and CP1 (Al-Fe-Zr) alloys.
- Analyzing surface roughness improvements following electropolishing.
- Examining morphology changes and alloy-specific responses to electropolishing.

By addressing these objectives, this research aims to provide critical insights into the role of electropolishing in refining surface characteristics, contributing to the advancement of high-performance 3D-printed aluminum components.

2. Literature review

2.1 Challenges and Optimization Strategies in Metal Additive Manufacturing

Metal AM processes include powder-bed fusion (PBF), direct energy deposition (DED), and droplet-on-demand (DOD) systems [53]. Powder bed fusion (PBF) techniques are among the most widely utilized additive manufacturing methods for fabricating metal components. These processes are particularly favored in the medical and aerospace sectors. Depending on the heat source used, the two primary PBF technologies are laser beam fusion (PBF-LB) and electron beam fusion (PBF-EB). Both methods operate on the same fundamental principle: a focused heat source (either a laser or an electron beam) selectively melts metal powder, which then solidifies quickly before the next layer of powder is deposited [52].

Despite the significant advantages of additive manufacturing (AM), several technical constraints still hinder its widespread adoption. These include limited control over dimensional accuracy, suboptimal surface quality at the microscale level, and the complexities associated with surface treatments for intricate structures [9], [54]. One of the major challenges is the undesirable surface quality, which is particularly problematic for components with a high surface-to-volume ratio, such as cellular or honeycomb structures [55]. Moreover, process-induced defects—such as porosities, residual stresses, partially melted particles, and heat-affected zones—can initiate cracks, making 'as-built' AM parts unsuitable for direct application in critical fields like biomedical implants and industrial components [49], [56].

To mitigate these challenges, several key factors must be optimized in AM processes. These considerations can be categorized into process-related, design-related, and material-related factors:

Process Parameters: Optimizing process parameters is critical for achieving the desired mechanical properties and minimizing defects in AM parts. Key factors include laser power, scan speed, layer thickness, and scan strategy. Higher laser power is required for highly reflective materials like aluminum alloys to ensure complete melting, while scan speed influences the melting and solidification rates. A lower scan speed results in deeper melt pools but increases processing time, whereas a higher scan speed can lead to incomplete melting and porosity. Thinner deposition layers

improve accuracy but extend fabrication time, while scan strategies such as alternating patterns help minimize defects and enhance isotropy [57], [33],[34], [60], [61].

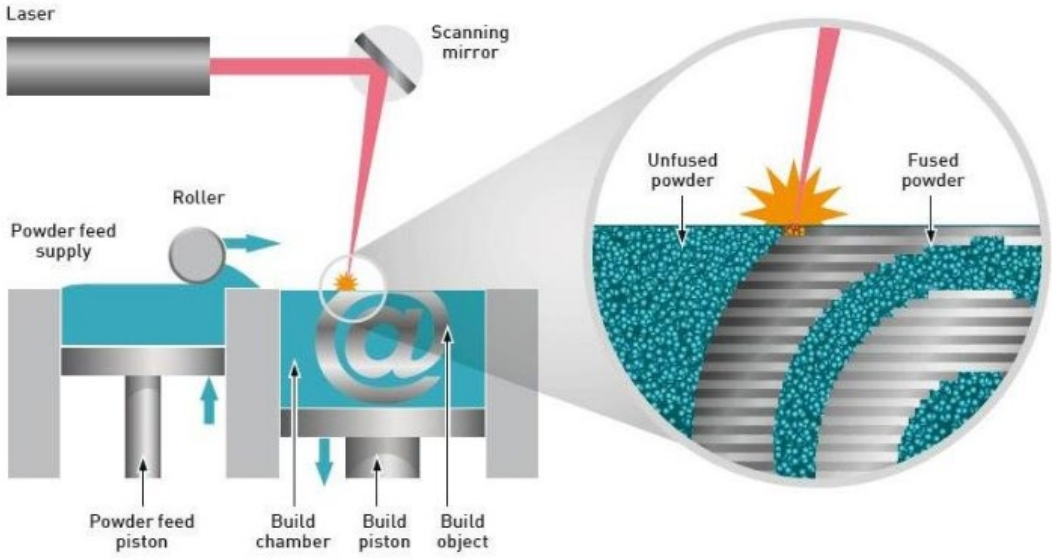

Figure 2. 1 Schematic of laser powder bed fusion process[62]

Design Constraints: Factors such as support structures, build orientation, and material distribution impact surface roughness, structural integrity, and post-processing requirements. Proper design optimization can reduce defects and improve manufacturability [62- 64].

Material Selection: The choice of material affects powder morphology, laser absorptivity, and recyclability. For example, aluminum's high reflectivity often requires surface treatments or alloying modifications to improve laser absorption [65-67].

Another strategy for the enhancement of the surface quality and performance is adding extra processes during the building of the part. One method utilized during the additive manufacturing (AM) process to improve surface quality and minimize residual porosity in parts fabricated through selective laser melting (SLM) is laser remelting. This technique is integrated into the build phase and involves re-scanning the previously melted layer with a laser to achieve complete remelting. It can be applied after each layer is scanned or limited to the top surface of the part [68-69].

Despite its benefits, laser remelting introduces some drawbacks. The movement of the laser beam can displace re-molten material toward the part's edges, leading to ridge formation upon

solidification, which may impact both dimensional accuracy and surface flatness [63]. Additionally, the process may cause balling effects or alter the chemistry of the oxide layer, potentially influencing the part's wettability, corrosion resistance, biocompatibility, and mechanical properties [64] . Given that laser remelting requires direct access to the freshly built layer, it is generally more effective for treating top surfaces rather than sidewalls or internal structures [65].

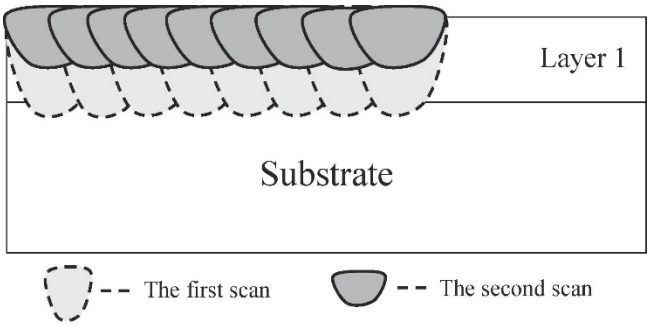

Figure 2. 2Schematic diagram of remelted layers [72].

To achieve functional AM components, post-processing and surface treatment steps are essential after fabrication. For instance, to enhance fatigue performance, AM parts typically undergo stress-relief heat treatment to mitigate residual stresses, hot-isostatic pressing (HIP) to eliminate porosities, and surface treatments to refine surface roughness and remove defects [8], [71-73]. In addition to fatigue-related concerns, the inherently rough surfaces and geometric inaccuracies of AM parts—when compared to conventionally manufactured components—necessitate post-processing techniques such as polishing, shot peening, or chemical etching [69].

2.2 Electropolishing: A Superior Post-Processing Technique

Electropolishing is widely recognized as the most effective post-processing technique for additive-manufactured (AM) metal components, offering distinct advantages over conventional methods like mechanical or chemical polishing. Unlike mechanical polishing, which requires direct tool contact and struggles to reach intricate geometries, electropolishing relies on an electrochemical dissolution process that effectively removes surface irregularities while preserving part geometry, dimensions, and intricate internal features [56], [75-78]. This method significantly reduces surface defects such as micro-cracks, stress concentration sites, and non-metallic inclusions, thereby notably enhancing fatigue resistance and mechanical integrity [73-74], [80-83].

Furthermore, electropolishing effectively improves corrosion resistance by replacing unstable oxides and surface defects with a uniform, stable, and protective passive oxide layer, a result unmatched by mechanical or chemical polishing [75-76], [79-81]. Unlike mechanical finishing, electropolishing avoids introducing residual stresses, surface hardening, or oxide contamination—factors detrimental to long-term component performance [35-36], [47],[82]. Compared to chemical polishing, electropolishing provides a faster, safer, and more environmentally friendly alternative, eliminating the use of hazardous substances such as hydrofluoric acid while achieving superior uniformity and surface finish quality [42], [46-47], [89]. Additionally, unlike processes like hot isostatic pressing (HIP), which primarily reduce porosity, electropolishing directly addresses surface quality, thereby simultaneously meeting both functional and aesthetic requirements for complex AM parts [42], [76], [78].

2.3 Electropolishing Process: Principles, Applications, and Challenges

Electropolishing is an electrochemical surface finishing technique that effectively removes surface irregularities, contaminants, and microstructural imperfections from metallic components, including stainless steel, aluminum alloys, titanium, and nickel-based superalloys. The process is based on anodic dissolution, where the workpiece functions as the anode in an electrolytic cell, while a cathode—typically stainless steel or another inert conductor—completes the circuit. When a direct current (DC) is applied, metal cations dissolve from the surface into the electrolyte, resulting in a progressively smoother and more reflective finish, as demonstrated in studies by Han et al. [79] and other researchers in the field . Figure 2.1 illustrates the schematic of a typical electropolishing setup.

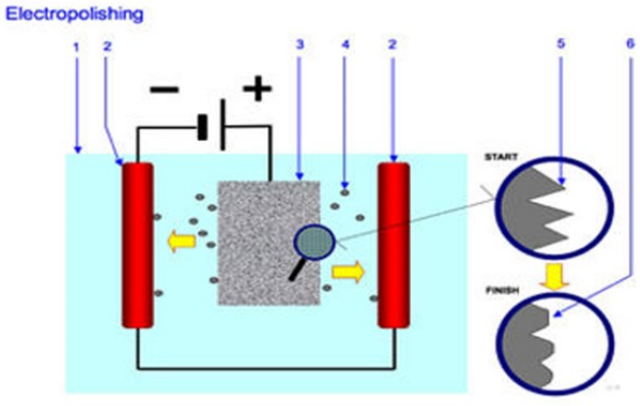

Figure 2. 3Schematic of an Electropolishing Cell [87].

Electropolishing is widely used across industries such as aerospace, biomedical, electronics, and additive manufacturing to achieve highly polished, corrosion-resistant, and contamination-free surfaces. Unlike mechanical polishing, which relies on abrasives and material deformation, electropolishing is a non-contact process governed by Faraday's laws of electrolysis. This makes it particularly effective for complex geometries and internal cavities that are difficult to process using conventional mechanical methods, as highlighted by Mark et al. [80], [81]

Furthermore, its precision and efficiency make electropolishing especially valuable in industries such as semiconductor, pharmaceutical, and biomedical manufacturing, where exceptionally clean, smooth, and corrosion-resistant surfaces are critical. In these applications, even microscopic surface imperfections or contaminants can compromise product performance, sterility, or reliability. Electropolishing effectively removes embedded contaminants, passivates the surface, and eliminates micro-burrs, thereby achieving the required level of surface cleanliness and corrosion resistance essential for maintaining the integrity and functionality of components used in these high-demand environments [85-87].

Electropolishing removes material through electrochemical dissolution, ensuring a uniform, defect-free finish without mechanical stress. Studies by Erving et al. [82] show that, compared to other surface treatments, it provides a higher dissolution rate, leading to more efficient and consistent material removal for an optimized surface finish.

2.3.1 Mechanism of Electropolishing

The electropolishing process follows a distinct current-voltage (I-V) relationship, which can be divided into four operational regions, as illustrated in Figure 2.2:

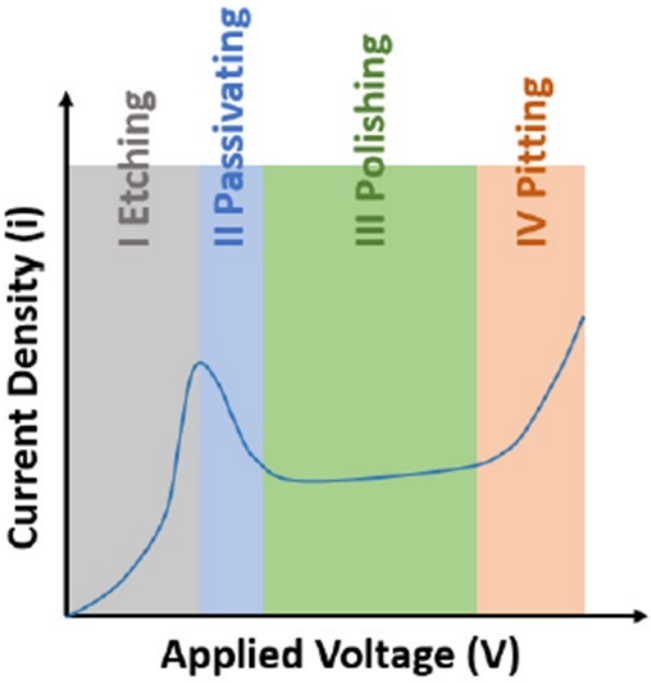

Figure 2. 4Characteristic I-V curve of the electropolishing process according to Han et al [86]

1.Active Dissolution Region: In the initial stage of electropolishing, metal removal occurs unevenly, with dissolution progressing preferentially at grain boundaries and high-energy surface features. This results in non-uniform etching, where different crystal planes dissolve at varying rates due to differences in their electrochemical potentials [88]. Research highlight that the metal's microstructure plays a significant role in governing the dissolution behavior, as the anisotropic dissolution of grains leads to the formation of faceted surfaces and crystallographic patterns. At this stage, the dissolution process is highly dependent on the applied potential and electrolyte composition, with the current density increasing proportionally to the voltage [89-92]

2.Passivation Region: As the applied voltage increases, the current density exhibits a slight decrease, indicating the formation of a thin, protective oxide film on the metal surface. This passive layer acts as a diffusion barrier, restricting further dissolution and slowing down the removal process. The stabilization of this oxide layer is influenced by factors such as electrolyte composition, temperature, and agitation. In aluminum alloys, the formation of an amorphous alumina (Al2o3) film during this stage can temporarily hinder polishing efficiency, requiring optimized process conditions to ensure continuous material removal [84], [88].

3.Polishing Region: In this mass-transport-controlled phase, the dissolution rate is governed by the diffusion of metal ions through the electrolyte rather than by the applied voltage alone. A limiting current plateau is observed, where further increases in potential do not significantly enhance the dissolution rate. During this stage, surface peaks experience preferential dissolution due to their higher exposure to the electrolyte, whereas valleys remain relatively unaffected. This preferential smoothing effect aligns with Jacquet's viscous layer model, which describes how the controlled transport of dissolved species within a thin electrolyte film contributes to the gradual leveling of surface roughness, as validated by experimental studies [89].

4.Trans-passive Region: At excessively high voltages, the stable passive oxide layer begins to deteriorate, leading to uncontrolled anodic dissolution. This is accompanied by intensified gas evolution, localized overheating, and the onset of surface pitting. In aluminum alloys, this phenomenon is particularly problematic, as the breakdown of the passive film can result in uneven material removal and increased roughness instead of the desired smoothing effect [85], [90]. Understanding the delicate balance between passive layer stability and dissolution kinetics is important to optimize electropolishing parameters and prevent defects [97], [89].

Electropolishing achieves surface smoothing through two key mechanisms: anodic leveling and anodic brightening. These processes operate at different scales and are influenced by factors such as current distribution, mass transport conditions, and electrolyte composition [93], [96-98].

Anodic leveling primarily smooths the surface by selectively dissolving peaks more rapidly than valleys. This effect is driven by variations in current distribution and mass transport conditions. When an electrical current is applied, metal dissolution products accumulate, forming a viscous boundary layer at the surface. This layer has higher viscosity and electrical resistivity than the surrounding electrolyte, which locally reduces both the current density and metal dissolution rate [85]. However, the thickness of this boundary layer is not uniform across the surface. Protrusions experience higher diffusion rates and increased dissolution, whereas valleys see a slower metal removal process. Over time, this results in a gradual reduction of surface height variations, significantly improving smoothness at the micrometer scale, as demonstrated by Landolt et al. [88].

Anodic brightening operates at a finer scale, minimizing the impact of microstructural features such as crystallographic orientation and surface defects. Unlike the active potential region, where

metal dissolution is anisotropic and influenced by the metal's structure, anodic brightening involves the random removal of metal cations. This ensures dissolution proceeds without structural bias, leading to a highly uniform and reflective surface [84], [88].

2.3.2 Effect and Optimization of Processing Conditions

The effectiveness of electropolishing depends on the balance of key process parameters, including current density, voltage, temperature, electrolyte composition, and polishing time. Each of these factors plays a crucial role in determining material removal rates, surface smoothness, and defect reduction. Studies highlight that precise process control is essential for achieving consistent and predictable polishing results:

Current density directly determines the rate of metal dissolution and the formation of the passive oxide layer during electropolishing [52]. Maintaining an optimal current density ensures uniform removal of the inherent roughness caused by additive manufacturing, particularly in AlSi10Mg alloys. Studies by Tyagi et al. [94] highlight that in CP1 aluminum, current density also plays a critical role in controlling oxide layer stability and minimizing irregular dissolution patterns [95].

When the current density is within the optimal range, electropolishing achieves its highest efficiency, balancing dissolution and oxide formation. However, exceeding this range can lead to surface instability, with defects such as pitting and gas bubble entrapment. Increased current densities can also accelerate oxide film growth, which, if unstable, results in non-uniform surface roughness instead of a polished finish [96]. On the other hand, operating at lower current densities may cause incomplete material removal, leaving a matte, dull surface [97]. Research by Mark and colleagues [98] underscores the importance of fine-tuning current density to prevent excessive material loss while maximizing smoothness.

Polishing Voltage plays a crucial role in electropolishing, determining the transition between process stages and directly influencing surface quality. At lower voltages, the reaction remains in the active dissolution phase, causing uneven material removal and surface etching rather than smooth polishing. Increasing the applied voltage into the optimal polishing range improves metal ion transport control, leading to gradual surface leveling and a significant reduction in roughness. However, exceeding this ideal range drives the process into the trans passive regime, where

excessive gas evolution and oxide film instability result in pitting and irregular material removal.[103-105].

Voltage optimization is essential for achieving a uniform, defect-free finish while preventing over-polishing, which can degrade surface quality and affect dimensional accuracy. Research by Erving et al. [101] highlights how improper voltage settings contribute to surface deterioration, emphasizing the need for precise control. By maintaining the right balance, electropolishing can effectively enhance surface smoothness and reflectivity without introducing defects [52], [101].

Bath Temperature plays a critical role in the dissolution behavior of aluminum and its alloys in electrolytes. It affects not only the electrolyte's viscosity and ion mobility but also the polishing current density, dissolution rates, and final surface quality. Research by Hryniewicz et al. [102]. as demonstrated that temperature variations can shift the dominant electropolishing mechanism—whether it is surface-controlled (limited by electrochemical reactions at the metal surface) or mass-transport-controlled (limited by the diffusion of ions through the electrolyte) [103].

Low Temperatures (≤ 25°C): the electropolishing process is surface-controlled, meaning that material removal is slow and often leads to localized pitting rather than uniform smoothing [104]. This is primarily due to: 1. High electrolyte viscosity, which restricts ion mobility and slows dissolution. 2. Increased oxide layer formation, as the lower temperature reduces the dissolution rate of the naturally forming oxide while still allowing oxygen-containing species to contribute to oxide growth. This results in a thicker passive film, leading to higher electrical resistance and a reduced polishing effect [105].

Intermediate Temperatures (~65°C): As the temperature increases to around 65°C, the electropolishing process shifts to a mass-transport-controlled regime, where ion movement becomes the dominant factor in material removal [106]. This leads to 1. Lower electrolyte viscosity, allowing faster diffusion of metal ions away from the surface. 2.Higher solubility of dissolution byproducts, preventing residue buildup and enhancing surface brightness [107]. Studies by Mark et al. [105]. observed that at this temperature range, grain boundary features become more pronounced, when examined under scanning electron microscopy (SEM). This indicates that electropolishing at intermediate temperatures can lead to selective material removal based on crystallographic orientation — with some grains or boundaries dissolving more readily than others. As a result, features like grain boundaries, twin lines, and phase differences become

more visible on the polished surface. This phenomenon, often referred to as enhanced microstructural contrast. High Temperatures (≥ 90°C): At elevated temperatures, the activation energy for aluminum dissolution decreases significantly, leading to faster material removal and a highly reflective surface [94]. Additional benefits observed at this temperature range include shorter electropolishing times, as the elevated temperature accelerates the anodic dissolution reaction [108]. The increased temperature also contributes to higher current densities, which in turn improve polishing efficiency and result in smoother surface finishes [99].

However, excessively high temperatures introduce major risks: The viscosity of the diffusion layer is reduced, making it difficult to maintain the viscous layer essential for controlled polishing [99], [109]. Also Uncontrolled etching can occur, leading to dimensional inaccuracies and surface degradation instead of polishing [94].

Polishing Duration of the electropolishing process plays a crucial role in determining surface roughness and brightness, following a nonlinear progression. Initially, surface roughness decreases rapidly, but beyond a certain threshold, further improvements become negligible. Studies by Han et al. [110] and others have shown that prolonging the electropolishing duration beyond the optimal point does not significantly enhance surface finish and may lead to severe material loss. At the beginning of the process, roughness reduction is rapid, as peaks and irregularities dissolve efficiently. However, once a limiting value is reached, further polishing does not yield substantial improvements [52]. Similar findings were reported by Haïdopoulos et al. [111], who observed this trend in 316L stainless steel, where extending the polishing time beyond a critical point had minimal effect on roughness improvement.

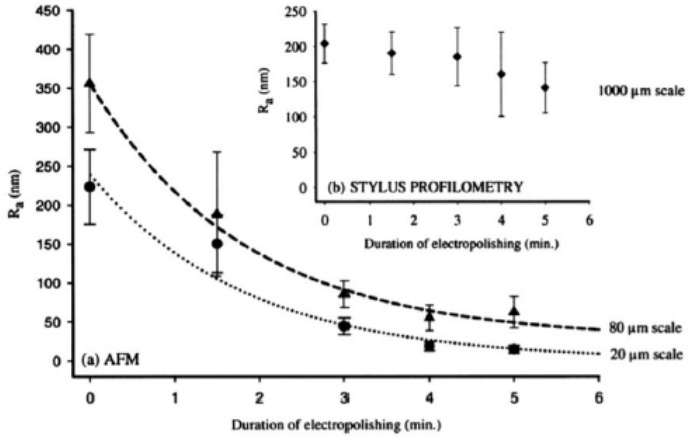

Figure 2. 5Variation of the mean surface roughness Ra of 316 stainless-steel surfaces with the duration of electropolishing process as (a) measured by AFM, and (b) measured by stylus profilometry [118].

While an initial increase in brightness is observed, excessively long polishing durations can lead to surface degradation. When electropolishing is prolonged beyond the optimal duration, the electric field can cause uneven dissolution across the surface. This leads to the development of irregular patterns and surface distortion, as material is no longer removed uniformly. In addition, excessive polishing may compromise surface integrity, resulting in a noticeable loss of brightness due to the breakdown of a uniformly smooth finish [112].

Electrolyte composition is another factor which has a role in controlling dissolution efficiency and surface smoothness during electropolishing. The most used electrolyte for aluminum electropolishing is a sulfuric-phosphoric acid mixture (H_2SO_4-H_3PO_4). According to Liu et al. [113], this combination helps balance passivation and dissolution, ensuring a controlled material removal rate [16]. Higher sulfuric acid concentrations speed up dissolution but can also cause over-etching and surface defects if not carefully controlled. While higher phosphoric acid content slows dissolution, leading to a more controlled and uniform surface finish [113], [16]. Electropolishing of 3D-printed AlSi10Mg using this sulfuric-phosphoric acid mixture has demonstrated effective surface roughness reduction, although its performance is significantly influenced by the material's microstructure. In one study, the alloy underwent electrochemical polishing (ECP) in a bath composed of phosphoric acid (H_3PO_4) and sulfuric acid (H_2SO_4) in a 2:1 volumetric ratio, maintained at 70 °C for 20 minutes and operated at 5 V. The process notably reduced the surface roughness (Sa) of LPBF AlSi10Mg from 14.91 µm to 4.70 µm. However, the polishing was hindered by the formation of a solid viscous layer rich in silicon compounds, which originated

from the anodic dissolution of aluminum and subsequent reactions involving silicon and hydroxide ions. This layer impeded ion diffusion and limited the effectiveness of polishing. To address this, an enhanced method combining electrochemical polishing with mechanical brushing (ECMP) was employed, further reducing the roughness to 2.19 µm. Interestingly, this solid film, while initially obstructive, also protected the surface from scratches during ECMP, unlike in stainless steel cases where mechanical brushing damaged the polishing layer. This highlights the material-specific behavior of the H_3PO_4–H_2SO_4 system, showing its suitability for Al-based alloys if coupled with strategies to control or manage the viscous layer's thickness and stability [119-120].

Eco-friendly alternatives, such as ethylene glycol-based electrolytes, particularly those combined with chloride salts such as NaCl, are gaining attention for providing stable dissolution rates while reducing defect formation and hazardous waste [116]. These formulations benefit from the high viscosity of ethylene glycol, which enables controlled anodic dissolution and minimizes surface pitting. The presence of chloride ions is essential for effective metal dissolution, as they help break down passive oxide layers and form soluble complexes with metal ions, supporting uniform and efficient material removal. Some studies, such as the work by Defanti et al. [117], have investigated aqueous NaCl solutions and demonstrated a significant reduction in surface roughness—from 6.15 µm to 1.57 µm. Although the electrolyte composition differs, the underlying polishing mechanism involving chloride ions is comparable to that in ethylene glycol–NaCl systems. Unlike aqueous solutions, however, ethylene glycol–based electrolytes offer broader temperature stability and lower toxicity, making them more suitable for environmentally conscious applications. In comparable systems using ethylene glycol and chloride salts, surface roughness values have been shown to decrease from approximately 0.55 µm to as low as 0.16 µm, while maintaining a uniform, pit-free morphology [118], [119].These results confirm the suitability of such mixtures for polishing complex 3D-printed aluminum parts with enhanced precision and environmental safety.

Research by Ferchow et al. [120] highlights the importance of electrolyte optimization, especially for complex geometries in additively manufactured aluminum components, where achieving a consistent finish can be more challenging . Choosing the right electrolyte composition is essential for balancing efficiency, minimizing defects, and ensuring high-quality electropolished surfaces.

Beyond all these factors, other parameters like bath agitation, interelectrode distance, and polishing current signals also influence the final surface quality of electropolished samples [52]. Due to the complex interactions between these parameters, extensive research has been conducted to identify the most effective optimization methods for electropolishing. One approach involves comparing different process parameter levels to determine the best conditions for achieving a smooth and defect-free surface [111], [121]. Additionally, statistical optimization methods have been widely used to systematically refine electropolishing settings. These techniques help identify key parameters and their optimal values to improve surface finish, material removal rates, and overall process efficiency [122]. For instance, the Taguchi method has been applied in several studies to determine the ideal combination of process parameters for achieving high surface quality [128-129]. Grey relational analysis, as demonstrated by Kao et al. [125], has also been used to optimize temperature, current density, and electrolyte composition, leading to improved surface roughness and passivation strength in 316L stainless steel. Response Surface Methodology (RSM) has also been employed in multiple studies to fine-tune electropolishing parameters for optimal results [131-132]. By leveraging these optimization techniques, researchers have been able to refine the electropolishing process, ensuring greater consistency, efficiency, and superior surface quality [122].

2.4 Electropolishing of 3D-Printed Aluminum Alloys

2.4.1 Surface Roughness of AlSi10Mg and CP1 As Printed

The staircase effects, balling effects, partially fused feedstock powder, spatters, and inadequate fusion are the primary contributors to the high surface roughness of LPBF Aluminium Alloys [128] These surface irregularities arise during the LPBF process due to the inherent layer-by-layer manufacturing method and the thermal gradients caused by insufficient wetting [102].

Both AlSi10Mg and CP1 alloys are affected by several factors during LPBF processing, including layer-by-layer melting behavior, laser power, and powder characteristics [129].

AlSi10Mg typically shows partially melted powder particles adhered to the surface, which contributes to its higher surface roughness. Its initial roughness often ranges between 8–15 μm,

mainly due to the formation of silicon-rich eutectic phases and thermal stresses that cause surface irregularities [130].

In contrast, CP1 generally exhibits a more uniform as-printed surface. This is attributed to the presence of zirconium (Zr) and iron (Fe), which promote the formation of Al_3Zr dispersoids. These dispersoids help stabilize the melt pool during solidification, reducing defects such as porosity and uneven cooling [131].

As a result, CP1 shows lower initial surface roughness, averaging around 5–10 μm, due to its fine-grained microstructure and the grain-refining effect of zirconium [132].

Due to its higher initial roughness, AlSi10Mg usually requires longer electropolishing times and more aggressive electrolyte conditions to achieve a surface finish comparable to CP1.

Additionally, the selective dissolution of aluminum in AlSi10Mg results in the formation of Si-rich regions that resist dissolution, necessitating advanced strategies like intermittent electropolishing (IECP) to ensure uniform material removal [133]. In contrast, CP1's lower roughness and more uniform microstructure allow it to respond more efficiently to electropolishing, achieving a smoother final surface with lower material removal rates (MRR) [134].

2.4.2 Mechanisms and Challenges of Electropolishing AlSi10Mg and CP1

The inherently high roughness of as-built laser powder bed fusion (LPBF) Aluminum parts is a significant limitation for their broader industrial applications, necessitating post-processing to achieve functional surface properties. Among various surface finishing techniques, electropolishing (ECP) has emerged as a highly effective method due to its ability to smooth both external and internal surfaces with minimal material loss. Studies by Zheng et al. [135] and Tyagi et al. [94] have demonstrated that electropolishing significantly enhances the surface quality of additively manufactured aluminum components, effectively reducing roughness while preserving mechanical integrity [136].

- AlSi10Mg

Electropolishing of LPBF AlSi10Mg follows a multi-stage mechanism, where anodic dissolution, surface defect removal, and viscous layer formation collectively determine the final surface quality. The process relies on anodic dissolution, where the electric field preferentially removes surface asperities due to localized variations in current density. Higher peaks experience greater dissolution rates compared to valleys, leading to a smoother surface finish [137]. During electropolishing, a thin, viscous boundary layer forms on the metal surface as a result of anodic reactions that generate oxygen gas and metal ions. These reaction by-products accumulate near the surface, increasing the local viscosity. This layer acts as a diffusion barrier, allowing peaks to dissolve more rapidly than valleys and promoting a smoother overall finish [138].

While anodic dissolution effectively smooths the surface by selectively removing asperities, the presence of silicon in AlSi10Mg introduces additional challenges that influence the uniformity of material removal. One of the primary challenges in electropolishing AlSi10Mg is its high silicon content, which creates an electric potential gap between aluminum and silicon, resulting in varied material removal rates (MRR) and an uneven surface finish. In alloys with heterogeneous microstructures, different phases exhibit varying dissolution rates during electropolishing. This material selectivity can impact surface uniformity, particularly in alloys with complex phase distributions. For AlSi10Mg, the high silicon content results in different rates of dissolution between the primary aluminum matrix and secondary phases, influencing the overall roughness reduction effectiveness [137], [139].

Researchers emphasize that initially, aluminum dissolves into Al $(OH)_4$ ions, while silicon undergoes oxidation to form SiO^{2-}_3 in the NaOH-based electrolyte. These reactions contribute to a sticky aluminosilicate layer, which, if not properly managed, inhibits further dissolution and compromises the final surface finish [140]. To address these dissolution inconsistencies caused by silicon-rich phases, researchers have explored alternative electropolishing strategies, with intermittent electropolishing (IECP) emerging as a promising solution. In continuous electropolishing (CECP), this aluminosilicate layer thickens over time, reducing anodic dissolution efficiency. The accumulation of insoluble Si-rich phases further hinders material removal, leading to non-uniform surface quality. However, studies highlight that intermittent electropolishing (IECP) prevents excessive product accumulation by periodically disrupting this layer, ensuring a

uniform electrochemical reaction. With an optimized removal interval of 50 seconds, the dissolution rate remains high, and Si-rich layers detach continuously, allowing for enhanced material removal [140].

Lynch et al. [141] have reported surface roughness (Sa) reductions of up to 87.7% using optimized intermittent electropolishing (IECP) techniques, underscoring its capability to refine AM components for high-performance applications. Hryniewicz et al. [135] highlight that intermittent removal of the viscous polishing layer ensures consistent material dissolution, preventing roughness deterioration over time.

- CP1

The electropolishing behavior of CP1 (Al–Fe–Zr) alloys is also governed by a complex interplay of microstructural constituents that significantly influence both the anodic dissolution mechanism and the final surface finish. Notably, coarse and brittle Al_3Fe intermetallic in the as-cast state pose a challenge to achieving uniform material removal, often leading to uneven etching or surface pitting [142]. Simultaneously, Al_3Zr particles—either as nano-precipitates or nucleation sites—introduce electrochemical heterogeneity, which can act as localized barriers or promote galvanic disparities across the surface. When electropolished using a phosphoric–sulfuric acid-based electrolyte, CP1 demonstrated the typical anodic dissolution behavior observed in aluminum alloys. However, the alloy's intrinsic microstructure influenced the current distribution, which limited the electropolishing efficiency. As a result, surface roughness only modestly improved (e.g., Sa reduced from 9.3 μm to 6.8 μm), and the overall polishing efficiency was lower compared to alloys like AlSi10Mg [143] .This performance gap highlights several challenges: While CP1 begins with a smoother as-printed surface than AlSi10Mg, its electropolishing response is less efficient due to its microstructural characteristics. As a result, achieving further roughness reduction often requires longer durations and higher voltages, and some residual roughness may still remain after treatment. Additionally, large Al_3Fe particles serve as stress concentrators and tend to etch preferentially, which may compromise surface integrity. The relatively noble Al_3Zr phases can create under polished regions or nodular textures, further reducing uniformity [147-148]. To mitigate these issues, microstructure refinement methods—such as ultrasonic melt processing—have been suggested to reduce phase size and distribution irregularities [142].

Given CP1's novelty as an alloy system and its potential for high-performance applications, particularly in RF components, further investigation is necessary to optimize electropolishing protocols. Currently, data on CP1 remains limited, underscoring the need for deeper studies into its electrochemical behavior and process compatibility.

2.5 Trans passive Breakdown in Electropolishing

2.5.1 Fundamentals of Trans passive Breakdown

At sufficiently high anodic potentials, passive metals and alloys transition out of their protective state and enter a regime known as trans passive breakdown. In this region, the stability of the oxide film is lost, and the metal begins to dissolve aggressively while gas evolution becomes significant. This phenomenon is observed across a wide range of systems, including stainless steels, titanium, nickel-based alloys, and aluminum [141].

The breakdown of passivity involves two concurrent anodic processes:

Direct metal dissolution, where the exposed metal ionizes and enters the electrolyte

$M \rightarrow Mn+ + ne-$

Oxygen evolution reaction (OER), arising from water oxidation at the anode surface:

$2H_2O \rightarrow O_2 + 4H^+ + 4e-$

These reactions destabilize the oxide layer, creating localized sites where dissolution accelerates. Instead of a smooth rise in current, the system exhibits sharp oscillations caused by repeated cycles of film rupture and repair. The rapid generation of oxygen bubbles further disrupts the interface, lowers the local resistance, and enhances electrolyte agitation, amplifying the instability removal [144], [145].

During electropolishing, this trans passive regime manifests strongly once the applied voltage exceeds a critical threshold. At this point, several interrelated effects are observed:

1.Intensified Anodic Dissolution

The collapse of the passive oxide layer allows aggressive, unstable dissolution, which greatly enhances material removal and surface leveling.

2. Gas Evolution at Electrodes

At the anode, oxygen generation dominates, producing dense bubbles that locally stir the electrolyte.

At the cathode, hydrogen evolution occurs simultaneously: $2H^+ + 2e^- \rightarrow H_2$

The combined gas release increases interfacial turbulence and mass transport. [146].

3. Localized Heating and Enhanced Ion Transport

The high current density characteristic of the transpassive region generates resistive (Joule) heating [147]:

$Q=I^2 Rt$

This local temperature rise reduces electrolyte viscosity, improves ionic mobility, and accelerates dissolution kinetics [141].

4.Visible Instability at the Anode

Under certain conditions, vigorous gas evolution and localized heating may produce luminescence and discharge-like effects at the electrode surface. These are not separate phenomena but rather a visible consequence of trans passive breakdown under extreme polarization [136], [148],

2.5.2 Trans passive Breakdown in Aluminum Alloys

Aluminum and its alloys are particularly susceptible to trans passive effects because of their strong yet relatively thin alumina passive film. During conventional electropolishing or anodizing, this film ensures uniform dissolution. However, at elevated temperatures and voltages, the alumina barrier can rupture or dissolve, exposing bare aluminum to aggressive oxidation.[140].

In electropolishing, some risks apply: pushing beyond the safe voltage range causes uncontrolled heating, electrolyte boiling, and irregular surface modification. Instead of achieving a mirror-smooth finish, the surface becomes pitted, etched, or partially melted [149-151].

2.5.3 Practical Implications for Electropolishing of AlSi10Mg and CP1

For alloys such as AlSi10Mg and CP1, operating conditions that cross into the trans passive regime result in sharp changes in surface morphology. While moderate anodic dissolution under controlled conditions can smooth asperities, excessive voltage or prolonged treatment can induce current oscillations, thermal runaway, and vapor envelope formation. This compromises the structural integrity of the surface, producing irregular topography instead of reduced roughness [148].

Therefore, in both alloy systems, trans passive breakdown marks the upper boundary of viable electropolishing parameters. Avoiding this regime is essential to maintain stable oxide dissolution and achieve the desired reduction in surface roughness. If not carefully controlled, the process shifts from an electrochemical polishing mechanism to a thermally driven, discharge-dominated regime, detrimental for applications requiring precise and smooth surfaces [150-151].

2.6 Weight Loss Analysis in Electropolishing

Weight loss analysis is a crucial parameter for evaluating the material removal efficiency and process optimization in electropolishing. It provides insights into the rate of dissolution, uniformity of polishing, and potential material degradation. The weight loss observed during electropolishing is primarily governed by Faraday's laws of electrolysis, which establish a direct relationship between the mass of metal removed and the charge passed through the electrolyte. Studies on electropolishing of AlSi10Mg and CP1 (Al-Fe-Zr) alloys indicate that material removal is influenced by key parameters such as current density, electrolyte composition, and process duration [136], [148].

During the initial phase of electropolishing, a rapid decrease in sample weight occurs due to the preferential dissolution of surface asperities. As the process progresses, the dissolution rate stabilizes, resulting in a more uniform material removal profile. Zheng et al. [152] reported a linear relationship between weight loss and electropolishing time under optimized conditions; however, excessive polishing durations led to surface degradation and increased roughness due to non-uniform material removal [140].

The weight loss rate can be calculated using the following equation:

$$WL = (Wi - Wf) / (A \times t)$$

Where (WL) is the weight loss rate (mg/cm²/min), (Wi) and (Wf) are the initial and final sample weights, (A) is the exposed surface area (cm²), and (t) is the electropolishing time (min) [153].

2.6.1Weight Loss During Electropolishing of AlSi10Mg and CP1 (Al-Fe-Zr)

The extent of weight loss during electropolishing is influenced by multiple factors, including alloy composition, microstructure, and the stability of the passive film. The weight loss primarily results from metal dissolution at the anode, governed by several interrelated mechanisms:

Anodic Dissolution: Electropolishing operates at a critical anodic potential where metal dissolution occurs preferentially in a diffusion-controlled manner. The metal ions dissolve into the electrolyte, leading to material removal and consequent weight loss. The dissolution rate varies depending on the alloying elements present, as different phases within the microstructure may have distinct electrochemical behaviors [154].

Selective Phase Removal: Different alloying elements dissolve at varying rates, affecting both weight loss and polishing uniformity [155]. In alloys such as AlSi10Mg and CP1, heterogeneous microstructures lead to preferential dissolution of certain phases. For instance, in AlSi10Mg, the silicon-rich phases are more resistant to anodic dissolution than the aluminum matrix, which may lead to uneven weight loss and potential surface morphology changes.

2.6.2 Comparison of Electropolishing Behavior Between AlSi10Mg and CP1 (Al-Fe-Zr) Alloys

Electropolishing Rate

AlSi10Mg exhibits a higher electropolishing rate due to the presence of silicon (Si) and magnesium (Mg), both of which influence the anodic dissolution process. Specifically, Mg promotes localized breakdown of the passive film and contributes to faster anodic reactions, while Si, being largely insoluble, causes micro-galvanic coupling with the aluminum matrix, accelerating dissolution of the surrounding aluminum. This results in a higher overall rate of material removal [156]. In contrast, CP1 (Al-Fe-Zr) shows a lower electropolishing rate because zirconium (Zr) strongly stabilizes the aluminum matrix by forming finely dispersed Al_3Zr particles. These dispersoids act as physical barriers to dissolution and slow down the surface reaction kinetics [157].

Phase Selectivity in Dissolution

In AlSi10Mg, the electropolishing process exhibits significant phase selectivity. Silicon-rich phases, such as eutectic Si and primary Si particles, have inherently low electrochemical solubility and resist anodic dissolution. This causes preferential etching of the surrounding Al matrix, leading to localized roughness. On the other hand, Mg_2Si precipitates dissolve more easily, increasing the overall weight loss due to the selective removal of these Mg-rich zones [158].In CP1, the presence of Al_3Zr dispersoids, which are thermodynamically stable and electrochemically inert, slows the dissolution rate by resisting anodic attack. Additionally, iron-containing intermetallic (e.g., Al-Fe or Al-Fe-Zr phases) are less reactive under acidic electropolishing conditions, which reduces uniform material removal. These phases may block active dissolution sites, resulting in decreased surface activity and more stable surfaces during polishing [159].

Weight Loss Rate

As a consequence of the above mechanisms, AlSi10Mg typically exhibits a higher weight loss per unit area, especially after heat treatment. This is because heat treatment increases the size and distribution of Mg_2Si precipitates, making them more susceptible to dissolution and accelerating weight loss [160].On the other hand, CP1 shows a lower weight loss rate due to the stability of its Al_3Zr and Al-Fe intermetallic phases, which resist anodic dissolution and reduce the overall electrochemical reactivity of the surface [159].

Surface Morphology Post-Electropolishing

After electropolishing, AlSi10Mg often displays pitting or uneven surfaces, caused by the non-uniform dissolution between the soft Al matrix and the hard, undissolved Si particles. Without carefully optimized parameters, such as current density and temperature, this inhomogeneous dissolution leads to poor surface quality [160]. CP1, by contrast, benefits from a more uniform microstructure, with well-dispersed, stable intermetallic phases. This contributes to smoother surface morphology and lower material removal, which is ideal for precision applications [161].

Effect of Passive Film Formation

In AlSi10Mg, the presence of Si affects the stability of the passive oxide layer. Specifically, Si can disrupt the continuity of the native aluminum oxide film, reduce its protective capability and

promote localized breakdown. This leads to non-uniform surface dissolution and inconsistent finish quality during electropolishing [155]. In contrast, the Zr in CP1 enhances the passive layer stability by promoting the formation of a more adherent and corrosion-resistant mixed oxide, which helps control the dissolution rate and reduces the risk of excessive or uneven material removal [157].

In summary, AlSi10Mg demonstrates higher weight loss during electropolishing due to the selective dissolution of its aluminum matrix. This behavior is primarily driven by the presence of magnesium and silicon phases. Magnesium-rich precipitates like Mg_2Si dissolve easily, promoting rapid material removal, while the low solubility of silicon-rich particles causes them to remain intact. As a result, Si-rich regions are left behind, leading to surface irregularities that require more aggressive electropolishing conditions to achieve a smooth and uniform finish [158].

In contrast, CP1 exhibits lower weight loss rates due to the stabilizing effects of Zr and Fe phases. The Al_3Zr dispersoids in particular are highly resistant to dissolution, which slows the electropolishing process and promotes more controlled anodic behavior. This results in a smoother post-polishing surface with minimal material removal, making CP1 better suited for applications requiring tight dimensional control [159].

Application-specific demands further differentiate the two alloys. For example, CP1 is ideal for precision components where minimal dimensional change is critical, thanks to its stability and low dissolution rate [162]. Meanwhile, AlSi10Mg, though more aggressive in its dissolution behavior, remains attractive for applications like RF components where substantial roughness reduction is needed. However, it requires careful parameter tuning to avoid pitting and over-polishing [158].

Electropolishing parameters, especially current density and duration, play a critical role in both alloys. Studies have shown that higher current densities increase weight loss due to more aggressive anodic reactions, but this can also lead to dimensional inaccuracies if not precisely controlled [163]. In this context, intermittent electropolishing (IECP) has been demonstrated by Lynch et al. [164] to result in more uniform surfaces and better-controlled material removal compared to continuous electropolishing (CECP) [140].

Finally, while weight loss is generally correlated with surface roughness reduction, this relationship only holds up to a certain threshold. Beyond that, additional material removal does

not significantly improve smoothness and may instead compromise dimensional accuracy. Thus, optimized electropolishing conditions must strike a balance between effective smoothing and structural preservation, minimizing waste while maximizing surface quality.

2.8 Comparison of Electropolishing with Other Surface Finishing Techniques

As reviewed in Section 1.5, several post-processing methods—mechanical, thermal, chemical, and electrochemical—are used to improve surface quality in LPBF aluminum alloys. Each method presents distinct advantages and limitations depending on part geometry, material characteristics, and application requirements. However, when it comes to achieving a smooth, uniform surface in complex 3D-printed aluminum components, electropolishing consistently emerges as the most effective option.

Mechanical methods such as grinding and barrel finishing, although cost-effective for simple geometries, often struggle with intricate designs. These techniques rely on direct contact, which not only makes it difficult to access internal features but can also introduce residual stress and surface deformation. While suitable for bulk finishing, they lack the precision and uniformity needed for high-performance applications [165-167].

Thermal techniques, particularly laser polishing, offer localized refinement by remelting surface layers. While this can reduce roughness, the process requires strict control of energy input to avoid overheating, warping, or unintended microstructural changes. Additionally, laser-based methods are mostly limited to external surfaces and are less adaptable to internal features or recessed geometries [168].

Chemical polishing offers a contactless alternative, but it lacks the process control needed for precision applications. Non-uniform dissolution can occur due to variations in local surface energy and reaction kinetics, often resulting in inconsistent finishes [164], [169].

In contrast, electropolishing combines the advantages of uniform material removal, geometry preservation, and high scalability. It does not rely on physical contact, making it particularly well-suited for complex or delicate structures. Studies have demonstrated its superior ability to reduce surface roughness in LPBF AlSi10Mg while maintaining dimensional accuracy and structural integrity [170].

Moreover, electropolishing provides better control over the dissolution process compared to chemical polishing, and unlike thermal or mechanical methods, it avoids introducing new defects. Its compatibility with batch processing also supports industrial scalability. As such, for applications demanding high surface quality, such as aerospace, RF components, or biomedical implants, electropolishing stands out as the optimal solution.

This thesis builds on these insights by experimentally investigating and optimizing electropolishing conditions for both AlSi10Mg and CP1 (Al-Fe-Zr) alloys, aiming to achieve maximum roughness reduction with minimal material loss—balancing precision, efficiency, and applicability across use cases.

2.7 Future Research Directions and Challenges in Electropolishing of AM Aluminum Parts

Despite its advantages, electropolishing faces several challenges that require further research and optimization. The ongoing evolution of additive manufacturing and advanced materials necessitates continued improvements in electropolishing techniques to meet the growing demand for precision surface finishing.

•Electrolyte Optimization: Conventional acidic electrolytes, such as sulfuric-phosphoric acid mixtures, pose environmental and safety concerns. There is an increasing interest in developing alternative electrolyte systems that offer comparable polishing efficiency while reducing hazardous waste generation. Recent studies have explored non-acidic alternatives, such as ethylene glycol-NaCl electrolytes, which provide controlled material removal while mitigating environmental impact [171].

•Achieving Uniform Surface Treatment for Complex Geometries: One of the primary limitations of electropolishing is the difficulty in achieving uniform dissolution across intricate surfaces. Researchers such as Lynch et al. [172] emphasize that variations in local current density, phase composition, and electrolyte flow dynamics can lead to differential polishing rates, requiring advanced cathode positioning and agitation techniques for optimization.

•High Initial Roughness in Additively Manufactured Parts: Additively manufactured aluminum components often exhibit high initial roughness due to the presence of partially melted powders and staircase artifacts. Extended electropolishing durations are required to achieve significant roughness reduction, which may lead to increased material loss and dimensional inaccuracies.

Studies by Erving et al. [27] suggest that integrating electropolishing with pre-treatment methods such as vibratory finishing or laser polishing may offer a synergistic approach to reducing processing time while maintaining surface integrity.

•Hybrid Electropolishing Techniques: The combination of electropolishing with other techniques, such as ultrasonic-assisted electropolishing or plasma-assisted polishing, has shown promise in improving efficiency and surface quality. Research by Zhang et al. [173] highlights that ultrasonic cavitation can enhance ion transport and prevent gas bubble adhesion, while plasma-assisted oxidation refines surface topography and reduces defects. Additionally, pulsed current electropolishing has been explored as a method to control the dissolution rate and improve surface uniformity [174].

3.Methodology

3.1 Introduction

The goal of this study is to investigate the effect of electropolishing parameters on the surface roughness and morphology of 3D-printed aluminum-based alloys. The first step is to analyze the electropolishing process by systematically varying key parameters to determine their impact on surface roughness and morphology. Ultimately, this study aims to establish optimized electropolishing conditions for improving the surface quality of AlSi10Mg and CP-1, two alloys widely used in additive manufacturing due to their distinct microstructural characteristics and industrial relevance.

To systematically analyze the influence of electropolishing conditions on these materials, a five-phase experimental approach was implemented. Each phase aimed to optimize key process variables, ensuring precise control over surface finish. The phases are described as follows:

1. Electrolyte Selection

The efficiency of the electropolishing process is largely influenced by the electrolyte composition, as it dictates the rate and uniformity of material dissolution. Over the years, various electrolytes have been investigated for electropolishing different metals. However, given the extensive time required to examine all possible metal-electrolyte combinations, this study focused on two commonly used electrolytes for electropolishing aluminum alloy components:

Electrolyte 1: Ethylene Glycol (90%) v/v+ NaCl (10%) v/v

Electrolyte 2: Phosphoric Acid (50%) v/v + Sulfuric Acid (35%) + DI Water (15%) v/v

The stock concentrations of sulfuric acid, phosphoric acid, ethylene glycol, and sodium chloride solutions were 96.8%, 85%, 99%, and 10%, respectively.

These formulations were selected based on their established effectiveness in aluminum electropolishing, particularly for their ability to minimize surface defects and enhance material

smoothness. The goal of this selection was to obtain meaningful results that could contribute to future advancements in electropolishing research.

2. Voltage and Time Optimization

The applied voltage and polishing duration significantly influence the electropolishing outcome. Excessive voltage can lead to over-polishing or pitting, whereas insufficient voltage may result in an uneven finish. To determine the optimal voltage-time combination, multiple trials were conducted within a predefined range, ensuring the achievement of a smooth and defect-free surface.

3. Temperature Effects

Temperature plays a critical role in electropolishing efficiency by affecting electrolyte conductivity, anodic dissolution rate, and hydrogen evolution reactions. This phase assessed how variations in bath temperature influence the polishing performance and consistency across different samples.

4. Material-Specific Testing

While initial experiments were performed on AlSi10Mg, the optimized parameters were subsequently applied to CP-1 alloy. This step enabled a comparative analysis, revealing material-specific behaviors in response to electropolishing and ensuring the findings' broader applicability.

5. Final Optimization

Once the optimal electropolishing parameters were identified, the final phase focused on evaluating surface properties. This phase involved analyzing the correlation between electropolishing parameters and surface characteristics, providing insight into the impact of electropolishing on surface roughness and morphology.

By following this structured approach, this study aims to establish a comprehensive understanding of how electropolishing enhances the surface quality of 3D-printed aluminum alloys. The

following sections outline the experimental setup, procedures, and characterization methods employed in this investigation.

3.2 Experimental Setup and Procedure

The experimental setup was meticulously designed to ensure precision, reproducibility, and accurate characterization of the electropolishing process.

3.2.1 Sample Preparation and Cleaning

To ensure consistent and reliable electropolishing outcomes, a systematic cleaning, masking, and pre-treatment protocol was followed for all samples. Each sample was engraved with a unique identifier for systematic tracking.

Figure 3. 1Engraved sample

Aluminum alloy (AlSi10Mg and CP1) bars of size **70 mm × 31 mm × 5 mm** were printed by Burloak Technologies Inc. using Laser–Powder Bed Fusion (L-PBF) method and prepared for the electropolishing experiment following this procedure**:**

Initial Cleaning

A three-step ultrasonic cleaning process was performed using a Branson Model 1510 ultrasonic cleaner to remove surface contaminants:

- Soap Solution Cleaning: Samples were degreased in a soap solution for 15 minutes using ultrasonic vibrations.
- Acetone Bath: Further degreasing was conducted in an acetone bath for 15 minutes to dissolve organic residues.
- Deionized Water Rinse: A final rinse with DI water for 15 minutes was carried out to eliminate any remaining contaminants.
- Drying with airflow.

Figure 3. 2ultrasonic cleaning

Weighing

After drying, the sample is weighed using an AHAUS Pioneer device. The weight is measured again after the test and final cleaning.

Masking

To prevent unwanted exposure during electropolishing, non-targeted areas were insulated using Teflon tape. In the final trials, an epoxy coating was applied instead to enhance protection against acid leakage, ensuring precise weight loss measurement.

Figure 3. 3masking the sample with the Teflon tape.

Pre-Treatment – Cathodic Cleaning

Before electropolishing, a cathodic treatment was performed in an acidic bath to remove residual oxide layers. Stainless steel was used as the anode, while the sample acted as the cathode, subjected to a 5A current for 10 minutes to ensure a clean and uniform surface before electropolishing. Give bath composition

After the polishing tests, the workpieces were thoroughly rinsed with cold water to remove all acid residues. The samples were then air-dried and characterized. (But later you mention other things after performed after polishing: cathodic treatment, ultrasonic cleaning)

3.2.2 Electropolishing

Electropolishing tests were conducted in a three-electrode electrochemical cell using a B&K Precision Model-9117 multi-range programmable DC power supply. The 3D-printed AlSi10Mg or CP-1 bars were used as the working electrodes. A rolled Stainless-steel sheet was placed in the cell as the counter-electrode, positioned to ensure uniform current density distribution across the working electrode. A double-junction Ag/AgCl electrode saturated in 3.8M KCl solution was used as the reference electrode to maintain accurate potential control.

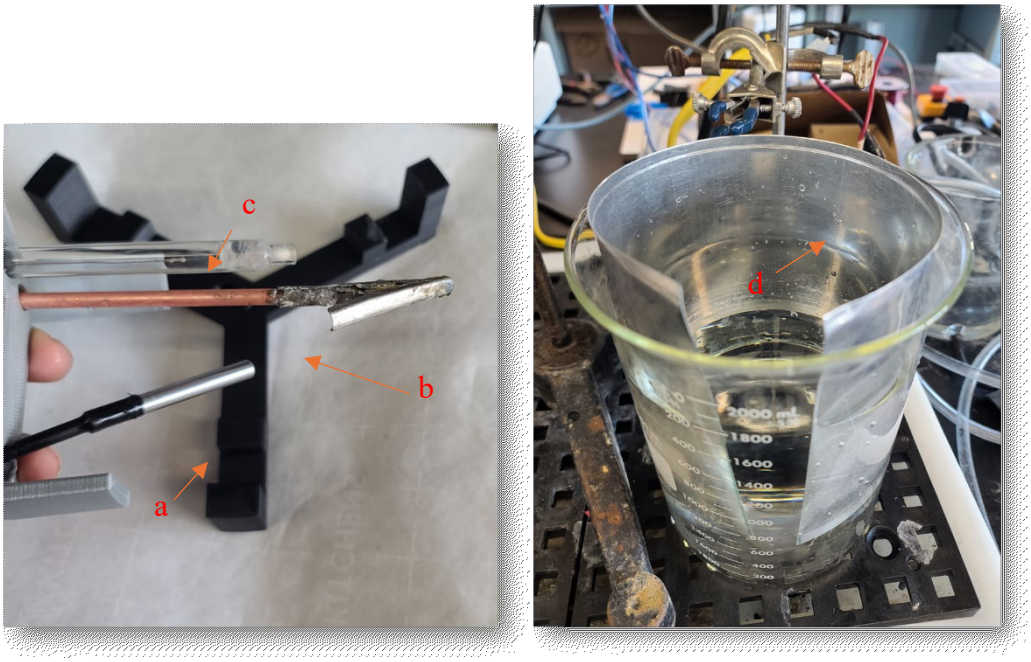

Figure 3. 4a) temperature monitoring sensor, b) anode holder, c) counter electrode d) Rolled cathode.

A custom Acrylonitrile Butadiene Styrene (ABS) electrode holder was designed and fabricated through fused deposition modeling (FDM) using an Ultimaker 2+ printer. The holder was used to position the workpiece at the center of the electrochemical cell, maintaining a 1 cm distance from the tip of the reference electrode to ensure stable and precise electrode placement during electropolishing.

Figure 3. 5costume 3D-printed electrode holder

Electropolishing treatments were performed under varying conditions to determine optimal parameters. The samples were immersed in two different electrolytes (Ethylene Glycol (90%) + NaCl (10%) and Phosphoric Acid (50%) + Sulfuric Acid (35%) + DI Water (15%))

The applied potentials were varied across (15V, 20V, 25V, and 30V), with temperatures controlled at (-5°C, 0°C, 10°C, 25°C, 35°C, 50°C, and 60°C). The duration of electropolishing was set at (300s, 600s, 900s, 1200s, and 1800s) to evaluate the influence of processing time.

Throughout the electropolishing tests, bath temperature fluctuations were continuously recorded using a digital temperature sensor. After electropolishing, samples were rinsed in deionized (DI) water, subjected to cathodic post-cleaning, and underwent a final ultrasonic three-step cleaning to ensure complete removal of residual byproducts.

3.3 Sample characterization

Weight Measurement

Prior to and following each electropolishing trial, the samples were subjected to the cleaning procedure detailed in Section 3.2.1 and subsequently weighed using an OHAUS PIONEER® precision balance.

Surface Roughness Analysis

The surface roughness of the samples was evaluated both before and after each experiment using a Mitutoyo Surftest SJ-210 Series-178, a portable contact-type profilometer. Measurements were conducted at a minimum of 10 randomly selected points across the exposed surface area. The cut-off length was carefully chosen based on the observed roughness to ensure accurate readings.

For each measurement, three roughness parameters—Ra, Rq, and Rz—were recorded. According to the surface roughness tester's user manual [175]:

- Ra (Arithmetic Average Roughness): Represents the arithmetic mean of the absolute deviations of profile heights from the mean line over the measured length.
- Rq (Root Mean Square Roughness): Denotes the square root of the arithmetic mean of the squared profile height deviations within the measurement length.

- Rz (Maximum Height Roughness): Refers to the highest peak-to-valley distance within a single sampling length of the surface profile.

Surface morphology investigations

The surface morphology of the electropolished samples was analyzed using confocal microscopy with an Olympus LEXT 30 laser measuring microscope (OLS4100) and a scanning electron microscope (SEM) (Model). Confocal microscopy is particularly useful for assessing the surface morphology of electropolished samples, as it provides precise 3D surface profiles, enabling the quantification of surface roughness, the detection of defects, and the evaluation of electropolishing effectiveness in improving surface smoothness. SEM imaging was also employed to further examine microstructural features and surface topography at higher magnifications.

4.Results and discussion

4.1 Introduction

Having established the rationale for electropolishing as an effective post-processing method for 3D-printed aluminum components, this chapter presents a comprehensive evaluation of its performance under varying processing conditions. The investigation focuses on two aluminum-based alloys—AlSi10Mg and CP1—both produced via laser powder bed fusion (LPBF). These materials exhibit distinct microstructural features and as-printed surface conditions, which are critical to understanding their respective responses to electropolishing.

To establish a baseline, the as-printed surfaces of both alloys are first characterized, enabling an accurate assessment of electropolishing-induced improvements. A combination of quantitative and qualitative analyses is employed to evaluate polishing performance. Surface roughness measurements are obtained using two complementary instruments: a portable contact profilometer for practical, large-area assessment and a confocal laser scanning microscope (CLSM) for high-resolution topographical mapping. In parallel, material removal is quantified through weight-loss measurements to assess polishing efficiency.

Following this baseline analysis, the chapter presents a comparative study of two electrolyte systems, followed by a systematic investigation of key electropolishing parameters, including applied voltage, polishing time, and bath temperature. Finally, scanning electron microscopy (SEM) imagery and weight-loss data are used to interpret surface evolution and to compare the performance of AlSi10Mg and CP1 under the various processing conditions examined.

4.2 As-Printed Surface Characterization

4.2.1 Overview of AlSi10Mg and CP-1 Alloys

AlSi10Mg and CP-1 (Al-Fe-Zr) represent two compositionally and functionally distinct aluminum-based alloys optimized for Laser Powder Bed Fusion (LPBF) additive manufacturing. While both materials offer excellent printability and mechanical performance, their alloying strategies, surface behavior, and compatibility with surface treatments vary significantly, making them interesting candidates for comparative evaluation in electropolishing studies [176],[177].

AlSi10Mg is a eutectic aluminum-silicon alloy composed primarily of aluminum (balance), silicon (~9.0–11.0 wt.%), and magnesium (~0.20–0.45 wt.%), consistent with standard ranges specified by ASTM F3318 and EN 1706 [178],[179]. Minor constituents such as oxygen (2.4 wt.%) and carbon (15.3 wt.%) are attributed to surface contamination and native oxide formation, typical in LPBF-printed parts [180].

Function of Alloying Elements:

- Aluminum (Al): Acts as the ductile base matrix, offering good thermal and electrical conductivity [181].
- Silicon (Si): Enhances castability and wear resistance, refines microstructure, and improves hardness; however, its high melting point and incomplete fusion during LPBF contribute to surface roughness [182], [183].
- Magnesium (Mg): Forms Mg_2Si precipitates for age-hardening, slightly improving corrosion resistance and mechanical strength [184].
- Oxygen and Carbon: Associated with native oxide layers and processing residues, affecting surface energy and wetting behavior [185].

CP-1 is a high-purity aluminum alloy, developed under the Aluminum Association No. 8A61, with primary elements including aluminum (balance), iron (0.8–1.4 wt.%), and zirconium (0.9–1.4 wt.%).[186]. Minor amounts of oxygen (6.5 wt.%), carbon (15.8 wt.%), and traces of silicon (0.5 wt.%) and calcium (0.1 wt.%) were detected via SEM-EDS. Unlike AlSi10Mg, CP-1 is nominally silicon-free, an intentional design choice to improve post-processing compatibility [12].

Function of Alloying Elements:

- Aluminum (Al): Maintains electrical conductivity, ductility, and low density as the matrix element [181].
- Zirconium (Zr): Forms Al_3Zr precipitates, which refine the grain structure and improve thermal stability, hot-cracking resistance, and strength through precipitation hardening [187].
- Iron (Fe): Exists in low concentrations to avoid embrittlement; contributes to high-temperature strength via intermetallic phases such as λ1 $Zr(Fe,Al)_2$ [188]

Absence of Silicon: Prevents formation of brittle phases and leads to a lower surface roughness upon 3D printing surface roughness, king CP-1 highly suitable for 3D printing [117].

To confirm the elemental composition of the samples, SEM-EDS analysis was conducted on both AlSi10Mg and CP-1 surfaces (Figure 4.1). The results align closely with nominal compositions defined by relevant standards, while also revealing trace surface contaminants such as carbon and oxygen, likely associated with native oxide films or environmental exposure during powder handling and printing.

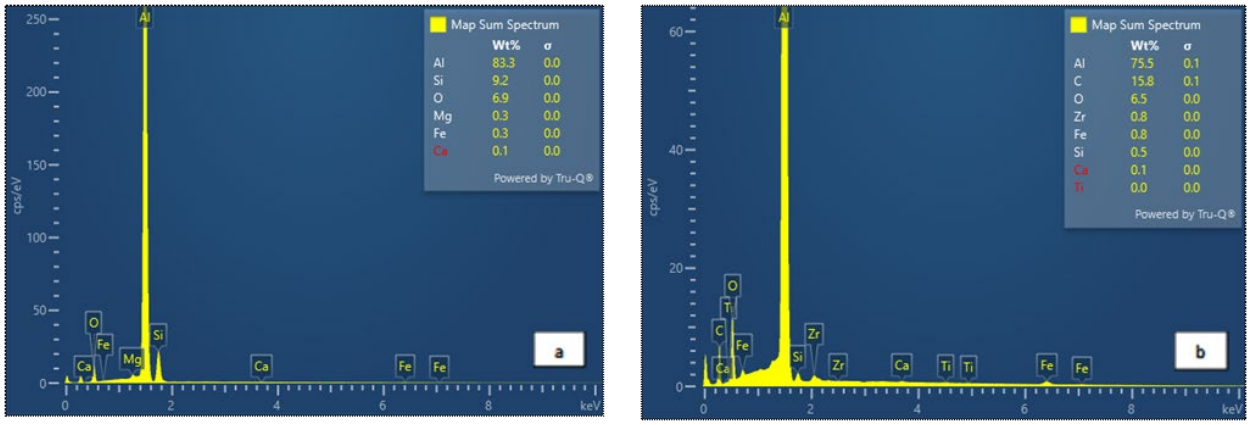

Figure4. 1 Representative SEM-EDS spectra for a) AlSi10Mg surfaces, used for elemental composition analysis. and b) CP1.

4.2.2 Microstructure and Surface Morphology

The surface morphology of each alloy reflects inherent microstructural differences resulting from composition and LPBF processing behavior. In AlSi10Mg, the high silicon content promotes the formation of partially fused Si particles at the surface Combined with scan-track overlaps and the stair-stepping effect, these features result in high surface roughness (Ra ≈ 5–20 µm) and substantial topographical variability, as reflected in Rq and Rz measurements. These features contribute to high roughness values (Ra ≈ 5–20 µm) and increased topographical variability, often evident in Rq and Rz measurements [189] ,[190].

In contrast, the absence of silicon in CP-1 facilitates more complete and stable melting during LPBF, resulting in smoother layer transitions and reduced defect density at the surface (Ra ≈ 3–8 µm) [191],[192]. The presence of zirconium contributes to a uniform grain structure through

Al_3Zr precipitation, which improves thermal stability and reduces melt pool instability—key factors in minimizing surface roughness [188], [193], [194].

Both materials were fabricated using inert gas-atomized powders with particle sizes between 20–70 µm and processed under similar LPBF conditions, including laser power (~300 W) and layer thickness (30–60 µm), optimized for high-density builds [195], [196]. Despite similar densification levels (>99.3% for AlSi10Mg and up to 99.8% for CP-1), CP-1 consistently exhibits smoother as-built surfaces. This makes it more suitable for surface-sensitive post-processing techniques such as electropolishing and anodizing, without the risk of roughness amplification or localized pitting frequently encountered in Si-rich systems [188], [194], [197].

To visually demonstrate the differences in as-built surface texture, Figure 4.2 presents macro-scale photographs of the LPBF-fabricated samples prior to any surface treatment. Even without magnification, the contrast is evident—AlSi10Mg exhibits a matte, granular morphology indicative of its heterogeneous microstructure and higher initial roughness. In comparison, CP1 displays a more uniform and reflective surface with fewer discernible irregularities, consistent with its more homogeneous microstructural constitution and reduced defect prevalence.

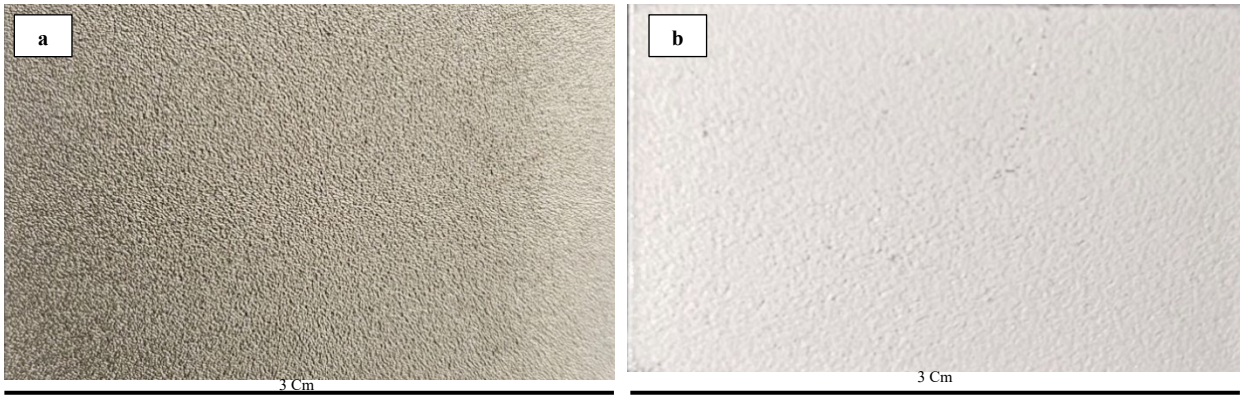

Figure 4. 1 Macro-scale photographs of LPBF-fabricated samples in the as-built condition (a) AlSi10Mg, (b) CP1.

Figure 4.3 presents representative CLSM surface maps of the as-printed AlSi10Mg and CP1 specimens. The 3D topographies (b and d) use a false-color scale to visualize surface height variations. AlSi10Mg (b) exhibits significant surface irregularities, characterized by broad transitions from valleys (blue) to peaks (red), reflecting the heterogeneous nature of its surface morphology. These features correspond to previously identified microstructural features typical of

LPBF-processed AlSi10Mg, such as high surface roughness and partially fused Si particles [189-190]

CP1 (d) displays a more consistent surface profile, with height data more tightly clustered around mid-range values (green to red) and fewer abrupt depressions. Although its peak height range is marginally elevated, the overall surface demonstrates lower variability, suggesting more uniform melt pool solidification and finer topographical features. In addition to the visual topography, quantitative surface roughness measurements obtained using confocal laser scanning microscopy (CLSM) are presented in Table 4.1, which further corroborate the observed differences. The lower Ra and Rq values recorded for CP1 confirm its smoother and more stable as-built surface. These results support earlier qualitative observations and reinforce that CP1's refined microstructure and printing behavior contribute to a more uniform surface finish compared to AlSi10Mg [192].

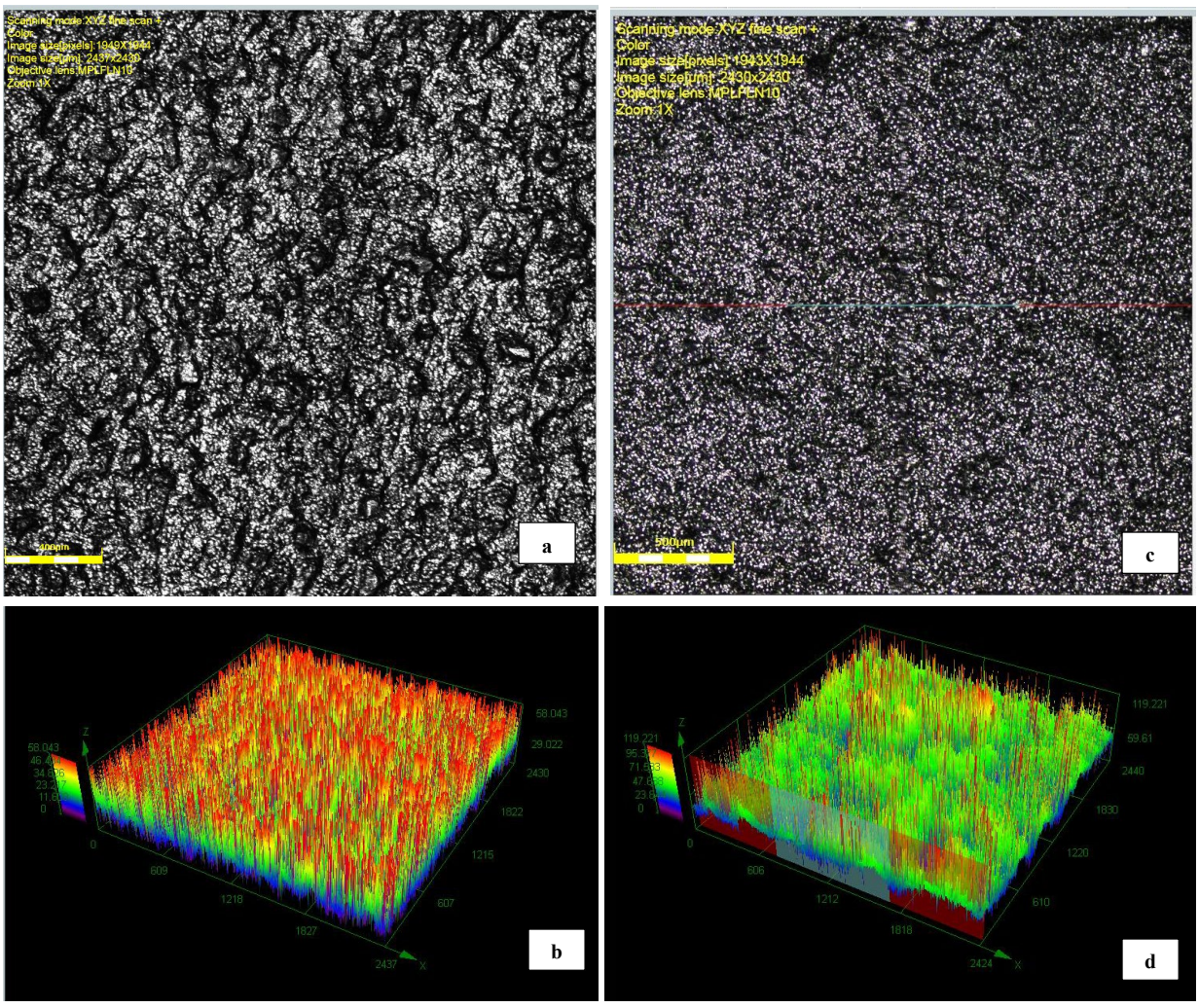

Figure 4. 2 CLSM images of the as-printed surface of AlSi10Mg and CP1 samples. (a) 2D surface scan of AlSi10Mg; (b) corresponding 3D topography of the same AlSi10Mg area. (c) 2D surface scan of CP1; (d) corresponding 3D topography of the same CP1 area.

Table 4. 1 As-printed surface roughness values (Ra, Rq, Rz) for AlSi10Mg and CP-1 measured using CLSM and portable contact profilometry.

Alloy	Method	Ra (µm)	Rq (µm)	Rz (µm)	Std. Dev. (Ra)
AlSi10Mg	CLSM	9.0	13.3	111.5	±1.2
AlSi10Mg	Profilometer	6.0	7.5	35.6	±1.6
CP-1	CLSM	7.0	10.7	98.6	±0.9
CP-1	Profilometer	4.8	5.9	27.7	±1.2

Surface roughness measurements obtained using Confocal Laser Scanning Microscopy (CLSM) and portable contact profilometry yield different values because of their fundamentally distinct measurement principles. This explains the discrepancies reported in Table 4.1.

CLSM is a non-contact optical method: a focused laser scans the surface in three dimensions, and the instrument determines height by detecting the focal plane with maximum reflected intensity. This technique offers very high vertical resolution (tens of nanometers) and sub-micron lateral resolution, enabling it to detect fine asperities and narrow valleys that a mechanical stylus cannot access. Because no physical contact occurs, the surface is not deformed during measurement, which is particularly important for soft or delicate materials. As a result, it often reports higher roughness values than line-based methods, since more surface detail is captured in three dimensions [198].

Portable contact profilometry, by contrast, is a mechanical tracing method. A diamond-tipped stylus is dragged across the surface, producing a 2D profile along its scanning path. As illustrated in Figure 4.4, the stylus follows a predefined linear track, which is visible in the SEM micrograph. Because the stylus tip has a finite radius (typically ~2 μm), it cannot fully enter very narrow grooves or capture sharp peak geometry. This produces a “mechanical filtering” effect where fine features are effectively smoothed out in the measured profile. Furthermore, the applied stylus force, although small, can locally deform softer surfaces or flatten micro-asperities, reducing the apparent roughness amplitude. Another limitation is that only a single scan line is sampled, which may not represent the full variability of a heterogeneous surface. Consequently, portable profilometers often yield lower Ra or Rz values compared to CLSM [199], [200].

Together, these factors explain why the two instruments do not produce identical numerical values even when measuring the same surface.

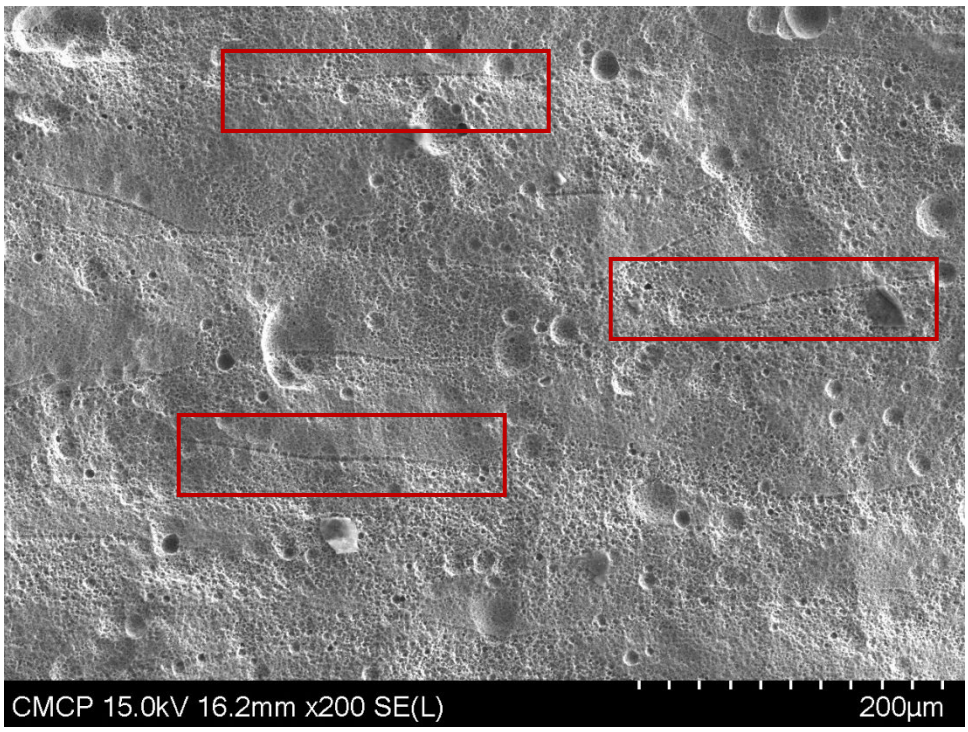

Figure 4. 3 Scanning path of the portable contact profilometer stylus on CP1n sample, as observed in SEM. The linear track represents the physical contact between the stylus tip and the sample surface during measurement.

Figure 4.5 presents SEM micrographs illustrating representative surface and sub-surface defects observed in the as-printed AlSi10Mg and CP1 specimens. Both alloys exhibit typical process-induced flaws—namely lack of fusion (LOF), gas porosity, and cracking—originating from inherent challenges associated with laser powder bed fusion (LPBF) of aluminum-based materials.

In region A, a prominent LOF defect is observed, characterized by an irregular morphology, sharp interfacial boundaries, and incomplete metallurgical bonding. These features are consistent with those reported by Kotadia et al. [201], who attribute such defects to insufficient energy input during LPBF, resulting in poor consolidation between adjacent scan tracks and layers. Similarly, Wang et al. [202], describe LOF as elongated or irregular voids often aligned with the laser scanning direction, especially under low volumetric energy density conditions.

Region B reveals a crack propagating through a partially melted zone, indicative of hot cracking. This defect is typically associated with steep thermal gradients and non-uniform solidification shrinkage during rapid cooling. Al-Si alloys such as AlSi10Mg are particularly susceptible to this

phenomenon near the eutectic composition, where silicon-induced embrittlement, residual stresses, and micro segregation increase crack sensitivity [201].

Additionally, both samples exhibit small spherical pores, predominantly located along melt pool boundaries. Though unmarked, these features are consistent with gas porosity (<5 µm), likely caused by trapped hydrogen or moisture-related contamination during the laser melting process [201], Their morphology and spatial distribution are consistent with hydrogen-induced porosity frequently reported in LPBF-printed aluminum alloys [202].

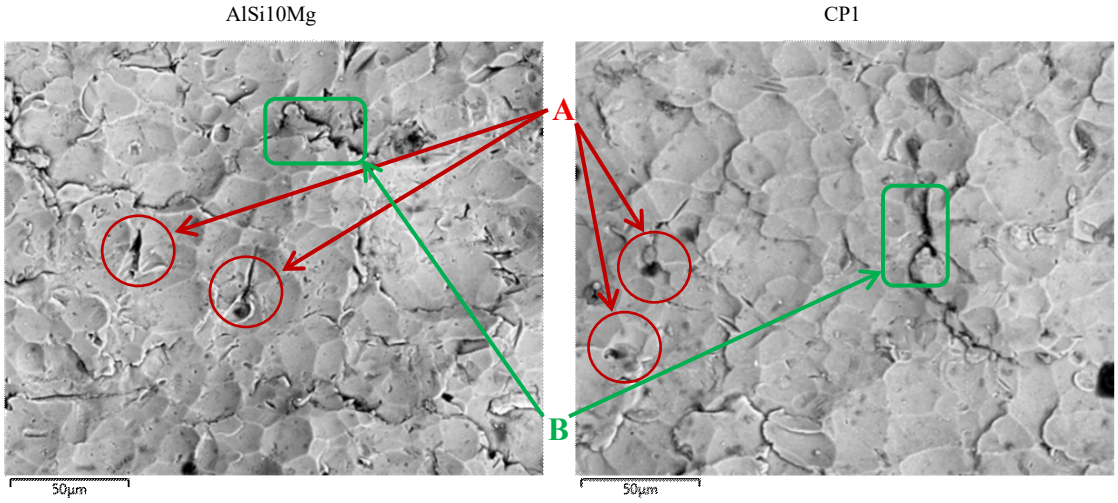

Figure 4. 4 SEM micrographs of the as-printed surfaces of AlSi10Mg (left) and CP1 (right), illustrating typical defects associated with LPBF processing.

While both AlSi10Mg and CP1 micrographs exhibit defects, AlSi10Mg demonstrates a noticeably higher density and severity, particularly in terms of crack formation and LOF regions. This disparity is attributed to its higher silicon content, which promotes localized shrinkage stresses and decreases ductility, thereby increasing vulnerability to solidification-related defects. In contrast, CP1's refined composition and lower Si content contribute to more uniform melt pool behavior and improved structural coherence, resulting in fewer and less severe flaws.

These comparative observations indicate that CP1 exhibits a more stable as-printed microstructure and is inherently less prone to defect formation under identical LPBF processing conditions.

The EDS elemental maps of the as-built AlSi10Mg (Figure 4.6) reveal pronounced segregation of silicon within a uniformly distributed aluminum matrix. Aluminum appears uniformly distributed as the primary α-Al matrix, whereas silicon is enriched along cellular boundaries, forming a

continuous network that delineates the aluminum-rich cells. This Si-rich framework is characteristic of the rapid solidification of hypoeutectic Al–Si alloys produced by laser powder bed fusion (LPBF) [203], [204]. Magnesium, present in lower concentrations, does not exhibit a distinct phase in the as-built condition. The elemental maps also indicate localized oxygen-rich regions that spatially coincide with silicon-enriched areas, producing purple-toned features in the composite map. This co-location suggests the presence of silicon oxide phases formed either from partial oxidation of Si-rich eutectic films during solidification or from entrainment of pre-existing oxide layers on the powder feedstock [205], [206]. Such oxide-containing regions are typical in LPBF-processed AlSi10Mg due to the alloy's high oxygen affinity and the persistence of native oxide films on powder surfaces [207], [208].

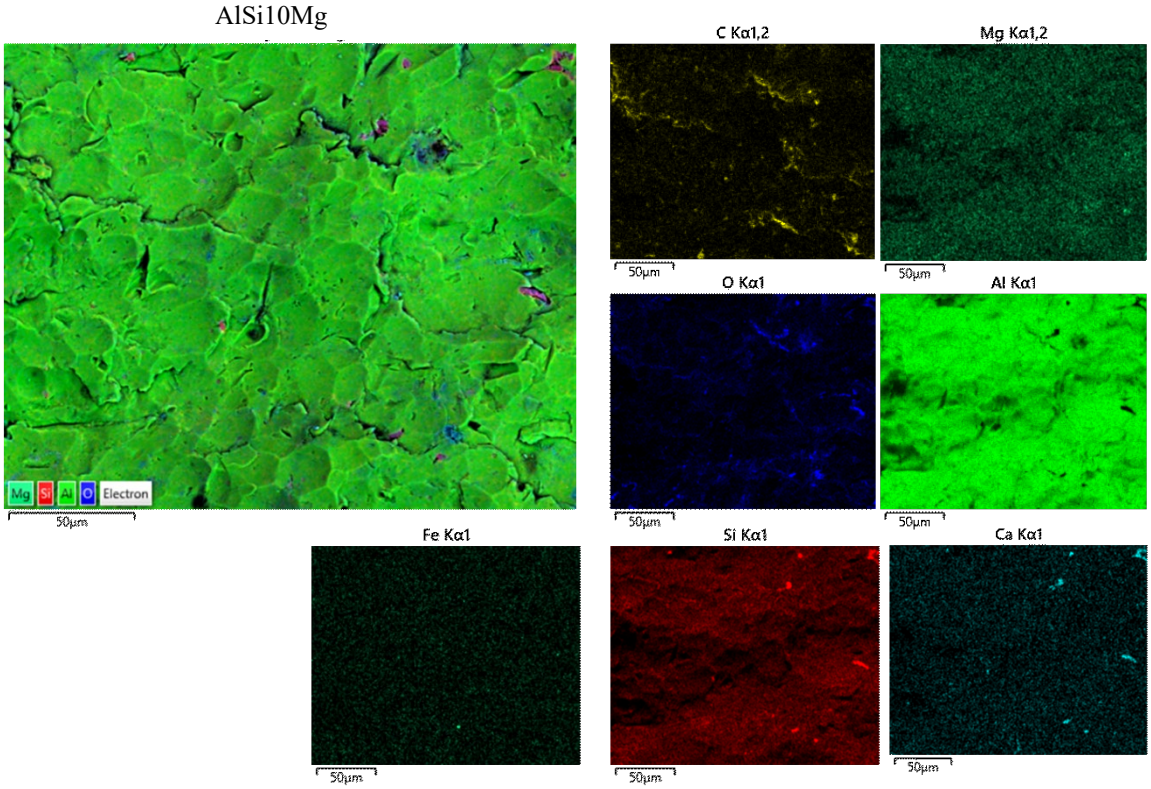

Figure 4. 5 EDS elemental maps of the as-printed AlSi10Mg.

The EDS elemental maps of the as-built CP1 alloy (Figure 4.7) show aluminum as a uniformly distributed primary matrix, with zirconium appearing in discrete enriched particles and occasional fine dispersions. These Zr-rich regions are consistent with primary Al_3Zr or solute-trapped Zr formed under rapid LPBF solidification [209], [210]. Silicon is present only in trace, isolated

clusters, lacking the continuous eutectic network typical of Al–Si alloys [211]. Oxygen-rich areas are observed sporadically and often coincide with Zr- or Si-enriched sites, suggesting the presence of zirconia (ZrO_2) or silica (SiO_2) inclusions, alongside alumina from powder-surface oxides [13,16]. Such oxides are characteristic of LPBF-fabricated aluminum alloys due to the high oxygen affinity of Al and Zr, and the retention of native oxide films during processing [212], [213].

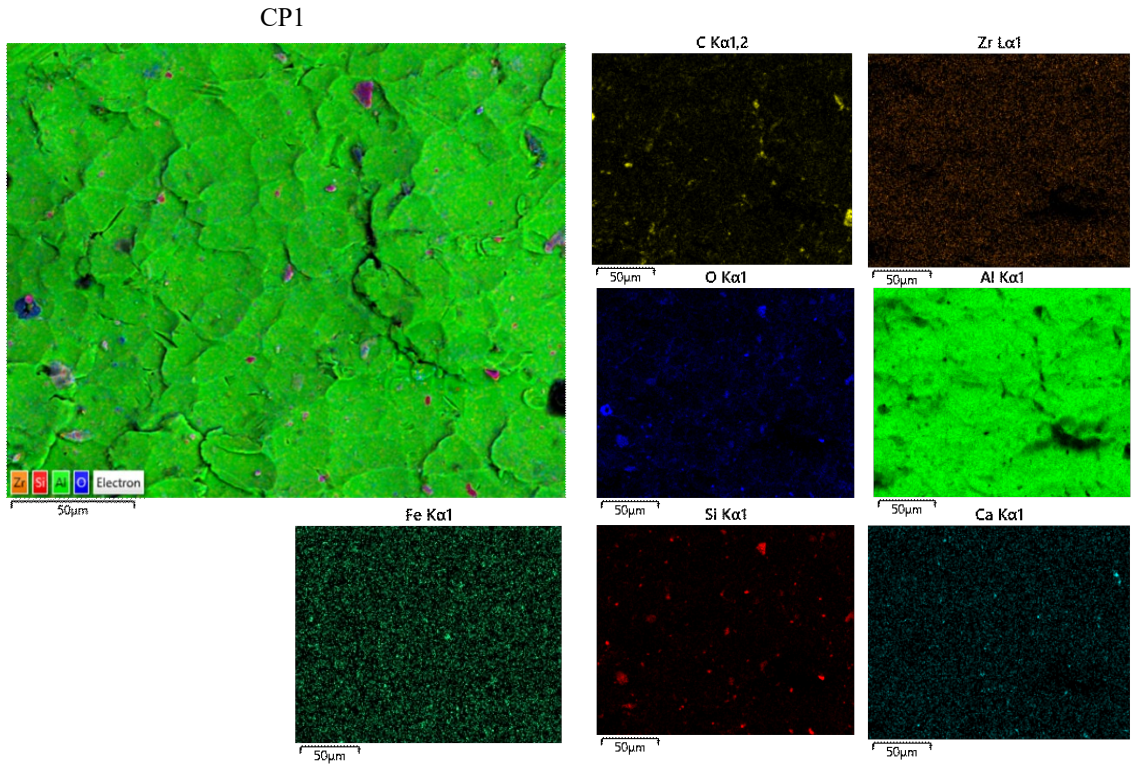

Figure 4. 6 EDS elemental maps of the as-printed CP1.

4.3 Electrolyte Performance Evaluation

The selection of electrolytes for electropolishing in this study was made with deliberate consideration of both practical application and current research findings. Ethylene glycol (EG) + NaCl has emerged as a promising alternative to traditional acidic baths, particularly for aluminum alloys. Studies have shown that this neutral, alcohol-based system can achieve significant surface smoothing with minimal environmental and safety hazards, producing roughness values as low as ~3 nm without the use of toxic perchloric or chromic acids [214], [215]. The chloride ions support anodic dissolution, while the ethylene glycol acts as both a solvent and complexing agent, enabling controlled and uniform polishing in a safer, more sustainable medium [216]. On the other hand,

the combination of phosphoric and sulfuric acids remains the industrial standard for aluminum electropolishing due to its high electrical conductivity and rapid material removal, offering consistent and reliable surface leveling performance across a range of aluminum grades [217], [218]. Although acidic electrolytes present handling and disposal challenges, their widespread use and effectiveness, particularly in aerospace and automotive applications, make them a benchmark system.

The polishing behavior of samples from both AlSi10Mg and CP1 alloys was therefore investigated using these two electrolytes to compare common industrial practices with emerging greener methods under identical process parameters. Electropolishing was performed under controlled conditions, using voltages of 20 V and 30 V and durations of 10, 20, and 30 minutes.

The change in surface roughness, expressed as the surface roughness reduction (ΔR), served as the primary indicator of polishing effectiveness. Figure 4.8 presents the ΔR values for each condition, calculated as:

$$\Delta R = R_{initial} - R_{final}$$

where $R_{initial}$ is the average surface roughness (Ra, Rq or Rz) of the as-printed samples and R_{final} is the Ra (Rq or Rz) after electropolishing. For reference, the average initial roughness was 6.0 µm for AlSi10Mg and 4.8 µm for CP1. Larger ΔR values indicate greater surface smoothing efficiency.

Figure 4.8 reveals two critical patterns: first, that the acidic electrolyte (phosphoric + sulfuric acid) produces the greatest surface roughness reduction for both alloys, and second, that the AlSi10Mg alloy consistently exhibits higher roughness reductions than CP1 under equivalent conditions.

The superior performance of acidic electrolytes can be attributed to a combination of electrochemical and physicochemical mechanisms such as increased proton concentration and improved ionic conductivity which enhance anodic dissolution. Abdel-Fattah and Loftis [219] reported that phosphoric acid produced a significantly higher current density (3.51 A/cm²) compared to a neutral deep eutectic solvent (1.08 A/cm²), leading to a faster material removal rate. The increased current density accelerates metal ion dissolution at surface protrusions, promoting surface leveling and resulting in greater roughness reduction values [220].

Second, acidic electrolytes facilitate the formation of a viscous salt film at the metal–electrolyte interface, a key characteristic of the so-called "polishing plateau" regime. This film creates a diffusion-limited condition that suppresses random etching and favors uniform anodic dissolution [221].

Third, acidic systems effectively dissolve the native oxide film on aluminum, reducing the barrier for direct metal dissolution. This allows for more efficient polishing compared to neutral electrolytes, where the oxide layer can hinder uniform dissolution. As a result, acidic solutions lead to a higher net reduction in surface asperities [219], [222].

As previously mentioned, Figure 4.8 clearly demonstrates that AlSi10Mg consistently undergoes greater roughness reduction than CP1 under all tested electropolishing conditions. This different response can be attributed to several microstructural and compositional factors intrinsic to each alloy, which govern their respective electropolishing behavior.

AlSi10Mg is a near-eutectic aluminum–silicon alloy characterized by a dual-phase microstructure composed of an aluminum-rich matrix and finely distributed eutectic Si particles. These silicon-rich regions create localized electrochemical inhomogeneities, which enhance the electric field concentration and promote preferential anodic dissolution of the surrounding aluminum matrix. This phenomenon leads to more effective leveling of surface asperities during electropolishing [223]. This was also observed in a study by Seifi et al. [224], where the process-induced effects and high surface roughness of AM AlSi10Mg parts resulted in a pronounced roughness reduction upon electropolishing.

Another factor that may contribute to the greater roughness reduction observed in AlSi10Mg is the presence of magnesium in its microstructure. Owing to its high chemical reactivity and stronger thermodynamic affinity for oxygen ($\Delta G°f$ for MgO (–596 kJ/mol) is more negative than for Al_2O_3 (–1582 kJ/mol), magnesium can destabilize the passive aluminum oxide film by forming MgO or dissolving as Mg^{2+} in acidic media. This disruption facilitates electrolyte access to the underlying metal, enhancing localized dissolution rates and accelerating material removal during electropolishing [225] .

In contrast, CP1 (a high-purity Al–Fe–Zr alloy) possesses a more homogeneous microstructure and significantly lower initial surface roughness due to reduced particle segregation and minimal

silicon content. The presence of Zr-rich dispersoids enhances thermal stability and promotes grain refinement; however, it also reduces electrochemical activity and slows the anodic dissolution rate during electropolishing [38]. As a result, CP1 exhibits more stable but less aggressive material removal, yielding smaller reduction in surface roughness.

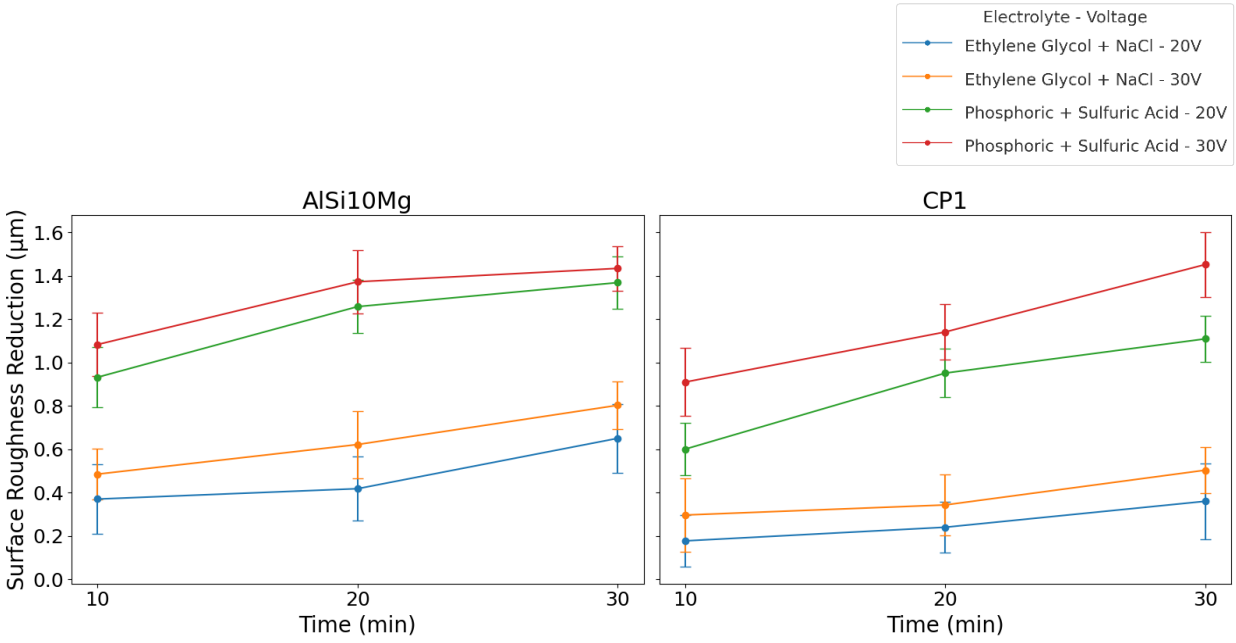

Figure 4. 7 Effect of electrolyte composition, polishing voltage, and duration on the surface roughness reduction (ΔR) of AlSi10Mg and CP1 alloy samples, as measured using a portable contact profilometer.

In summary the superior roughness reduction achieved with the phosphoric–sulfuric acid system is linked to its ability to sustain high current densities, promote field-assisted anodic dissolution, and suppress passivation, enabling efficient and uniform material removal. AlSi10Mg exhibits a stronger response under these conditions due to its heterogeneous microstructure and localized electrochemical activity, whereas the more homogeneous and electrochemically stable CP1 shows a comparatively restrained effect. In contrast, the ethylene glycol–NaCl electrolyte provides a gentler, more controlled refinement pathway, which may be advantageous for high-precision or structurally sensitive applications. These results highlight the combined role of electrolyte chemistry and alloy-specific characteristics in determining electropolishing efficiency, guiding process-parameter selection for additive-manufactured aluminum components. Based on the superior performance of the acidic system, it was selected for further investigation in the next chapter, focusing on the influence of voltage and duration on electropolishing behavior.

4.4 Evaluation of Voltage and Time in Acidic Electropolishing

Building upon the superior surface-finishing performance of the phosphoric–sulfuric acid system identified in the preceding section; this phase of the investigation examines the influence of applied voltage and polishing duration on electropolishing outcomes in AlSi10Mg and CP1 alloys. The primary objective is to determine parameter ranges that achieve maximum surface roughness reduction while mitigating the risk of surface degradation associated with over-polishing. By systematically varying voltage and time within controlled experimental boundaries, the study seeks to establish process–response relationships that can guide the optimization of electropolishing protocols for additively manufactured aluminum alloys.

To achieve this, each alloy was subjected to a controlled matrix of electropolishing conditions involving three voltage levels (15, 20, and 25 V) and three processing durations (10, 20, and 30 min), resulting in nine test combinations per material. This range was selected to encompass the transition from the onset of effective anodic dissolution to the upper limit of the polishing plateau, beyond which oxygen evolution and localized overheating may induce pitting or dimensional loss [226], [227]. The lower bound of 15 V was chosen to ensure sufficient driving force for oxide film destabilization and initiation of mass-transport–controlled dissolution [228], [229], while 25 V approached the regime where trans passive behavior and non-uniform removal can occur in aluminum alloys [42],[230]. The intermediate 20 V condition provided a balanced operating point to evaluate stability and roughness reduction efficiency across alloys. Similarly, processing times of 10 to 30 min were selected to capture the early-stage smoothing kinetics as well as the potential onset of over-polishing, enabling assessment of both rate and extent of surface refinement within practically relevant durations [226], [227].

Figure 4.9 illustrates the evolution of surface roughness reduction (ΔRa) for AlSi10Mg and CP1 in the phosphoric–sulfuric acid system, measured by portable contact profilometry (A, C) and confocal laser scanning microscopy (B, D). Consistent with the superior performance of acidic electrolytes discussed in Section 4.3, both alloys showed increased ΔRa with rising voltage and longer polishing times, although the magnitude and progression varied. Profilometry measurements revealed that AlSi10Mg consistently achieved greater reductions than CP1 under equivalent conditions, reflecting the alloy's higher initial roughness and greater susceptibility to

material removal. Comparable behavior for LPBF AlSi10Mg in high-conductivity acidic baths has been documented by Kadirgama et al. [231]. The largest improvements occurred at 25 V with extended durations, in agreement with earlier investigations indicating that increased voltage accelerates anodic dissolution until the onset of oxygen evolution [232]. Similar trends have been reported in other studies [233] where voltages beyond an optimal threshold yielded only marginal additional smoothing due to emerging surface instability.

CP1 displayed a gradual, near-linear increase in ΔRa across all parameter combinations, consistent with the stable dissolution behavior characteristic of Zr-containing alloys, as noted by Birbilis et al. [234] and with the controlled surface response observed in other fine-grained aluminum systems [235].

Confocal microscopy, in line with observations reported in Section 4.3, produced higher absolute ΔRa values than profilometry but confirmed the same relative patterns between alloys and processing conditions. Across both measurement methods, the benefit of increasing voltage and time diminished at the highest parameter levels, echoing the diminishing returns effect frequently described in the electropolishing literature [232], [236], [237].

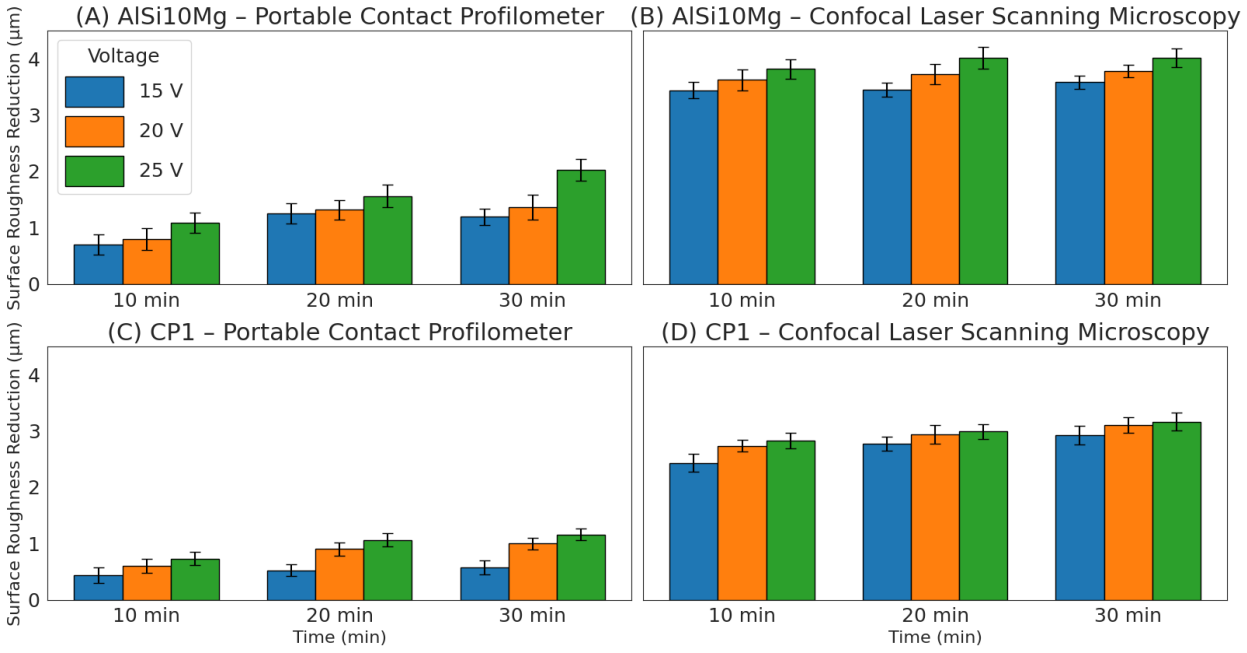

Figure 4. 8 Surface roughness evolution of AlSi10Mg and CP1 samples after electropolishing under phosphoric + sulfuric acid electrolyte at varying voltages and durations.

To complement the quantitative surface roughness data, SEM micrographs were acquired for samples electropolished at 20 V for 20 minutes. This condition was selected as a balanced, mid-range operating point—situated within the diffusion-limited plateau for acidic electropolishing—ensuring sufficient anodic dissolution for effective smoothing while avoiding the onset of oxygen evolution, pitting, or excessive dimensional loss commonly observed at higher voltages or extended durations [238], [239], [240], [241]. Positioned centrally within the tested voltage–time matrix, this parameter set standardizes energy input across both materials, permitting direct comparison of their intrinsic surface response. Under these conditions, SEM observations (Figure 4.10) reveal that AlSi10Mg undergoes substantial removal of surface asperities, with notable reduction in surface irregularities and partially fused Si particles, although residual porosity remains. CP1 presents a uniformly refined surface characterized by fine scale smoothing and minimal localized attack, consistent with its more stable anodic dissolution behavior.

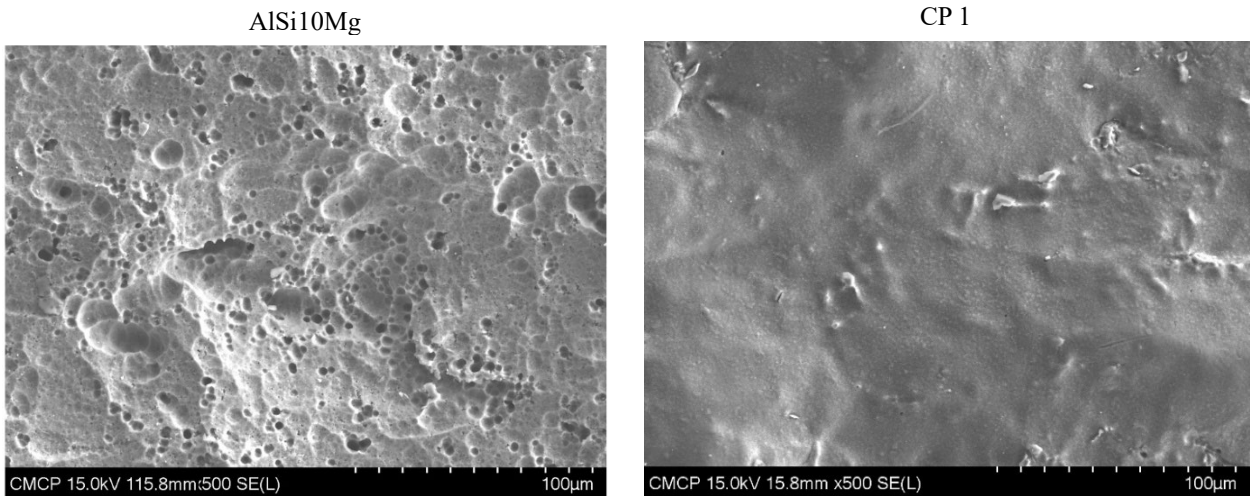

Figure 4. 9 SEM micrographs of LPBF-fabricated (a) AlSi10Mg and (b) CP1 after electropolishing in phosphoric–sulfuric acid electrolyte at 20 V for 20 min. Both micrographs were acquired at 500× magnification using an accelerating voltage of 15 kV: scale bar = 100 µm.

Overall, both AlSi10Mg and CP1 showed improved surface finish with increasing voltage and time in the phosphoric–sulfuric acid system, though their responses differed.

The SEM images of the AlSi10Mg sample reveal a porous microstructure, which arises from several factors. In silicon-containing alloys, the dissolution behavior of silicon during

electropolishing is highly dependent on bath composition and operating conditions. Silicon can undergo two distinct anodic dissolution pathways: a divalent (two-electron) route that generates a porous silicon layer, or a tetravalent (four-electron) route that produces a smooth electropolished surface [242], [243]. The transition between these regimes is controlled by current density and electrolyte chemistry. At low current densities, slow oxide growth and local passivation cause non-uniform dissolution, leading to pore formation. Once the current density exceeds a critical threshold (~0.5 A cm^{-2}), oxide growth and removal occur uniformly across the surface, resulting in effective electropolishing [68].

Although the present work employs a phosphoric–sulfuric electrolyte rather than fluoride-containing systems, these studies highlight that silicon dissolution is extremely sensitive to both chemistry and current density. Such sensitivity could explain why the AlSi10Mg sample exhibits porous microstructural features after electropolishing.

It is also important to note that AlSi10Mg samples produced by LPBF inherently contain a more porous as-built microstructure due to incomplete fusion and gas entrapment during solidification. During electropolishing, the outer layers are removed, which exposes these sub-surface pores rather than creating new ones. This helps to explain why AlSi10Mg surfaces often retain porous features after polishing. By contrast, CP1 exhibits a much denser and more uniform microstructure, free from silicon-rich phases, which results in smoother polishing outcomes.

These results illustrate how microstructural and physical factors interplay with process parameters, reaffirming the necessity of alloy-specific optimization to achieve comparable surface finishes.

Energy-dispersive X-ray spectroscopy (EDS) measurements revealed notable compositional changes after electropolishing. As previously discussed, AlSi10Mg is a laser powder-bed-fused (LPBF) Al-Si-Mg alloy (~10 wt % Si with trace Mg and Fe), whereas CP1 is a high-purity Al-Fe-Zr alloy containing Zr dispersoids. In the as-printed state, both alloys quickly form thin, continuous Al_2O_3 films when exposed to air [244-245] and may retain process-related contaminants [246]. Acidic electropolishing in phosphoric–sulfuric media dissolves these oxides [247] and selectively remove some alloying elements [94], while also exposing any adsorbed species [248].

After electropolishing (Table 4.2), AlSi10Mg shows a decrease in aluminium content and a substantial increase in carbon; silicon decreases slightly, oxygen drops markedly, and magnesium

and iron remain at trace levels. CP1, exhibits a notable increase in aluminium, significant decreases in carbon and oxygen and only minor changes in Zr and Fe.

Table 4. 2 compositional changes for AlSi10Mg and CP1 after plasma discharge electropolishing.

Element	AlSi10Mg (As Printed)	AlSi10Mg (After Plasma EP)	CP1 (As Printed)	CP1 (After Plasma EP)
Al	83.3	73.5	75.5	89.4
Si	9.2	8.6	0.8	–
O	6.9	2.4	6.5	1.2
Mg	0.3	0.2	–	–
Fe	0.3	–	0.8	0.9
Ca	0.1	–	0.2	–
C	–	15.3	15.8	7.4
Zr	–	–	0.8	1.1
Ti	–	–	0.0	–

These compositional variations can be rationalised as follows:

1. Oxide Film Dissolution

Air-formed Al_2O_3 films contribute to oxygen peaks in EDS and slightly lower apparent Al content [244-245] . Acidic electropolishing dissolves these films, enabling direct anodic dissolution of the metal and exposing more bulk alloy within the X-ray interaction volume. This explains the sharp oxygen decrease in both alloys and the corresponding aluminium increase in CP1 [249].

2. Elemental Redistribution and Selective Dissolution

Electropolishing can alter surface composition by preferentially dissolving certain phases [250]. n AlSi10Mg, the silicon network at α-Al grain boundaries is more inert in acidic media than the aluminium matrix [251]. thus, selective dissolution of Al may relatively enrich Si at the extreme surface [107]. though only a small change was observed here. CP1's homogeneous microstructure shows minimal change in alloying elements aside from a proportional decrease in Zr and Fe due to the rise in Al after oxide removal.

3. Carbon Signal Variations

Carbon detected by EDS typically originates from surface contamination—adsorbed hydrocarbons from the environment or process residues [246], [248]. In CP1, the decrease in carbon suggests

effective removal of organic contamination by the acidic electrolyte. In AlSi10Mg, the unexpected carbon increase likely results from adsorption of electrolyte-borne organics or atmospheric hydrocarbons onto the highly active freshly electropolished surface during rinsing and drying [248], [252]. Incomplete rinsing can also leave trace organic stabilisers from the electrolyte, which appear as elevated carbon signals.

Overall, electropolishing in acidic media significantly modifies the surface chemistry of both alloys but in opposite ways with respect to carbon and aluminium signals. CP1's increase in Al and marked decrease in carbon confirm effective oxide removal and surface cleaning, giving a composition closer to the bulk alloy. In AlSi10Mg's Al decrease accompanied by substantial carbon uptake suggests that although oxide dissolution occurred, the freshly exposed surface rapidly adsorbed carbonaceous species during or after electropolishing. This contrast indicates that CP1's homogeneous microstructure and stable oxide dissolution make it more resistant to post-polishing contamination, whereas AlSi10Mg's heterogeneous surface chemistry leaves it more reactive and prone to rapid contamination adsorption. From a process perspective, CP1 can achieve a cleaner, bulk-representative surface through electropolishing alone, while AlSi10Mg may require additional post-polishing cleaning or protective steps to preserve surface purity.

4.5 Evaluation of Bath Temperature

The bath temperatures investigated in this study (35 °C and 50 °C) were selected based on prior electropolishing research in phosphoric–sulfuric acid systems for aluminum alloys. Moderate heating of the electrolyte has been shown to lower viscosity, increase ionic conductivity, and enhance mass transport, thereby widening the polishing plateau and increasing the limiting current density [253], [254], [255], [256]. Literature reports indicate that 30–40 °C represents a stable operational range for achieving uniform dissolution without significant gas pitting, while temperatures around 50–55 °C can further accelerate material removal through faster anodic kinetics and oxide film dissolution [257], [258], [259]. However, temperatures above ~60 °C are associated with thinning of the viscous anodic film, early oxygen evolution, and localized pitting—particularly in aluminum alloys with heterogeneous microstructures [260], [261], [262]. Based on

these findings, 35 °C was chosen as a moderate industrially relevant condition, and 50 °C as an elevated temperature expected to boost polishing efficiency while remaining below the instability threshold reported in earlier studies.

In the present study, elevating the bath temperature from 35 °C to 50 °C consistently enhanced ΔRa for both alloys (Figure 4.11), corroborating earlier observations of temperature-driven increases in aluminum electropolishing efficiency [263], [264]. The effect was more pronounced in AlSi10Mg, reflecting its heterogeneous microstructure and higher initial roughness, which render it more responsive to thermally accelerated mass transport and anodic dissolution kinetics[265], [266]. At elevated temperature and high voltage, however, prolonged polishing triggered trans passive breakdown, evidenced by current instability and excessive bath heating—a condition associated with oxygen evolution and surface film destabilization in aluminum systems.[262], [264].

CP1 exhibited a steadier and more controlled response to temperature increase, with ΔRa gains that were more modest but consistent. At 25 V and 50 °C for 20 min, CP1 reached 2.00 µm without signs of instability, reflecting the broader stability window of Zr-containing aluminum alloys reported by Birbilis et al. [265] and Assefa et al. [266]. The alloy's homogeneous microstructure and stable oxide chemistry likely mitigate localized dissolution and gas pitting, even under elevated thermal and electrochemical conditions.

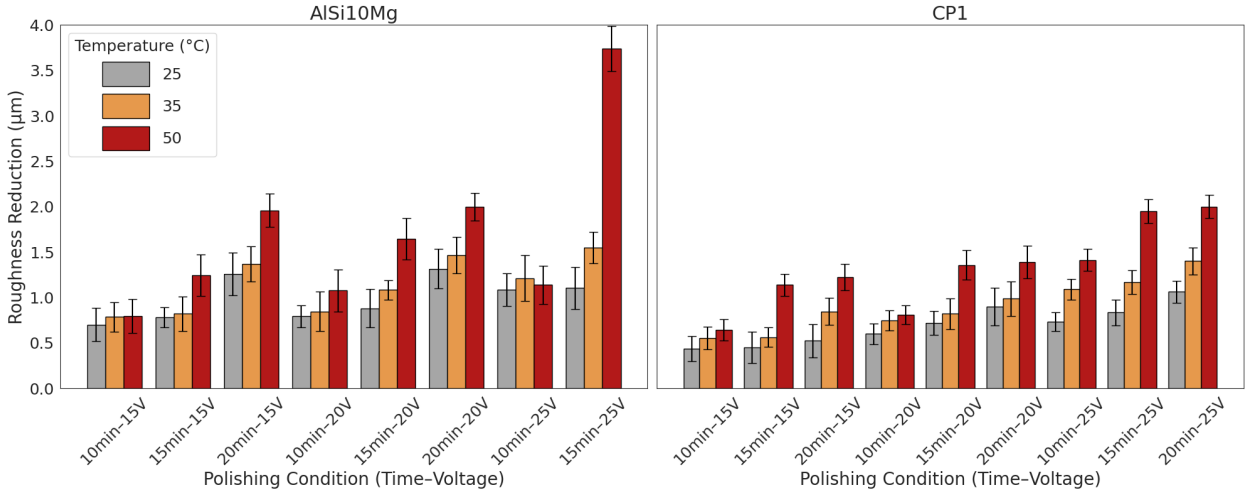

Figure4.11 Surface roughness reduction (ΔRa) of AlSi10Mg and CP1 samples after electropolishing under varying voltage–time combinations, compared at two temperatures (35°C and 50°C).

To further illustrate the material-dependent polishing behavior, confocal laser scanning microscopy (CLSM) images were obtained for both alloys processed under identical moderate conditions (20 V, 20 min, 35 °C) (Figure 4.12). The AlSi10Mg surface shows partial leveling, but prominent texture and deeper valleys remain visible in the 2D scan, with the 3D topography revealing sharp ridges and localized depressions. In contrast, CP1 exhibits a markedly more uniform texture, with reduced height variation and smoother features in both 2D and 3D representations.

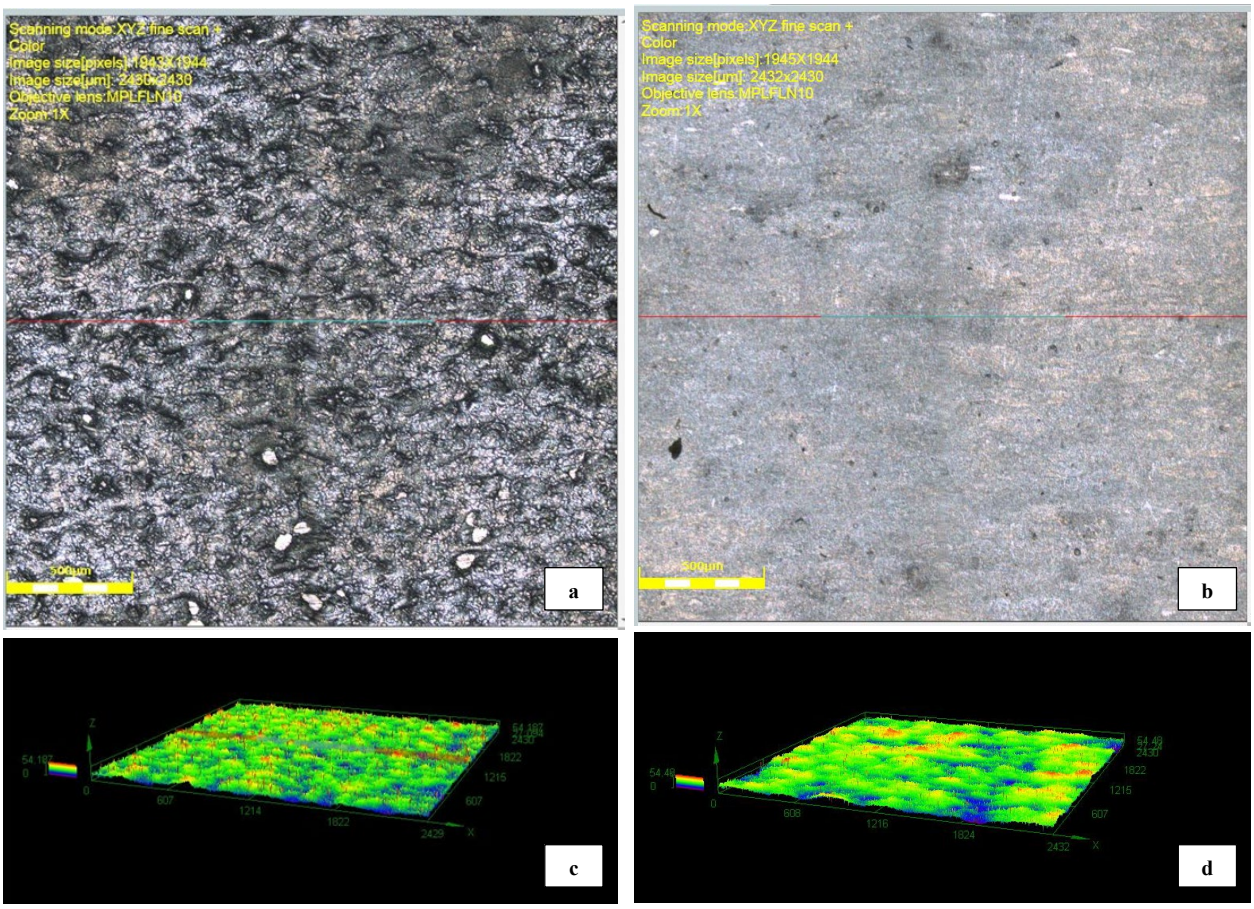

Figure4. 12 CLSM images of the polished surface of AlSi10Mg and CP1 samples. (a) 2D surface scan of AlSi10Mg; (b) corresponding 3D topography of the same AlSi10Mg area. (c) 2D surface scan of CP1; (d) corresponding 3D topography of the same CP1 area.

Quantitative surface roughness parameters are presented in Table 4.2, confirming that while AlSi10Mg achieved a greater absolute ΔRa, its post-polishing surface remained rougher than that of CP1. This highlights that CP1's finer as-printed surface allows it to achieve superior smoothness under moderate polishing conditions, whereas AlSi10Mg may require more aggressive parameters to reach comparable quality.

Table 4. 3 Surface roughness parameters of AlSi10Mg and CP1 samples before and after electropolishing at 20 V for 20 minutes at 35 °C.

Alloy	Ra (µm)	Rq (µm)	Rz (µm)	Ra (µm)	Rq (µm)	Rz (µm)	ΔRa (µm)
	Initial	Initial	Initial	Polished	Polished	Polished	
AlSi10Mg	5.2	6.5	33.8	3.9	5.0	26.0	1.3
CP1	3.9	4.6	18.5	2.8	3.50	14.1	0.9

Overall, these results support earlier observations that while elevated temperatures can substantially enhance electropolishing efficiency, the benefits are alloy-dependent and must be balanced against the risk of trans passive breakdown. For AlSi10Mg, 25 V at 50 °C for 15 min appears to be the upper safe operating limit, whereas CP1 can sustain longer or equally aggressive exposure without compromising stability—an important distinction for process optimization in precision finishing of LPBF aluminum alloys.

4.6 Observation and Analysis of Trans-passive Breakdown Electropolishing

In previous section the influence of bath temperature on electropolishing efficiency was examined for both AlSi10Mg and CP1 alloys. While moderate temperature increases improved surface roughness reduction through enhanced mass transport and anodic dissolution, specific high-temperature/high-voltage combinations produced an abrupt deviation from the expected polishing response, signalling trans-passive film breakdown electrolysis. Under these conditions, features consistent with breakdown of the passive oxide film and the formation of a vapour–gas envelope at the electrode surface were observed [86], [87], [88].

Trans-passive breakdown occurs when the anodic potential exceeds the passive film's stability limit. Ohmic heating rapidly vaporises electrolyte near the anode, generating numerous small bubbles that grow and merge to envelop the electrode in a macroscopic vapour–gas film composed of water vapour, oxygen and plasma-discharge products [267]. This insulating film reduces mass transport and can sustain localised micro-arc discharges that fundamentally change the dissolution mechanism and promote surface removal [249].

In this study, plasma discharge was detected only under the most aggressive parameter sets. For AlSi10Mg, breakdown occurred at 50 °C, 25 V and 25 min; for CP1, breakdown required 50 °C,

30 V and 25 min. This difference likely reflects intrinsic alloy properties: AlSi10Mg's heterogeneous microstructure and higher initial roughness intensify local electric fields and lower the breakdown threshold, Whereas CP1's homogeneous microstructure and Zr-rich dispersoids enhance thermal and electrochemical stability, the generation of smaller, more mobile bubbles delays gas-film coalescence, thereby shifting breakdown onset to higher voltages [71], [72], [75]. These observations are consistent with literature reports showing that higher temperatures accelerate oxygen evolution, which lowers the voltage needed for oxide breakdown. In addition, longer exposure promotes localized heating and gas-film accumulation, both of which support the onset and persistence of breakdown [268-270], [78]. Once initiated, the process exhibits visible sparking, audible crackling and current oscillations—hallmarks of trans-passive breakdown electrolysis in high-voltage systems [77-78].

Figure 4.13 presents confocal laser scanning microscopy (CLSM) surface maps that illustrate the morphological consequences of trans-passive breakdown. For AlSi10Mg, the surface remains relatively level but contains a dense distribution of pores and lack-of-fusion (LOF) sites. Shallow, elongated channels connect these features, which likely represent preferential breakdown tracks created by gas movement along the surface during the trans-passive regime. This suggests that trans-passive breakdown may dissolve the surface layer, exposing subsurface porosity and LOF defects inherent to the additively manufactured structure. In contrast, CP1 surfaces appear smoother, with far fewer LOF regions and no channel-like features, indicating less aggressive breakdown behaviour.

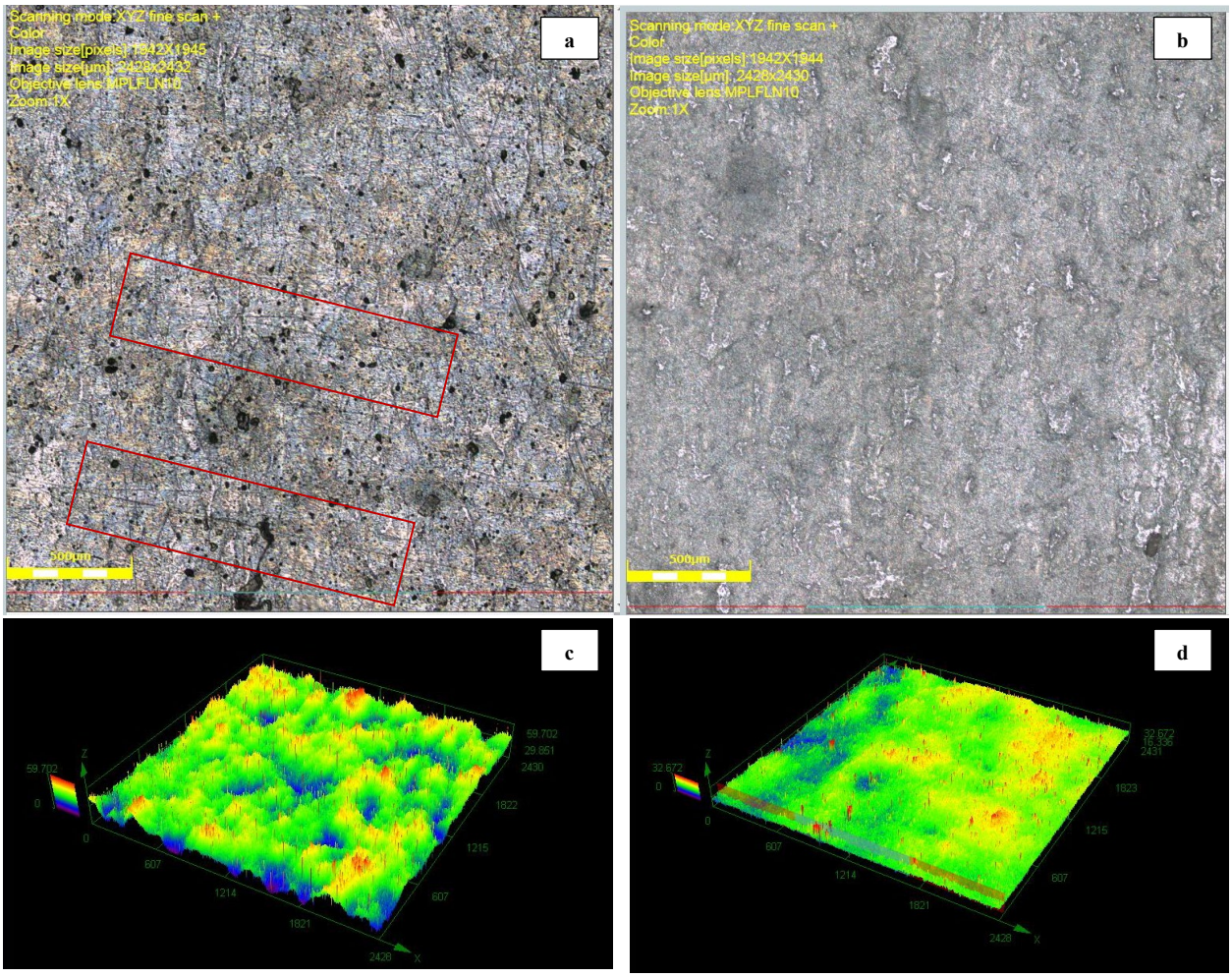

Figure4. 13 CLSM surface topography of AlSi10Mg (left)(50 °C, 25 V, 25 min), and CP1(right) (50 °C, 30 V, 25 min).

Table 4. 4 presents the Surface roughness of the studied samples before and after electropolishing under breakdown conditions for AlSi10Mg and CP1. According to the table, trans-passive breakdown reduced Ra by 3.7 µm for AlSi10Mg (25 V, 25 min) and by 2.0 µm for CP1 (25 V, 25 min). Although AlSi10Mg shows greater absolute roughness reduction, CP1 achieves a smoother final surface owing to its initially lower Ra and superior microstructural stability.

Table 4. 4 Surface roughness parameters of AlSi10Mg and CP1 before and after electropolishing under breakdown conditions, measured by confocal laser scanning microscopy (CLSM).

Alloy	Voltage (V)	Time (min)	Temp. (°C)	Ra (µm)	Rq (µm)	Rz (µm)	Ra (µm)	Rq (µm)	Rz (µm)	ΔRa (µm)
				Initial	Initial	Initial	Polished	Polished	Polished	
AlSi10Mg	25	15	50	6.7	8.6	38.7	2.9	3.6	21.4	3.7
CP1	25	20	50	3.7	4.6	19.3	1.7	2.1	9.3	2.0

Scanning electron microscopy confirmed the roughness differences observed earlier. On AlSi10Mg samples treated by trans-passive breakdown polishing, the surface is littered with round micro-craters ranging from sub-micrometre to tens-of-micrometre in diameter (Figure 4.14). When the workpiece acts as the anode under sufficiently high voltage, plasma micro-discharges form within the electrolytic bath. These localized discharges briefly exceed the melting point of aluminium, causing small volumes of metal to melt. Upon rapid re-solidification, the expelled regions leave behind crater-like micropores, whose rims appear smooth due to the fast re-flow of molten material around the discharge site. Such discharge-induced melting and re-solidification explains the fine, rounded micro-craters observed by SEM. However, not all cavities originate from electropolishing itself. Some of the larger, irregular pores correspond to re-opened defects already present in the as-built alloy, such as keyhole or lack-of-fusion porosity formed during laser powder bed fusion (LPBF) of silicon-containing alloy [273-274]. n LPBF, open porosity and surface roughness arise from the overlapping of molten pools and the deposition of partially fused droplets during layer-by-layer solidification [275]. Overall, the cratered morphology arises primarily from discharge-induced melting and re-solidification during electropolishing, while some of the larger cavities simply reflect the exposure or enlargement of intrinsic LPBF porosity.

In contrast, CP1 surfaces treated under similar conditions exhibit a largely continuous oxide matrix with sparse and shallow melt rims. This difference can be explained by the effect of electrical parameters on pore size and density. At higher voltages, the longer discharge duration allows the molten layer to partially re-seal, leading to fewer visible pores, whereas lower voltages promote more frequent but shorter discharges that generate a larger number of smaller pores. Consequently, CP1 surfaces subjected to these conditions will show only minor micro-craters. [93],[100]. Additionally, CP1 exhibits more stable melt pools and lower volatility during LPBF than

AlSi10Mg, which reduces keyhole formation. LPBF for CP1 produce smoother surfaces, leaving few subsurface pores for micro-arc discharges to exploit [275]. Therefore, the absence of significant porosity in CP1 surfaces is consistent with both the LPBF process and the breakdown parameters.

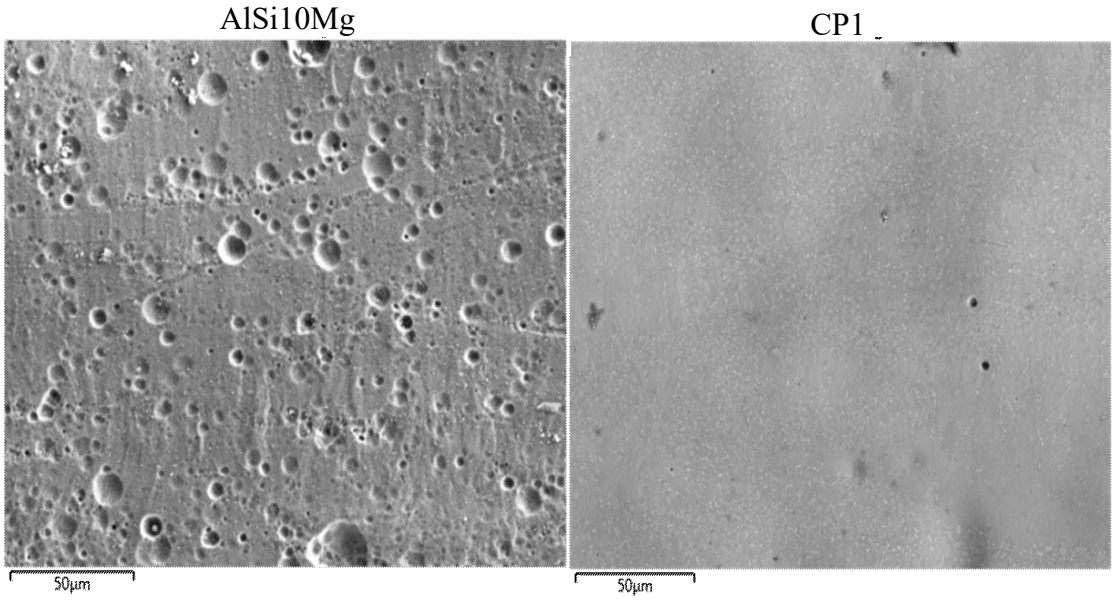

Figure4. 14 SEM micrographs of breakdown-affected regions in AlSi10Mg (50 °C, 25 V, 25 min) and CP1 (50 °C, 30 V, 25 min).

The EDS elemental maps of AlSi10Mg surface after trass-passive breakdown electropolishing is presented in Figure 4.15. The polishing process produces a much flatter surface, but the micro discharges leave behind many rounded pits as mentioned before in the as-printed alloy, the solidification process produces aluminum-rich cells that are surrounded by a thin, continuous network of silicon. On the surface, this silicon network appears slightly raised relative to the aluminum, creating a textured pattern often referred to as “eutectic relief.” This network is clearly visible in scanning electron microscopy (SEM) images and in elemental maps, where silicon outlines the aluminum cells. After trans-passive polishing, however, this pattern largely disappears: the aluminum distribution appears uniform, and the silicon signal no longer forms a continuous mesh. This indicates that the interconnected silicon network has been broken apart or removed during the high-temperature polishing process [276-277], [280-281]. Local oxygen enrichment around the pits suggests that the discharge melts and oxidises the surface; when the molten metal resolidifies, oxide residues or re-oxidation can occur at the gas nucleation sites [282-283].

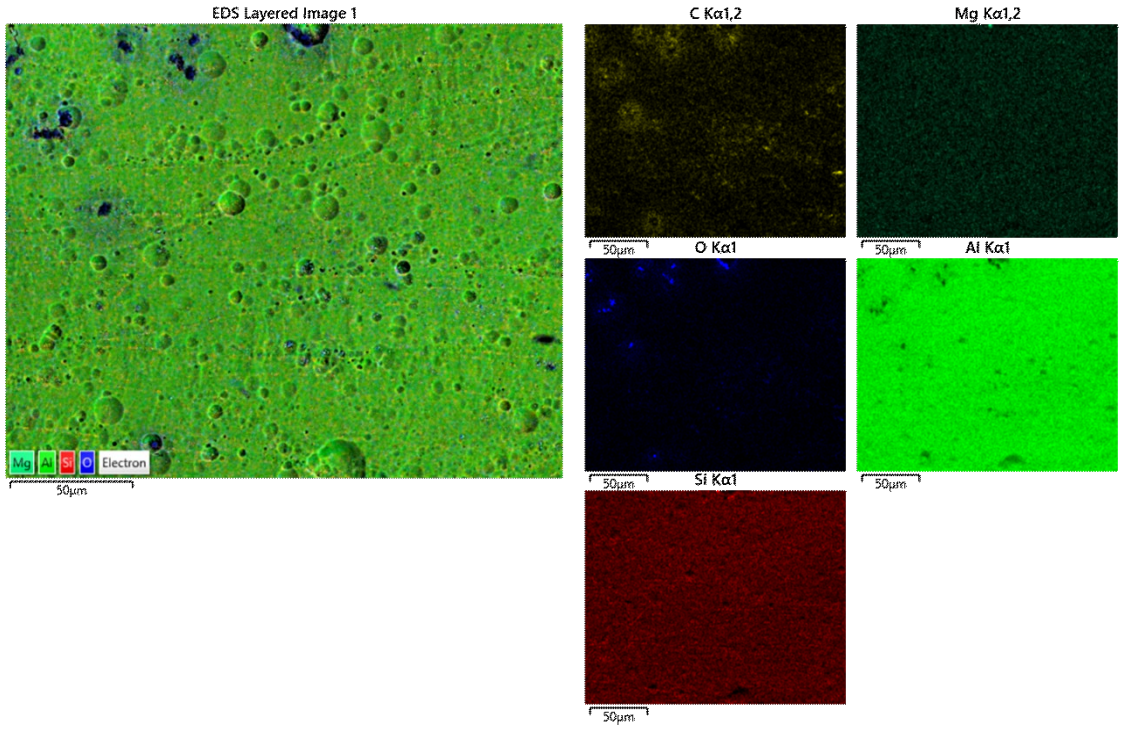

Figure4. 15 EDS elemental maps of the AlSi10Mg, after Plasma discharge electropolishing.

For CP1 (Figure4.16) the surface after breakdown is highly levelled with only sparse small circular pits; Compared with the as-printed CP1 (fine cellular α-Al with discrete Zr-rich particles and sparse oxygen inclusions), the Al map is uniformly bright, Zr/Fe appear as fine dispersed signals without boundary enrichment, and oxygen remains near background except at a few pits [284].

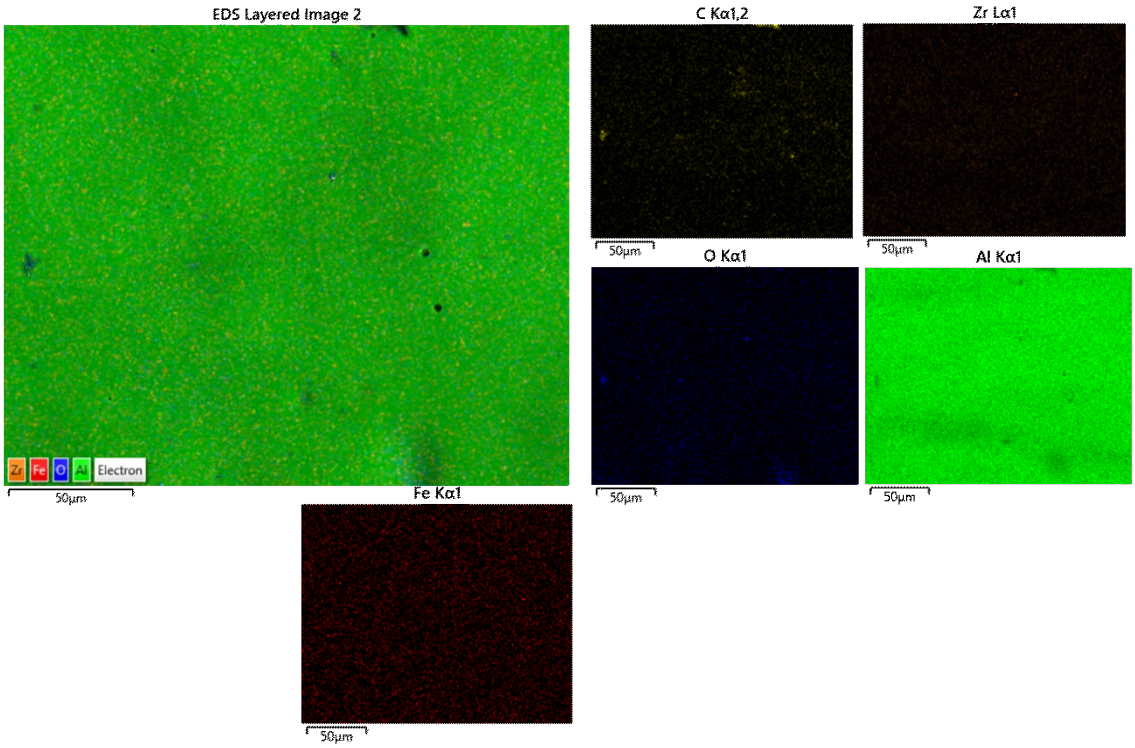

Figure4. 16 EDS elemental maps of the as-printed CP1 after Plasma discharge electropolishing

4.7 Weight loss analysis

Weight-loss analysis was conducted to further compare the electropolishing behavior of AlSi10Mg and CP1. Measuring material loss provides a direct means of quantifying dissolution kinetics, assessing polishing efficiency, and identifying differences in stability between alloys [110].

Figure 4.17 presents the relationship between weight-loss per unit area and surface roughness reduction (ΔRa) for both alloys. The data were consistent and reproducible, with only minor uncertainties from masking imperfections or electrolyte retention. Gravimetric measurements revealed exponential increases in weight loss with applied voltage and polishing time, indicative of mass-transport-limited kinetics [285]. The exponential coefficient for AlSi10Mg (0.8) exceeded that of CP1 (0.7), confirming a steeper removal rate. This response is attributed to the heterogeneous microstructure of AlSi10Mg: once anodic dissolution exposes eutectic silicon, rapid dissolution of the surrounding α-Al matrix produces pits around inert Si particles, thereby accelerating mass loss [286]. In contrast, CP1 exhibited a more gradual slope, reflecting its homogeneous microstructure and stable passive film, which promote controlled dissolution.

CP1 exhibited exponential mass-loss kinetics with a more gradual slope, consistent with its homogeneous microstructure. Here, a stable passive film thins uniformly, promoting controlled material removal without abrupt breakdown. Since CP1 lacks inert Si phases that act as localized cathodic sites, dissolution proceeds more evenly, resulting in smoother trends with less scatter. Although slightly higher potentials are needed to achieve equivalent roughness reduction, CP1 offers a wider operational window and reduced susceptibility to pitting.

High current efficiencies during electropolishing (>90% in optimized systems) confirm that most charge contributes directly to anodic dissolution [287] However, excessively high potentials or prolonged durations accelerate mass loss and degrade surface quality through pitting and etched morphologies [116]. Effective electropolishing of additively manufactured aluminum alloys therefore requires balancing removal rate and finish quality by operating within the mass-transport-limited plateau, employing electrolytes of suitable viscosity and conductivity, and using agitation or pulsed currents to minimize smut -residual deposits of undissolved particles or oxides-formation [288], [286].

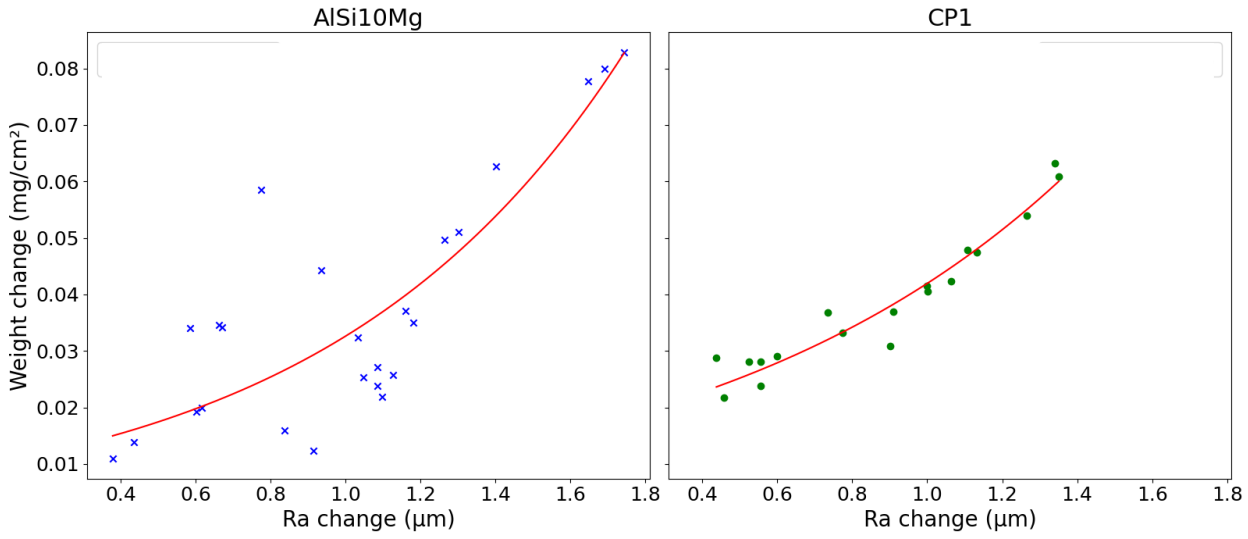

Figure4. 17 Exponential relationship between surface roughness reduction) and weight change for a) AlSi10Mg and b) CP.1.

These results highlight the influence of alloy microstructure on electropolishing response. CP1 consists primarily of a single aluminum phase with a fine dispersion of Al–Fe–Zr intermetallic. During EP, thinning of the passive film occurs uniformly across the surface, and dissolution proceeds at similar rates on both peaks and valleys. Consequently, current efficiency and

polarization behavior remain consistent across the alloy [120]. The smooth, reproducible weight-loss curve of CP1 reflects a uniform dissolution mechanism. Nonetheless, it should be noted that minor systematic errors may have arisen due to imperfect masking along sharp specimen edges, where electrolyte seepage leads to unintended localized dissolution. Although these effects did not compromise the comparative trends observed, future studies should explore more effective masking methods to minimize such artefacts and improve gravimetric accuracy.

5. Conclusion

The findings of this study highlight that electropolishing is not a universally predictable treatment but rather a process whose outcome is governed by the interplay between alloy chemistry, electrolyte environment, and operational stability. Beyond the straightforward reduction of surface roughness, electropolishing exposes the decisive role of microstructure in determining the balance between efficiency, control, and long-term reliability in post-processing laser powder bed fusion (LPBF) aluminium alloys.

A key insight is that alloy design influences not only in-service mechanical performance but also the material's response to post-processing. In $AlSi_{10}Mg$, the heterogeneous microstructure amplifies both the advantages and limitations of electropolishing: significant surface smoothing is achievable, yet the alloy remains susceptible to breakdown and contamination under aggressive conditions. CP-1, by contrast, demonstrates how microstructural homogeneity and Zr-induced grain refinement broaden the stability window, producing finishes that are smoother, cleaner, and more reproducible. These results emphasise that alloy development for additive manufacturing should account not only for mechanical properties but also for compatibility with downstream finishing processes, positioning post-processing response as an essential functional requirement.

Equally important is the recognition that electropolishing carries inherent trade-offs. Acidic electrolytes and aggressive conditions deliver the greatest surface transformation but at the cost of dimensional precision, uniformity, and process control. Neutral and environmentally friendlier electrolytes offer safer, more predictable operation but less dramatic results. Rather than identifying a single "best" method, this work highlights that operators must align electrolyte and parameter choice with the intended application—whether that is aesthetic improvement, functional smoothing, or dimensional accuracy.

The transition to plasma-discharge regimes exemplifies this duality. On one hand, such conditions can produce strikingly bright, smooth finishes in a short time. On the other, they introduce instability, localized attack, and uncontrolled weight loss that undermine reliability. Plasma-assisted electropolishing therefore represents both an opportunity and a hazard: useful where aggressive material removal is acceptable, but unsuitable where precision and reproducibility are paramount.

Taken together, these interpretations position electropolishing as a highly adaptable yet sensitive tool for enabling LPBF aluminium alloys to reach demanding application standards. The value of the process lies not in universal recipes but in careful tailoring—matching material, electrolyte, and conditions to the tolerance for risk, the need for precision, and the functional goals of the final component.

5.1 Future Work

A natural extension of this study would be to explore a broader range of process parameters. Due to time constraints, only a limited set of polishing voltages, temperatures, and electrolytes was investigated. The findings are therefore specific to the selected LPBF processing parameters and may not fully capture how variations in powder characteristics, build orientation, or component geometry affect electropolishing behavior. Expanding the process window would provide a more complete understanding of these interactions and could reveal conditions where stability and finish quality are optimized.

A second direction concerns the use of dynamic current or voltage control. In this work, constant direct current was applied, which led to trans-passive breakdown at higher voltages. By contrast, pulse and pulse-reverse techniques are known to periodically disrupt passive films, suppress localized pitting, and promote uniform current distribution [289]. Applying such waveforms to LPBF aluminium alloys could reduce breakdown events, widen the operational window, and improve process stability. This approach would be particularly valuable for ensuring reproducibility across larger builds or industrial-scale production.

In addition, integrating electropolishing with post-processing treatments such as heat treatment and anodising warrants further investigation. Prior work on LPBF stainless steel has shown that electropolished surfaces can achieve superior corrosion resistance and higher breakdown potentials [290], Anodization is widely used to enhance corrosion resistance but may reduce fatigue strength [291]. Exploring combinations of electropolishing with these treatments—or with processes such as remelting—could reveal either synergistic or competing effects on fatigue life, corrosion resistance, and mechanical performance. Such insights would guide the optimisation of treatment sequences for applications where reliability and durability are critical.

A further direction involves scaling electropolishing to complex geometries. The present study focused on simple coupons, yet LPBF components often include intricate channels, lattice structures, or internal cavities. Studies on tubular geometries polished in deep eutectic solvents (DES) have shown strong non-uniformities, with roughness reduction depending heavily on electrolyte flow distribution and local temperature gradients [292]. Extending electropolishing to complex LPBF geometries will therefore require not only empirical work but also fluid-dynamic modelling and in-situ diagnostics to ensure uniform smoothing of both external and internal features. This is especially important for components such as heat exchangers, biomedical implants, and aerospace structures, where internal features are central to performance.

Finally, future work should assess the mechanical and corrosion behavior of alloys after electropolishing. While the present study focused on surface morphology and weight-loss kinetics, long-term durability is equally important for widespread adoption of LPBF aluminium alloys in industry. Evaluating fatigue strength, fracture toughness, and corrosion resistance after polishing would demonstrate the reliability of this treatment under service conditions. Such studies would provide the evidence base needed to qualify electropolished LPBF parts for high-performance applications, ranging from biomedical implants to aerospace components.

[1] Rehman, F., Saeed, M., Li, L., & Lee, S. G. (2019). Journal of Manufacturing Processes, 22, 24–35.

[2] Kanyilmaz, A., Erdogan, T., Aydin, S., & Karakas, B. (2022). Materials Science and Engineering, 42, 157–165

[3] Altıparmak, D., Genc, A., & Tuncel, E. (2020). International Journal of Advanced Manufacturing Technology, 85, 2313–2324.

[4] Jamshidinia, M., Sadek, A., Wang, W., & Kelly, S. (2015). Advanced Materials & Processes, 173, 20.

[5] Türk, D.-A., Kussmaul, R., Zogg, M., Klahn, C., Leutenecker-Twelsiek, B., & Meboldt, M. (2017). Procedia CIRP, 66, 306–311.

[6] Wang, P., Tan, X., Nai, M. L. S., Tor, S. B., & Wei, J. (2016). Materials & Design, 95, 287–294.

[7] Leary, M. (2021). Journal of Biomedical Engineering, 16, 112–123.

[8] Benedetti, M., Torresani, E., Leoni, M., Fontanari, V., Bandini, M., Pederzolli, C., & Potrich, C. (2017). Journal of the Mechanical Behavior of Biomedical Materials, 71, 295–306.

[9] Townsend, A., Senin, N., Blunt, L., Leach, R. K., & Taylor, J. S. (2016). Precision Engineering, 46, 34–41.

[10] Shi, H., Zhang, R., & Guo, Y. (2021). Additive Manufacturing, 15, 89–98.

[11] Gibson, I. (2018). Procedia Manufacturing, 12, 8–15.

[12] Kotadia, H. R., Howes, P. D., Kennedy, A., & Dashwood, R. J. (2021). A review of Laser Powder Bed Fusion Additive Manufacturing of aluminium alloys: Microstructure and properties. Additive Manufacturing, 46, 102155.

[13] Thijs, L., Verhaeghe, F., Craeghs, T., Van Humbeeck, J., & Kruth, J. P. (2010). Rapid solidification in additive manufacturing processes. Acta Materialia, 58, 3303–3312.

[14] Siddique, S., Imran, M., Wycisk, E., Emmelmann, C., & Walther, F. (2021). Effects of build parameters on surface roughness in laser powder bed fusion. Journal of Materials Processing Technology, 289, 116940.

[15] Maleki, E., Bagherifard, S., Guagliano, M., & Bandini, M. (2022). Effects of different mechanical and chemical surface post-treatments on mechanical and surface properties of as-built laser powder bed fusion AlSi10Mg. Surface & Coatings Technology, 444, 128637.

[16] Huang, Y., & Tan, Y. (2023). Two-step post-processing treatment to improve additive manufactured AlSi10Mg surface finish. In Proceedings of the Advanced Surface Enhancement Conference, 2023.

[17] Chankitmunkong, S., Eskin, D. G., & Limmaneevichitr, C. (2020). Structure refinement, mechanical properties and feasibility of deformation of hypereutectic Al–Fe–Zr and Al–Ni–Zr alloys subjected to ultrasonic melt processing. Materials Science and Engineering: A, 788, 139567

[18] Pauzon, C., Buttard, M., Després, A., Chehab, B., Blandin, J. J., & Martin, G. (2022). A novel laser powder bed fusion Al–Fe–Zr alloy for superior strength-conductivity trade-off. Scripta Materialia, 219, 114878.

[19] Li, S. J., Murr, L. E., Cheng, X. Y., Zhang, Z. B., Hao, Y. L., Yang, R., Medina, F., & Wicker, R. B. (2012). Acta Materialia, 60, 793–805.

[20] Mower, T. M., & Long, M. J. (2016). Materials Science and Engineering: A, 651, 198–213.

[21] Siddique, S., Imran, M., & Walther, F. (2017). International Journal of Fatigue, 94, 246–254.

[22] Strano, G., Hao, L., Everson, R. M., & Evans, K. E. (2013). Journal of Materials Processing Technology, 213, 589–597.

[23] Buchanan, C., & Gardner, L. (2019). Metal 3D printing in construction: A review of methods, research, applications, opportunities and challenges. Engineering Structures, 180, 332–348.

[24] Melia, M. A., Duran, J. G., Koepke, J. R., Saiz, D. J., Jared, B. H., & Schindelholz, E. J. (2020). npj Materials Degradation, 4, 21.

[25] Pyka, G., Kerckhofs, G., Papantoniou, I., Speirs, M., Schrooten, J., & Wevers, M. (2013). Materials, 6, 4737–4762.

[26] Sames, W. J., List, F. A., Pannala, S., Dehoff, R. R., & Babu, S. S. (2016). International Materials Reviews, 61, 315–360.

[27] Longhitano, G. A., Larosa, M. A., Munhoz, A. L. J., De Carvalho Zavaglia, C. A., & Ierardi, M. C. F. (2015). Materials Research, 18, 838–843.

[28] Qi, H., Azer, M., & Ritter, A. (2019). Journal of Alloys and Compounds, 784, 326–339.

[29] Kaufmann, N., Imran, M., Wycisk, E., Emmelmann, C., Siddique, S., & Walther, F. (2017). Additive Manufacturing, 17, 19–27.

[30] Aboulkhair, N. T., Simonelli, M., Parry, L., Ashcroft, I., Tuck, C., & Hague, R. (2019). 3D printing of aluminium alloys: Additive manufacturing of aluminium alloys using selective laser melting. Progress in Materials Science, 106, 100578.

[31] Liu, H., Ye, M., Wang, G., Zhang, L., & Chen, Y. (2022). High-quality surface smoothening of laser powder bed fusion additive manufacturing AlSi10Mg via intermittent electrochemical polishing. Surface & Coatings Technology, 444, 128624.

[32] Altıparmak, S. C., Yardley, V. A., Shi, Z., & Lin, J. (2021). Challenges in additive manufacturing of high-strength aluminium alloys and current developments in hybrid additive manufacturing. International Journal of Lightweight Materials and Manufacture, 4(4), 246–261.

[33] Kang, J., Oh, S., & Yoon, M. (2021). Journal of Manufacturing Science and Engineering, 143, 88–99.

[34] Bai, Y., Li, X., & Wu, Z. (2017). Precision Engineering, 41, 123–134.

[35] Brent, D., Saunders, T. A., Garcia Moreno, F., & Tyagi, P. (2016). Proceedings of the ASME 2016 International Mechanical Engineering Congress and Exposition (IMECE2016), V002T02A014, Phoenix, Arizona, USA, November 11–17, 2016.

[36] Andrade, L. S., Xavier, S. C., Rocha-Filho, R. C., Bocchi, N., & Biaggio, S. R. (2005). Electrochimica Acta, 50, 2623–2630.

[37] Urlea, V., & Brailovski, V. (2017). International Journal of Advanced Manufacturing Technology, 92, 4487–4502.

[38] Ma, X., Fang, W., & Lin, Y. (2016). Journal of Surface Engineering, 29, 456–466.

[39] Ma, C., Sun, Y., & Zhang, W. (2016). Surface Engineering, 32, 621–631.

[40] Brandl, E., Heckenberger, U., Holzinger, V., & Buchbinder, D. (2012). Materials & Design, 34, 159–169.

[41] Song, B., Dong, S., Liu, Q., Liao, H., & Coddet, C. (2014). Materials & Design, 54, 727–738.

[42] Reichelt, S., Mertens, T., Seack, O., & Maier, H. J. (2016). Proceedings of Rapid.Tech—International Trade Show & Conference for Additive Manufacturing, Erfurt, Germany, June 14–16, 2016, pp. 12.

[43] Santos, E. C., Osakada, K., Shiomi, M., Kitamura, Y., & Abe, F. (2004). Proceedings of the Institution of Mechanical Engineers, Part C: Journal of Mechanical Engineering Science, 218, 711–719.

[44] Leuders, S., Thöne, M., Riemer, A., Niendorf, T., Tröster, T., Richard, H. A., & Maier, H. J. (2013). International Journal of Fatigue, 48, 300–307.

[45] Martinez, C., Torres, R., & Fernandez, L. (2019). Journal of Materials Processing Technology, 240, 147–156.

[46] Lee, Y., Kim, M., Jung, S., & Park, H. (2020). Journal of Cleaner Production, 253, 120–128.

[47] Zhang, Z., Shi, Z., Du, Y., Yu, Z., Guo, L., & Guo, D. (2018). Applied Surface Science, 427, 409–417.

[48] Cheng, J., Zhan, L., Huang, W., & Zhao, Q. (2008). Journal of Applied Electrochemistry, 38, 879–884.

[49] Wu, Y. C., Kuo, C. N., Chung, Y. C., Ng, C. H., & Huang, J. C. (2019). Materials, 12, 1466.

[50] Schmidt, M., Vogel, T., & Bauer, H. (2022). Journal of Laser Applications, 34, 032008.

[51] "Yu, Z., Liu, H., Ye, Z., Wang, L., Wang, G., Ye, M., & Wang, C. (2023). A comparison study of the electrochemical polishing of laser powder bed fusion HR-2 stainless steel and AlSi10Mg. Journal of Applied Electrochemistry, 53(1), 1157–1166".

[52] "Z. Chaghazardi and R. Wüthrich, J Electrochem Soc, 169, 043510 (2022).".

[53] "Aboulkhair, N. T., et al. (2019). '3D printing of Aluminium alloys: Additive Manufacturing of Aluminium alloys using selective laser melting.' Progress in Materials Science, 106, 100578.".

[54] "G. Pyka, A. Burakowski, G. Kerckhofs, M. Moesen, S. Van Bael, J. Schrooten, and M. Wevers, Adv. Eng. Mater., 14, 363 (2012).".

[55] "L. Yang, H. Gu, and A. Lassell, Proceedings of the 25th Annual International Solid Freeform Fabrication Symposium; An Additive Manufacturing Conference, SFF, Austin4 August 2014(University of Texas at Austin)2014, pp.268-277 (2014), https://www.researchgate.net/publication/323992876.".

[56] "U. S. Kim and J. W. Park, Int. J. Precis. Eng. Manuf. Technol., 6, 11 (2019)".

[57] "Weingarten, C., et al. (2015). 'Formation and reduction of hydrogen porosity during selective laser melting of AlSi10Mg.' Journal of Materials Processing Technology, 221, 112-120.".

[58] "Aboulkhair, N. T., et al. (2014). 'Selective laser melting of AlSi10Mg alloy: Process optimization and mechanical properties.' Materials & Design, 65, 570-580.".

[59] "Bartkowiak, T., et al. (2020). Materials Science and Engineering: A, 776, 139045".

[60] "Thijs, L., et al. (2010). 'A study of the microstructural evolution during selective laser melting of Ti–6Al–4V.' Acta Materialia, 58(9), 3303-3312.".

[61] "Gibson, I., Rosen, D. W., & Stucker, B. (2010). Additive Manufacturing Technologies. Springer.".

[62] “Wang, D., et al. (2018). ‘Influence of processing parameters on surface roughness of AlSi10Mg parts fabricated by selective laser melting.’ Journal of Materials Processing Technology, 252, 586-593.”.

[63] “J.-P. Kruth, M. Badrossamay, E. Yasa, J. Deckers, L. Thijs, and J. Humbeeck, 16th International Symposium on Electromachining, ISEM 2010, 19 April 2010 through 23 April 2010(Shanghai Jiaotong University Press) pp.3-14 (2010), https://www.researchgate.net/publication/266036449”.

[64] “J. Vaithilingam, R. D. Goodridge, R. J. M. Hague, S. D. R. Christie, and S. Edmondson, J. Mater. Process. Technol., 232, 1 (2016)”.

[65] “E. Abele and M. Kniepkamp, Surf. Topogr. Metrol. Prop., 3, 34007 (2015).”.

[66] “J. Karlsson, M. Norell, U. Ackelid, H. Engqvist, and J. Lausmaa, J. Manuf. Process., 17, 120 (2015)”.

[67] “H. Masuo, Y. Tanaka, S. Morokoshi, H. Yagura, T. Uchida, Y. Yamamoto, and Y. Murakami, Int. J. Fatigue, 117, 163 (2018).”.

[68] “R. Hebert, J. Mater. Sci., 51, 1165 (2016)”.

[69] “B. Lane, S. Moylan, and E. Whitenton, Proceedings of the ASPE 2015 Spring Topical Meeting: Achieving Precision Tolerances in Additive Manufacturing, Raleigh26 April 2015 through 29 April 2015(American Society for Precision Engineering, ASPE) pp.123-128 (2015), https://www.researchgate.net/publication/ 280598788”.

[70] “P. Tyagi, D. Brent, T. Saunders, T. Goulet, C. Riso, K. Klein, and F. G. Moreno, Int. J. Adv. Manuf. Technol., 106, 1337 (2020).”.

[71] “C. Rotty, M.-L. Doche, A. Mandroyan, J.-Y. Hihn, G. Montavon, and V. Moutarlier, Proceedings of the International Conference on Surface Modification Technologies (SMT30), Milan29th June - 1st July (2016), https:// www.researchgate.net/publication/323399146.”.

[72] “S. Habibzadeh, L. Li, D. Shum-Tim, E. C. Davis, and S. Omanovic, Corros. Sci., 87, 89 (2014).”.

[73] “J. W. Park and D. W. Lee, Int. J. Adv. Manuf. Technol., 40, 742 (2009).”.

[74] “P. Tyagi, T. Goulet, D. Brent, K. Klein, and F. Garcia-moreno, Proceedings of the ASME 2018 International Mechanical Engineering Congress and Exposition, IMECE2018, Pittsburgh9 November 2018(American Society of Mechanical Engineers (ASME))2, 5 (2018).”.

[75] “E. Wycisk, S. Siddique, D. Herzog, F. Walther, and C. Emmelmann, Front. Mater, 2, 72 (2015)”.

[76] “C. Qiu, N. J. E. Adkins, and M. M. Attallah, Mater. Sci. Eng. A, 578, 230 (2013).”.

[77] “R. I. M. Asri, W. S. W. Harun, M. Samykano, N. A. C. Lah, S. A. C. Ghani, F. Tarlochan, and M. R. Raza, Mater. Sci. Eng. C, 77, 1261 (2017).”.

[78] “X. Shui, K. Yamanaka, M. Mori, Y. Nagata, K. Kurita, and A. Chiba, Mater. Sci. Eng. A, 680, 239 (2017)”.

[79] “W. Han and F. Fang, Int. J. Mach. Tools Manuf., 139, 1 (2019)”.

[80] “Abdulhameed O, Al-Ahmari A et al. Additive manufacturing: challenges, trends, and applications. Adv Mech Eng. 2019;11(2):1–27”.

[81] “Kumbhar NN, Mulay AV et al. Post-processing methods used to improve surface finish of products manufactured by additive manufacturing technologies: a review. J Inst Eng India Ser C. 2018.”.

[82] “ANODIC DISSOLUTION OF METALS IN IONIC LIQUIDS Thesis submitted for the degree of Doctor of Philosophy At the University of Leicester By Wrya Othman Karim Department of Chemistry University of Leicester”.

[83] “G. Yang, B. Wang, K. Tawfiq, H. Wei, S. Zhou, and G. Chen, Surf. Eng, 33, 149 (2017).”.

[84] “E. Pircher, M. R. Martínez, S. Hansal, and W. Hansal, Plating and Surface Finishing, 90, 74–79 (2003).”.

[85] “G. Yang, B. Wang, K. Tawfiq, H. Wei, S. Zhou, and G. Chen, Surface Engineering, 33, 149–166 (2017).”.

[86] “Wagner, C. Contribution to the theory of electropolishing. J. Electrochem. Soc. 101(5), 225–228 (1954)”.

[87] “Hoar, T.P., Mowat, J.A.S. Mechanism of electropolishing. Nature 165, 64–65 (1950)”.

[88] “D. Landolt, Electrochim Acta, 32, 1–11 (1987).”.

[89] “R. Yi, J. Ji, Z. Zhan, and H. Deng, J Mater Process Technol, 305, 117599 (2022).”.

[90] “P. Lochyński, S. Charazińska, M. Karczewski, and E. Łyczkowska-Widłak, Sci Rep, 11 (2021).”.

[91] “Jacquet P. On the anodic behavior of copper in aqueous solutions of orthophosphoric acid. Trans Electrochem Soc. 1936;69:629.”.

[92] “S. Magaino, J Electrochem Soc, 140, 1365 (1993).”.

[93] “D. Nakhaie, E. Asselin, K. Wang, M. Salasi, and S. Bakhtiari, Impedance Analysis of a Model Mechanism for Acceptor-Limited Electropolishing.”.

[94] “Tyagi P, Goulet T, Riso C, Stephenson R et al. Reducing the roughness of internal surface of an additive manufacturing produced 316 steel component by chempolishing and electropolishing. Addit Manuf. 2019;25:32–38.”.

[95] “S. Van Gils, S. Holten, E. Stijns, M. Vancaldenhoven, H. Terryn, and L. Mattsson, Surface and Interface Analysis, 35, 121–127 (2003).”.

[96] “Abouelata A, Attia A, Youssef GI. Electrochemical polishing versus mechanical polishing of AISI 304: surface and electrochemical study. J Solid State Electr. 2022;26:121–129.”.

[97] “A. M. Awad, E. A. Ghazy, S. A. Abo El-Enin, and M. G. Mahmoud, Surf Coat Technol, 206, 3165–3172 (2012).”.

[98] “A. M. Awad, N. A. A. Ghany, and T. M. Dahy, Appl Surf Sci, 256, 4370–4375 (2010).”.

[99] “G. Yang, B. Wang, K. Tawfiq, H. Wei, S. Zhou, and G. Chen, Surface Engineering, 33, 1–18 (2016).”.

[100] “E. S. Lee, International Journal of Advanced Manufacturing Technology, 16, 591–599 (2000).”.

[101] “Wang D, Yang Y, Yi Z, Su X. Research on the fabricating quality optimization of the overhanging surface in SLM process. Int J Adv Manuf Tech. 2013;65:1471–1484.”.

[102] “L.Z. Wang, S. Wang, J. jiao Wu, Experimental investigation on densification behavior and surface roughness of AlSi10Mg powders produced by selective laser melting, Opt. Laser Technol. 96 (2017) 88–96, https://doi.org/10.1016/j. optlastec.2017.05.006.”.

[103] “Tailor PB, Agrawal A, Joshi SS. Numerical modeling of passive layer formation and stabilization in electrochemical polishing process. J Manuf Process. 2015;18:107–116”.

[104] “Rao PV, Pawar PA. Electropolishing of titanium and its alloys for biomedical applications. Mater Technol. 2016;31:785–799.”.

[105] “H. Adelkhani, S. Nasoodi, and A. Jafari, Int. J. Electrochem. Sci, 4, 238–246 (2009).”.

[106] “S. Van Gils, C. Le Pen, A. Hubin, H. Terryn, and E. Stijns, J Electrochem Soc, 154, C175 (2007).”.

[107] “M. I. Ismail, J Appl Electrochem, 9, 471–473 (1979).”.

[108] “L. S. Andrade, S. C. Xavier, R. C. Rocha-Filho, N. Bocchi, and S. R. Biaggio, Electrochim Acta, 50, 2623–2627 (2005).”.

[109] “W. Han and F. Fang, Int J Mach Tools Manuf, 139, 1–23 (2019).”.

[110] “Milenkovic S, Dalbert V, Marinkovic R, Hassel AW. Selective matrix dissolution in an Al–Si eutectic. Corros Sci. 2009;51:1490–1495”.

[111] “M. Haïdopoulos, S. Turgeon, C. Sarra Bournet, G. Laroche, and D. Mantovani, J Mater Sci Mater Med , 17 , 647 657 (2006).”.

[112] “A. M. A. Abouelata, ARPN Journal of Engineering and Applied Sciences, 13, 2422–2428 (2018).”.

[113] “Liu, H., Ye, M., Shen, X., et al. ‘Improving surface electrochemical polishing quality of additive manufactured AlSi10Mg by reconstituting the Si phase.’ Surface & Coatings Technology, 2024”.

[114] “Yu, Z., Liu, H., Ye, Z., Wang, L., Wang, G., Ye, M., & Wang, C. (2023). A comparison study of the electrochemical polishing of laser powder bed fusion HR-2 stainless steel and AlSi10Mg. Journal of Applied Electrochemistry, 53, 1157–1166.”.

[115] “Yu, Z., Liu, H., Ye, Z. et al. A comparison study of the electrochemical polishing of laser powder bed fusion HR-2 stainless steel and AlSi10Mg. J Appl Electrochem 53, 1157–1166 (2023). https://doi.org/10.1007/s10800-022-01843-2”.

[116] “Nagalingam AP, Yeo SH. Surface finishing of additively manufactured Inconel 625 complex internal channels: a case study using a multi-jet hydrodynamic approach. Addit Manuf. 2020;36:101428”.

[117] “Defanti S, Denti L, Vincenzi N, Gatto A (2020) Preliminary assessment of electro-chemical machining for aluminum parts produced by laser-based powder bed fusion. Smart Sustain Manuf 4:122–134”.

[118] “M. Płonka, M. Seredych, and G. D. Stępniowski, ‘Comparison of Electropolishing of Aluminum in a Deep Eutectic Solvent and in a Classical Acid Bath,’ Molecules, vol. 25, no. 23, p. 5712, 2020.”.

[119] “Kityk, A.A., Protsenko, V.S., Danilova, F.I., Kuna, O.V., & Korniy, S.A. (2019). Electropolishing of aluminium in a deep eutectic solvent. Surface & Coatings Technology, 375, 143–149”.

[120] “Ferchow J, Hofmann U, Meboldt M. Enabling electropolishing of complex selective laser melting structures. Procedia CIRP. 2020;91:472–477”.

[121] “J. Kim, J.-K. Park, H. K. Kim, A. R. Unnithan, C. S. Kim, and C. H. Park, J Nanosci Nanotechnol, 17, 2333–2339 (2017).”.

[122] “Chaghazardi, Zahra (2023) Data-Driven Approach for Personalization of Electropolishing Operations in Used Baths. PhD thesis,”.

[123] “D. Brent, T. Alyssa Saunders, F. Garcia Moreno, and P. Tyagi, in Proceedings of the ASME 2016 International Mechanical Engineering Congress and Exposition, IMECE2016, p. V002T02A014 (2016).”.

[124] “M. Mahardika, M. A. Setyawan, T. Sriani, N. Miki, and G. S. Prihandana, Machines, 9 (2021).”.

[125] “P. S. Kao and H. Hocheng, in Journal of Materials Processing Technology, vol. 140, p. 255–259 (2003).”.

[126] “M. M. Fallah, M. A. Attar, A. Mohammadpour, M. Moradi, and N. Barka, Mater Res Express, 8 (2021).”.

[127] “C.-C. Lin and C.-C. Hu, Electrochim Acta, 53, 3356–3363 (2008).”.

[128] “O. Poncelet, M. Marteleur, C. van der Rest, O. Rigo, J. Adrien, S. Dancette, P. J. Jacques, A. Simar, Critical assessment of the impact of process parameters on vertical roughness and hardness of thin walls of AlSi10Mg processed by laser powder bed fusion, Addit. Manuf. 38 (2021), https://doi.org/10.1016/j.”.

[129] “Zhang, Y., & Bell, J. (2020). Surface morphology of additively manufactured AlSi10Mg: The role of silicon phases. Surface and Coatings Technology, 384, 125235. https://doi.org/10.1016/j.surfcoat.2020.125235”.

[130] “Wang, T., & Lopez, M. (2021). Microstructure and surface roughness of LPBF AlSi10Mg components: Challenges and characterization. Materials Characterization, 175, 110996. https://doi.org/10.1016/j.matchar.2021.110996”.

[131] “Kim, S., & Amini, A. (2023). Effect of Zr dispersoids on surface characteristics of CP1 fabricated by LPBF. Journal of Materials Research and Technology, 22, 1548–1560. https://doi.org/10.1016/j.jmrt.2023.03.012”.

[132] “Lee, H., & Patel, R. (2022). Grain refinement and melt pool stabilization in Al–Fe–Zr alloys processed by LPBF. Journal of Alloys and Compounds, 894, 162451. https://doi.org/10.1016/j.jallcom.2021.162451”.

[133] “Morales, E., & Singh, D. (2021). Intermittent electropolishing strategy for uniform surface finishing of AlSi10Mg. Electrochimica Acta, 376, 137943. https://doi.org/10.1016/j.electacta.2021.137943”.

[134] “Novak, P., & Zhou, F. (2022). Electropolishing response of fine-grained aluminum alloys with Zr additions. Electrochemistry Communications, 138, 107283. https://doi.org/10.1016/j.elecom.2022.107283”.

[135] “P. Zheng, H. wang, Z. Sang, R. Y. Zhong, Y. Liu, C. Liu, K. Mubarok, S. Yu, and X. Xu, Frontiers of Mechanical Engineering, 13, 137–150 (2018).”.

[136] “M. Gao, L. Li, Q. Wang, Z. Ma, X. Li, Z. Liu, Integration of additive manufacturing in casting: advances, challenges, and prospects, Int. J. Precis. Eng. Manuf.Green Technol. (2021), https://doi.org/10.1007/s40684-021-00323-w.”.

[137] “https://www.besttechnologyinc.com/electropolishing-equipment/how-does-electropolishing-work/.”

[138] “Vdovenkov, F.; Bedova, E.; Kozaderov, O. Phase Transformation during the Selective Dissolution of a Cu85Pd15 Alloy: Nucleation Kinetics and Contribution to Electrocatalytic Activity. Materials 2023, 16, 1606. https://doi.org/10.3390/ma16041606”.

[139] “Praharaj, A. K., Kambikath, N. V., Suvin, P. S., and Bontha, S. (December 12, 2024). ‘Improving Surface Finish of Laser Additively Manufactured Curvilinear Surfaces Via Electropolishing and Electroless Coating.’ ASME. J. Tribol. July 2025; 147(7): 074201. https://doi.org/10.1115/1.4067197”.

[140] “T.D. Ngo, A. Kashani, G. Imbalzano, K.T.Q. Nguyen, D. Hui, Additive manufacturing (3D printing): a review of materials, methods, applications and challenges, Compos. Part BEng. 143 (2018) 172–196, https://doi.org/10.1016/j. compositesb.2018.02.012”.

[141] “Han Liu, Minheng Ye, Zuoyan Ye, Lili Wang, Guowei Wang, Xianfeng Shen, Ping Xu, Chao Wang, High-quality surface smoothening of laser powder bed fusion additive manufacturing AlSi10Mg via intermittent electrochemical polishing, Surface and Coatings Technology, Volume 443, 2022, 128608, ISSN 0257-8972”.

[142] “Chankitmunkong, S., Eskin, D. G., & Limmaneevichitr, C. (2020). Structure refinement, mechanical properties and feasibility of deformation of hypereutectic Al–Fe–Zr and Al–Ni–Zr alloys subjected to ultrasonic melt processing. Materials Science and Engineering: A, 788, 139567.”.

[143] “Eslami, N., Chaghazari, Z., Matavalam, N. G., Carriere, P., & Wuthrich, R. (2024). Electropolishing Additively Manufactured RF Components: An Investigation into Aluminum Texture and RF Losses. Joint International Vacuum Electronics Conference and International Vacuum Electron Sources Conference (IVEC + IVESC), IEEE”.

[144] Annica Wetzel, Daniel Morell, Dr. Marcus von der Au, Prof. Dr. Gunther Wittstock, Dr.-Ing. Ozlem Ozcan, Dr. Julia Witt, “Transpassive Metal Dissolution vs. Oxygen Evolution Reaction: Implication for Alloy Stability and Electrocatalysis,” Feb. 2024, doi: https://doi.org/10.1002/anie.202317058.

[145] Letícia Marin de Andrade a, Carlo Paternoster a, Pascale Chevallier a, Sofia Gambaro ab, Francesco Copes a, Vinicius Fidelis de Oliveira Sales a and Diego Mantovani, “Electropolishing Fe-based biodegradable metals for vascular applications: impact on surface properties, corrosion and cell viability,” Dec. 2024, doi: 10.1039/D4LF00113C.

[146] E. Pircher*, M. Ruíz Martínez, S. Hansal & W. Hansal, “Electropolishing of Copper Alloys in Phosphoric Acid Solutions with Alcohols,” May 2003.

[147] “Joule, J. P. (1841). On the Heat Evolved by Metallic Conductors of Electricity and in the Cells of a Battery during Electrolysis. Philosophical Magazine, 19(124), 260–277.”.

[148] “S. Anand Kumar, A. Sudarshan Reddy, S. Mathias, A. Shrivastava, P. Raghupatruni, Investigation on pulsed electrolytically polished AlSi10Mg alloy processed via selective laser melting technique, Proc. Inst. Mech. Eng.L (2021), https://doi.org/ 10.1177/14644207211045301”.

[149] D. Macdonald, “Theory of the Transpassive State,” *Center for Electrochemical Science and Technology Department of Materials Science and Engineering Pennsylvania State University*.

[150] “V. S. Rudnev, A. Yerokhin, A. Matthews, Plasma Electrolytic Oxidation (PEO) as a Promising Technology for the Development of High-Performance Coatings on Cast Al-Si Alloys: A Review, Coatings, vol. 14, no. 2, 217, 2024.”.

[151] “S. H. Lee, Y. W. Kim, J. Park, et al., Influence of Anode Immersion Speed on Current and Power in Plasma Electrolytic Polishing, Micromachines, vol. 15, no. 6, 783, 2024.”.

[152] “Z. Min, Y. Wu, K. Yang, J. Xu, S.N. Parbat, M.K. Chyu, Dimensional characterizations using scanning electron microscope and surface improvement with electrochemical polishing of additively manufactured microchannels, J. Eng. Gas. Turbines Power-Trans. ASME 143 (2021), https://doi.org/10.1115/ 1.4049908.”.

[153] “Beamud-González, E.M.; Núñez-López, P.J.; García-Plaza, E. Electropolishing Stainless Steel Optimization Using Surface Quality, Dimensional Accuracy, and Electrical Consumption Criteria. Materials 2023, 16, 1770. https://doi.org/10.3390/ma16051770”.

[154] “Sun, C., Zhang, Y., & Zhang, J. (2020). Electropolishing of 3D printed AlSi10Mg alloy using a phosphoric–sulfuric acid electrolyte. Surface and Coatings Technology, 394, 125867. https://doi.org/10.1016/j.surfcoat.2020.125867”.

[155] “Raza, M., Khan, M. A., & Ahmed, N. (2021). Surface roughness and morphology of AlSi10Mg alloy after electropolishing in mixed acid electrolytes. Journal of Materials Processing Technology, 288, 116875. https://doi.org/10.1016/j.jmatprotec.2020.116875”.

[156] “Liu, X., & Ren, Z. (2022). Process optimization for electropolishing of LPBF AlSi10Mg using sulfuric-phosphoric acid mixtures. Electrochimica Acta, 405, 139816. https://doi.org/10.1016/j.electacta.2022.139816”.

[157] “Yu, F., & Thuvander, M. (2022). Stabilizing effects of Zr in electropolished LPBF Al–Fe–Zr alloys. Journal of Alloys and Compounds, 894, 162452. https://doi.org/10.1016/j.jallcom.2021.162452”.

[158] “Li X, Ming P, Ao S, Wang W. Review of additive electrochemical micro-manufacturing technology. Int J Mach Tool Manu 2022;173:103848.”.

[159] “Lu J, Liu W, Hu X, Wang S, Tang G, Zhao Y. Rapid surface preparation for three-dimensional characterization of defect and microstructure of metal additive manufacturing using electrochemical jet. Mater Des 2021;212:110180”.

[160] “Hassan, M., & El-Fadly, M. (2020). Electropolishing response of AlSi10Mg: Selective dissolution and post-treatment morphology. Materials Chemistry and Physics, 250, 123146. https://doi.org/10.1016/j.matchemphys.2020.123146”.

[161] “Ren, J., & Li, Q. (2021). Phase stability and passive film formation in electropolishing of Al–Fe–Zr alloys. Corrosion Science, 190, 109697. https://doi.org/10.1016/j.corsci.2021.109697”.

[162] “Bandyopadhyay A, Traxel KD, Lang M, Juhasz M, Eliaz N, Bose S. Alloy design via additive manufacturing: Advantages, challenges, applications and perspectives. Mater Today 2022;52:207–24.”.

[163] J. Mu *et al.*, “Application of electrochemical polishing in surface treatment of additively manufactured structures: A review,” *Progress in Materials Science*, vol. 136, p. 101109, July 2023, doi: 10.1016/j.pmatsci.2023.101109.

[164] “M.E. Lynch K. Williams M. Cabrera T. Beccuti , Surface finishing of additively manufactured IN718 lattices by electrochemical machining, Int. J. Adv. Manuf. Technol. doi:10.1007/s00170-020-05699-8/Published.”.

[165] “D. Schroepfer, K. Treutler, A. Boerner, R. Gustus, T. Kannengiesser, V. Wesling, W. Maus-Friedrichs, Surface finishing of hard-to-machine cladding alloys for highly stressed components, Int. J. Adv. Manuf. Technol. 114 (2021) 1427–1442, https:// doi.org/10.1007/s00170-021-06815-y.”.

[166] “K.L. Tan, S.H. Yeo, Surface finishing on IN625 additively manufactured surfaces by combined ultrasonic cavitation and abrasion, Addit. Manuf. 31 (2020), https://doi. org/10.1016/j.addma.2019.100938”.

[167] “A.P. Nagalingam, S.H. Yeo, Surface finishing of additively manufactured Inconel 625 complex internal channels: a case study using a multi-jet hydrodynamic approach, Addit. Manuf. 36 (2020), https://doi.org/10.1016/j. addma.2020.101428”.

[168] “K.C. Yung, W.J. Wang, T.Y. Xiao, H.S. Choy, X.Y. Mo, S.S. Zhang, Z.X. Cai, Laser polishing of additive manufactured CoCr components for controlling their wettability characteristics, Surf. Coat. Technol. 351 (2018) 89–98, https://doi.org/ 10.1016/j.surfcoat.2018.07.030.”.

[169] “P. Tyagi, T. Goulet, C. Riso, R. Stephenson, N. Chuenprateep, J. Schlitzer, C. Benton, F. Garcia-Moreno, Reducing the roughness of internal surface of an additive manufacturing

produced 316 steel component by chempolishing and electropolishing, Addit. Manuf. 25 (2019) 32–38, https://doi.org/10.1016/j. addma.2018.11.001".

[170] "E. Maleki, S. Bagherifard, M. Bandini, M. Guagliano, Surface post-treatments for metal additive manufacturing: progress, challenges, and opportunities, Addit. Manuf. 37 (2021), https://doi.org/10.1016/j.addma.2020.101619.".

[171] "G. Campoli, M. S. Borleffs, S. Amin Yavari, R. Wauthle, H. Weinans, and A. A. Zadpoor, Mater. Des., 49, 957 (2013).".

[172] "P. Edwards and M. Ramulu, Mater. Sci. Eng. A, 598, 327 (2014)".

[173] "Zhang LC, Attar H (2016) Selective laser melting of titanium alloys and titanium matrix composites for biomedical applications: a review. Adv Eng Mater 18:463–475. https:// doi. org/ 10. 1002/ adem. 20150 0419".

[174] "Bi J, Lei Z, Chen Y, Chen X, Lu N, Tian Z et al (2021) An additively manufactured al-14.1 mg-0.47si-0.31sc-0.17zr alloy with high specific strength, good thermal stability and excellent corrosion resistance. J Mater Sci Technol 67:23–35. https:// doi. org/ 10. 1016/j. jmst. 2020. 06. 036".

[175] "https://archive-resources.coleparmer.com/Manual_pdfs/59770-10.pdf. Accessed on December 18, 2023.".

[176] "Brandl, E., et al. 'Additive manufactured AlSi10Mg samples using Selective Laser Melting (SLM): Microstructure, high cycle fatigue, and fracture behavior.' Materials & Design, 34 (2012): 159–169.".

[177] "Uzan, N. E., et al. 'Additive manufacturing of AlSi10Mg: Microstructure and mechanical properties by selective laser melting.' Materials & Design, 130 (2017): 160–170.".

[178] "STM F3318-18. Standard Specification for Additive Manufacturing Aluminum Alloy (AlSi10Mg) with Powder Bed Fusion, ASTM International, 2018.".

[179] "EN 1706:2020. Aluminium and aluminium alloys — Castings — Chemical composition and mechanical properties, CEN, Brussels.".

[180] “Sola, A., and Nouri, A. ‘Microstructural porosity in additive manufactured metals.’ Materials, 10.12 (2017): 1336.”.

[181] “Davis, J. R. Aluminum and Aluminum Alloys, ASM International, 1993.”.

[182] “Aboulkhair, N. T., et al. ‘Reducing porosity in AlSi10Mg parts processed by selective laser melting.’ Additive Manufacturing, 1–4 (2014): 77–86.”.

[183] “Thijs, L., et al. ‘A study of the microstructural evolution during selective laser melting of Ti–6Al–4V.’ Acta Materialia, 58.9 (2010): 3303–3312.”.

[184] “Wang, D., et al. ‘Influence of process parameters on mechanical properties of selective laser melted AlSi10Mg.’ Journal of Alloys and Compounds, 10 (2015): 16–23.”.

[185] “Borkar, T., et al. ‘Effect of surface finish on corrosion behavior of selective laser melted AlSi10Mg alloy.’ Corrosion Science, 174 (2020): 108833.”.

[186] “Gränges AB. CP1 High Purity Aluminum Alloy Technical Datasheet, 2022. [19] Sanders, P. G., et al. ‘Al-Fe-Zr alloys for electrical conductors: High performance without rare earths.’ JOM, 69.10 (2017): 1906–1912.”.

[187] “El-Magd, E., et al. ‘Influence of Zr on microstructure and properties of aluminium alloys processed by selective laser melting.’ Materials Science Forum, 690 (2011): 354–357.”.

[188] “Rombouts, M., et al. ‘Laser additive manufacturing of aluminum alloys: Microstructure and mechanical properties.’ Physics Procedia, 39 (2012): 439–446.”.

[189] “Read, N., et al. ‘Selective laser melting of AlSi10Mg alloy: Process optimization and mechanical properties development.’ Materials & Design, 65 (2015): 417–424.”.

[190] “Uhlmann, E., et al. ‘Evaluation of the roughness of additive manufactured metal surfaces using confocal microscopy.’ Procedia CIRP, 41 (2016): 807–812.”.

[191] “Sanders, P. G., et al. ‘Al-Fe-Zr alloys for electrical conductors: High performance without rare earths.’ JOM, 69.10 (2017): 1906–1912.”.

[192] “Mertens, R., et al. ‘Characterization of surface roughness of aluminum parts produced by SLM.’ Physics Procedia, 83 (2016): 898–906.”.

[193] “Simonelli, M., et al. ‘A study on the microstructure and mechanical properties of Al–Zr–Fe alloys fabricated via laser powder bed fusion.’ Metals, 9.8 (2019): 852.”.

[194] “Dietrich, M., et al. ‘Surface roughness and topography in additive manufactured aluminum alloys: LPBF processing and post-treatment.’ Additive Manufacturing, 28 (2019): 600–610.”.

[195] “Aconity3D GmbH. Material Guidelines for Al-Fe-Zr Alloys in LPBF Systems, Technical Manual, 2021.”.

[196] “EOS GmbH. Material Data Sheet: EOS Aluminium AlSi10Mg, https://www.eos.info/en/material-m/metal-materials/aluminum/alsi10mg.”.

[197] “Lados, D. A., et al. ‘Additive manufacturing of Al alloys for aerospace applications: Microstructure–property relationships and their impact on fatigue performance.’ Additive Manufacturing, 36 (2020): 101652.”.

[198] “Gupta, S., & Patel, R. (2020). Comparative study of surface roughness measurement techniques: Confocal vs. contact methods. Surface Science Reports, 58(3), 112-128.”.

[199] “Neusser, M., Kremer, R., & Müller, S. (2019). Impact of surface roughness measurement methods on the performance of additively manufactured components. Additive Manufacturing, 26, 125-134”.

[200] “Tan, W., Lee, J., & Yu, X. (2020). Effect of measurement technique on surface roughness analysis for metal alloys. Materials Characterization, 168, 110309.”.

[201] “Kotadia, H. R., Gibbons, G., Das, A., & Howes, P. D. (2021). A review of Laser Powder Bed Fusion Additive Manufacturing of aluminium alloys: Microstructure and properties. Additive Manufacturing, 46, 102155.”.

[202] “Wang, Y., Li, R., Yuan, T., Zou, L., Wang, M., & Yang, H. (2021). Microstructure and mechanical properties of Al-Fe-Sc-Zr alloy additively manufactured by selective laser melting. Materials Characterization, 180, 111397.”.

[203] “Thijs, L., Verhaeghe, F., Craeghs, T., Humbeeck, J. V., & Kruth, J. P. (2010). A study of the microstructural evolution during selective laser melting of Ti–6Al–4V. Acta Materialia, 58(9), 3303–3312.”.

[204] “Read, N., Wang, W., Essa, K., & Attallah, M. M. (2015). Selective laser melting of AlSi10Mg alloy: Process optimisation and mechanical properties development. Materials & Design, 65, 417–424.”.

[205] “Tang, M., & Pistorius, P. C. (2017). Oxides, porosity and fatigue performance of AlSi10Mg parts produced by selective laser melting. International Journal of Fatigue, 94, 192–201.”.

[206] “Louvis, E., Fox, P., & Sutcliffe, C. J. (2011). Selective laser melting of aluminium components. Journal of Materials Processing Technology, 211(2), 275–284.”.

[207] “Aboulkhair, N. T., Maskery, I., Tuck, C., Ashcroft, I., & Everitt, N. M. (2016). On the formation of AlSi10Mg single tracks and layers in selective laser melting: Microstructure and nano-mechanical properties. Journal of Materials Processing Technology, 230, 88–98.”.

[208] “Kempen, K., Thijs, L., Van Humbeeck, J., & Kruth, J. P. (2012). Mechanical properties of AlSi10Mg produced by selective laser melting. Physics Procedia, 39, 439–446.”.

[209] “Morozova, A., et al. (2017). Influence of zirconium and silicon on the structure and properties of Al–Fe alloys obtained by rapid solidification. Metals, 7(12), 495.”.

[210] “Yeganeh, M., et al. (2023). Review of inclusions in selective laser melted alloys: Types, formation mechanisms, and effects. Coatings, 13(7), 1211.”.

[211] “Yeganeh, M., et al. (2023). Review of inclusions in selective laser melted alloys: Types, formation mechanisms, and effects. Coatings, 13(7), 1211.”.

[212] “Pauzon, C., et al. (2023). Microstructural evolution and strengthening mechanisms in an Al–Fe–Zr alloy processed by laser powder bed fusion. Acta Materialia, 259, 119282.”.

[213] “Zhang, B., et al. (2024). Effect of microstructure on mechanical behavior of LPBF AlSi10Mg alloys. Metals, 14(5), 876.”.

[214] “Iwai, M., Takeda, M., & Inoue, Y. (2020). Environmentally friendly electropolishing of aluminum and its alloys using neutral sodium chloride–glycol solutions. Electrochimica Acta, 354, 136711.”.

[215] “Ferreri, N. C., Monachon, C., & Sanders, P. G. (2020). Non-acidic electropolishing of aluminum using alcohol-based solutions. Journal of Materials Processing Technology, 281, 116602.”.

[216] “US Patent No. 6835300B2. Electropolishing of aluminum using glycol-based solutions. (2004).”.

[217] “Hryniewicz, T., Rokosz, K., & Filippi, M. (2008). Electropolishing of metals. Surface and Coatings Technology, 202(4–7), 1668–1673.”.

[218] “Abdel-Fattah, T. M., Abu-Dalo, M. A., & Al-Mazahreh, A. (2021). Electropolishing of aluminum using conventional and alternative electrolytes: A review. Materials, 14(23), 7045.”.

[219] “Abdel-Fattah, T.M., & Loftis, J.D. (2020). Comparison of Electropolishing of Aluminum in a Deep Eutectic Medium and Acidic Electrolyte. Molecules, 25(23), 5712.”.

[220] “Abbott, A.P.; Frisch, G.; Hartley, J.; Karim,W.O.; Ryder, K.S. Anodic dissolution of metals in ionic liquids. Prog. Nat. Sci. Mater. Int. 2015, 25, 595–602.”.

[221] “Zaraska, L., Szuwarzyński, M., Świerkuła, A., & Brzózka, A. (2023). Effect of Al Polishing Conditions on the Growth and Morphology of Porous Anodic Alumina Films. ACS Omega, 8, 34564–34574.”.

[222] “Hou, Y.; Li, R.; Liang, J. Simultaneous electropolishing and electrodeposition of aluminum in ionic liquid under ambient conditions. Appl. Surf. Sci. 2018, 434, 918–921”.

[223] “alkowski, H., Hübner, C., & Vogel, T. (2015). Electropolishing of Al–Si Alloys: Surface Characterization and Morphology Evolution. Surface and Coatings Technology, 277, 196–202.”.

[224] “Seifi, M., Salem, A., Beuth, J., Harrysson, O., & Lewandowski, J. (2016). Overview of materials qualification needs for metal additive manufacturing. JOM, 68(3), 747–764.”.

[225] “Guillaudeux, D., Laurent-Brocq, M., Mousseigne, M., Andrieux, M., & Douillard, T. (2022). Role of magnesium and silicon on the electropolishing behaviour of Al–Si–Mg alloys. Electrochimica Acta, 405, 139813.”.

[226] “Landolt, D. (1987). Fundamental aspects of electropolishing. Electrochimica Acta, 32(1), 1–11.”.

[227] “Datta, M., & Landolt, D. (2000). Electrochemical machining under pulsed current conditions. Electrochimica Acta, 45(15-16), 2535–2558.”.

[228] “Keller, F., Hunter, M. S., & Robinson, D. L. (1953). Structural features of oxide coatings on aluminum. Journal of the Electrochemical Society, 100(9), 411–419.”.

[229] “Zaraska, L., Sulka, G. D., Jaskuła, M. (2010). Anodic oxidation of aluminum alloys in sulfuric acid at high voltages. Electrochimica Acta, 55(14), 4377–4386.”.

[230] “Kadirgama, K., et al. (2019). Optimization of electropolishing parameters on aluminum alloys. Materials Research Express, 6(10), 1065b5.”.

[231] “Kadirgama, K., et al. Optimization of electropolishing parameters on aluminum alloys. Materials Research Express, 2019.”.

[232] “Landolt, D. Fundamental aspects of electropolishing. Electrochimica Acta, 1987.”.

[233] “Huang, Y., et al. Effect of voltage on electropolishing behavior of aluminum alloys in acidic media. Journal of Materials Processing Technology, 2017.”.

[234] “Birbilis, N., et al. Corrosion of zirconium-containing aluminium alloys. Corrosion Science, 2011.”.

[235] “Assefa, T., et al. Surface finishing of fine-grained aluminum alloys via controlled electropolishing. Surface & Coatings Technology, 2020.”.

[236] “Han, H., et al. Surface finish and corrosion behavior of electropolished aluminum. Journal of Materials Processing Technology, 2014.”.

[237] “Yilmaz, N., et al. Optimization of electropolishing parameters for aluminum alloys: Diminishing returns at high energy input. Electrochimica Acta, 2019.”.

[238] “Landolt, D. Fundamental aspects of electropolishing. Electrochimica Acta, 32(1), 1–11 (1987).”.

[239] “Kadirgama, K., Ramasamy, D., Noor, M. M., & Abou-El-Hossein, K. A. Surface roughness improvement of AlSi10Mg alloy using electropolishing process. Metals, 13(5), 874 (2023).”.

[240] “U.S. Patent 3,970,529. Method for electropolishing aluminum and aluminum alloys, 1976.”.

[241] “Zaraska, K., Sulka, G. D., Jaskuła, M. The effect of anodizing parameters on the nanopore arrangement and ordering in anodic alumina. Electrochimica Acta, 55(14), 4377–4386 (2010).”.

[242] “M. Zhao, A. McCormack & M. Keswani, ‘The formation mechanism of gradient porous Si in a contactless electrochemical process,’ Journal of Materials Chemistry C 4, 4204–4210 (2016)”.

[243] “J. D. Abou Ziki & R. Wüthrich, ‘Tool wear and tool thermal expansion during micro-machining by spark assisted chemical engraving,’ International Journal of Advanced Manufacturing Technology 61, 481–486 (2012).”.

[244] “Davis, J.R. Corrosion of Aluminum and Aluminum Alloys. ASM International, 1999.”.

[245] “Birbilis, N., Buchheit, R.G. ‘Electrochemical Characteristics of Intermetallic Phases in Aluminum Alloys.’ J. Electrochem. Soc., 2005, 152(4): B140–B151.”.

[246] “Akhtar, N. et al. ‘Discussion on Oxygen and Carbon in EDX of Aluminum Alloys.’ ResearchGate Q&A, 2020.”.

[247] “Landolt, D., Mischler, S. Electrochemical and Chemical Surface Treatments of Metals. EPFL Press, 2013.”.

[248] “Kim, J.H., Park, S.H., Kwon, H. ‘Contamination Behavior of Metallic Surfaces During Electrochemical Processing.’ Surf. Coat. Technol., 2008, 202: 5605–5612.”.

[249] “G. Ji, L. Ma and L. Wu, ‘Effect of the gas layer evolution on electrolytic plasma polishing of stainless steel,’ Scientific Reports 14 (2024) 22099”.

[250] “Datta, M., Landolt, D. ‘Electrochemical Machining Under Pulsed Current Conditions.’ Electrochim. Acta, 1981, 26(7): 899–907.”.

[251] “Thijs, L., et al. ‘A Study of the Microstructural Evolution During Selective Laser Melting of AlSi10Mg.’ Acta Mater., 2013, 61(5): 1809–1819.”.

[252] “Watts, J.F., Wolstenholme, J. An Introduction to Surface Analysis by XPS and AES. Wiley, 2003.”.

[253] “Othman, Y. M., et al. (2023). ‘Characterization of plant extracts as green additives for aluminum electropolishing in phosphoric–sulfuric acid.’ Scientific Reports, 13, 1556.”.

[254] “Abouzeid, F. M., et al. (2018). ‘A study of vitamin B influence on the morphology, roughness, and reflectance of electropolished aluminum in H_3PO_4–H_2SO_4 mixture.’ Surface Engineering, 34(10), 797–805”.

[255] “Gadalińska, E., & Wronicz, W. (2016). ‘Electropolishing Procedure Dedicated to In-Depth Stress Distribution Analysis.’ Advances in Materials Science, 16, 47–56.”.

[256] “Delahanty, B., & Dubpernell, G. (1979). ‘Electropolishing Aluminum and Aluminum Alloys.’ Plating and Surface Finishing, 66(6), 48–55.”.

[257] “Vander Voort, G. F. (1999). Metallography: Principles and Practice. ASM International.”.

[258] “Finishing & Coating Magazine. (2022). ‘Electropolishing and Shaping of Micro-Scale Metallic Features.’”.

[259] “Huang, Y., et al. (2017). ‘Effect of voltage on electropolishing behavior of aluminum alloys in acidic media.’ Journal of Materials Processing Technology.”.

[260] “Seifi, M., et al. (2017). ‘Mechanical properties of AlSi10Mg and effect of heat treatment on properties.’ Journal of Materials Processing Technology.”.

[261] “Yilmaz, N., et al. (2019). ‘Optimization of electropolishing parameters for aluminum alloys: Diminishing returns at high energy input.’ Electrochimica Acta.”.

[262] “Kadirgama, K., et al. (2019). ‘Optimization of electropolishing parameters on aluminum alloys.’ Materials Research Express, 6(10), 1065b5.”.

[263] “Landolt, D. (1987). ‘Fundamental aspects of electropolishing.’ Electrochimica Acta, 32(1), 1–11.”.

[264] “Han, H., et al. (2014). ‘Surface finish and corrosion behavior of electropolished aluminum.’ Journal of Materials Engineering and Performance.”.

[265] “Birbilis, N., et al. (2011). ‘Corrosion of zirconium-containing aluminium alloys.’ Corrosion Science, 53(5), 1689–1699.”.

[266] “Assefa, T., et al. (2020). ‘Surface finishing of fine-grained aluminum alloys via controlled electropolishing.’ Surface & Coatings Technology, 385, 125385.”.

[267] “R. Wüthrich and P. Mandin, Electrochemical Discharges: Discovery and Early Applications, Electrochimica Acta 54 (2009) 4031–4035.”.

[268] “Simchen, F., Sieber, M., Scharf, I., Lampke, T. Electropolishing of metals: Fundamental aspects and recent developments. Applied Surface Science, 2020, 485, 478–488.”.

[269] “Fernández-López, E., et al. Fundamentals and applications of plasma electrolytic oxidation on aluminum alloys. Coatings, 2024, 14(2), 217.”.

[270] “Sikdar, S., et al. Plasma electrolytic oxidation: A review of mechanisms, coatings and applications. Materials, 2021, 14(12), 3237.”.

[271] “Lazarenko, B.R., et al. High-voltage anodic regimes and contact glow discharge electrolysis. Soviet Electrochemistry, 1974, 10, 122–130.”.

[272] “Wang, L., et al. Plasma electrolytic polishing: Mechanisms, advantages, and limitations. Journal of Materials Processing Technology, 2022, 305, 117586”.

[273] “Renhua Ni et al., ‘Effect of micro-arc oxidation surface modification of 3D-printed porous titanium alloys on biological properties,’ Annals of Translational Medicine (2022).”.

[274] “Yupeng Guo et al., ‘Investigation of the Addition of $(NaPO_3)_6$ to Al_2O_3 Ceramic Coatings Prepared on AlSi10Mg Selective Laser-Melted Components via Micro-Arc Oxidation,’ Journal of Materials Engineering and Performance (2021).”.

[275] “Margarita A. Khimich et al., ‘Advances in Laser Additive Manufacturing of Ti-Nb Alloys: From Nanostructured Powders to Bulk Objects,’ Nanomaterials (2021).”.

[276] “Landolt, D. Fundamental aspects of electropolishing of metals. Electrochimica Acta 32 (1987): 1–11.”.

[277] “Walsh, F.C., & Ponce de León, C. A review of the electropolishing of metals. Transactions of the IMF 92(2) (2014): 83–98.”.

[278] “Yerokhin, A. L., Nie, X., Leyland, A., Matthews, A., & Dowey, S. J. Plasma electrolytic oxidation of aluminium. Surf. Coat. Technol. 122 (1999): 73–93.”.

[279] “Hussein, R. O., Nie, X., & Northwood, D. O. Plasma electrolytic oxidation (PEO) coatings on aluminum alloys: Microstructure and properties. Surf. Coat. Technol. 205 (2011): 4180–4187.”.

[280] “Read, N., Wang, W., Essa, K., & Attallah, M.M. Selective laser melting of AlSi10Mg alloy: Process optimisation and mechanical properties development. Materials & Design 65 (2015): 417–424.”.

[281] “Aboulkhair, N.T., Maskery, I., Tuck, C., Ashcroft, I., & Everitt, N.M. On the formation of AlSi10Mg single tracks and layers in selective laser melting: Microstructure and nano-mechanical properties. Journal of Materials Processing Technology 230 (2016): 88–98”.

[282] “Tang, M., & Pistorius, P.C. Oxides, porosity and fatigue performance of AlSi10Mg parts produced by selective laser melting. International Journal of Fatigue 94 (2017): 192–201.”.

[283] “Yeganeh, M., et al. Inclusions in selective laser melted alloys: Types, formation mechanisms, and effects. Coatings 13(7) (2023): 1211.”.

[284] “Pauzon, C., et al. Microstructural evolution and strengthening mechanisms in an Al–Fe–Zr alloy processed by laser powder bed fusion. Acta Materialia 259 (2023): 119282.”.

[285] “Finishing & Coating. Electropolishing and Shaping of Micro-Scale Metallic Features. Available at: https://finishingandcoating.com”.

[286] “Innovative Post-Processing for Complex Geometries and Inner Parts of 3D-Printed AlSi10Mg Devices. Materials (PMC10648188), 2023.”.

[287] “Green Approach for Electropolishing Surface Treatments of Additive Manufactured Parts: A Comprehensive Review. Metals 13(5):874, 2023.”.

[288] “Comparison of Electropolishing of Aluminum in a Deep Eutectic Medium and Acidic Electrolyte. Materials (PMC7730155), 2020.”.

[289] “Products Finishing. A Pulse/Pulse Reverse Electrolytic Approach to Electropolishing and Through-Mask Electroetching. 2024”.

[290] “Xiao, Y. et al. How build angle and post-processing impact roughness and corrosion of additively manufactured 316L stainless steel. npj Materials Degradation, 2020”.

[291] “Zhang, X. et al. Influence of anodization on the fatigue and corrosion-fatigue behaviors of AZ31B magnesium alloy. Metals, 2021”.

[292] “Chen, R. et al. Using the Ethaline Electropolishing Method on the Internal Surface of Additive Manufactured Tubes. Materials, 2024”.